EXPLORING THE
HYDRAULIC PERFORMANCE OF
CONICAL PILE HEAD BREAKWATER – AN
EXPERIMENTAL INVESTIGATION

Thesis

Submitted in partial fulfilment of the requirements for the degree of
DOCTOR OF PHILOSOPHY

by

ARUNAKUMAR H S

DEPARTMENT OF WATER RESOURCES AND
OCEAN ENGINEERING
NATIONAL INSTITUTE OF TECHNOLOGY KARNATAKA,
SURATHKAL, MANGALURU - 575 025
June, 2023

EXPLORING THE
HYDRAULIC PERFORMANCE OF
CONICAL PILE HEAD BREAKWATER – AN
EXPERIMENTAL INVESTIGATION

Thesis

Submitted in partial fulfilment of the requirements for the degree of
DOCTOR OF PHILOSOPHY

by

ARUNAKUMAR H S

(187068AM001)

Under the Guidance of

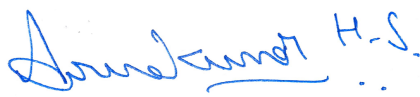**Dr. PRUTHVIRAJ U.**   **Prof. KIRAN G. SHIRLAL**

DEPARTMENT OF WATER RESOURCES AND

OCEAN ENGINEERING

NATIONAL INSTITUTE OF TECHNOLOGY KARNATAKA,

SURATHKAL, MANGALURU - 575 025

June, 2023

D E C L A R A T I O N

By the Ph.D. Research Scholar

I hereby *declare* that the Research Thesis entitled "**Exploring the Hydraulic Performance of Conical Pile Head Breakwater – An Experimental Investigation**" which is being submitted to the **National Institute of Technology Karnataka, Surathkal** in partial fulfilment of the requirements for the award of the Degree of **Doctor of Philosophy** in **Department of Water Resources and Ocean Engineering** is a *bonafide report of the research work* carried out by me. The material contained in this Research Thesis has not been submitted to any University or Institution for the award of any degree.

187068, ARUNAKUMAR H S

(Register Number, Name & Signature of the Research Scholar)

Department of Water Resources and Ocean Engineering

Place: NITK-Surathkal

Date: 30 - 06 - 2023

CERTIFICATE

This is to *certify* that the Research Thesis entitled "**Exploring the Hydraulic Performance of Conical Pile Head Breakwater – An Experimental Investigation**" submitted by **Arunakumar H S** (Register Number: 187068) as the record of the research work carried out by him, is *accepted as the Research Thesis submission* in partial fulfilment of the requirements for the award of degree of **Doctor of Philosophy**.

Dr. Pruthviraj U. 30/6/23

(Research Guide)

Prof. Kiran G. Shirlal

(Research Guide)

(Chairman – DRPC)

Chairman (DRPC)
Dept. of Water Resources & Ocean Engineering

DEPARTMENT OF WATER RESOURCES AND OCEAN ENGINEERING

NATIONAL INSTITUTE OF TECHNOLOGY KARNATAKA,

SURATHKAL, MANGALURU - 575 025

ACKNOWLEDGMENT

ABSTRACT

Conventional pile breakwater is a pervious structure built using prismatic circular piles and it has been proven to provide partial protection efficiently. Increasing the size of the pile breakwater in the vicinity of the free surface increases its hydraulic efficiency, as most of the wave energy is concentrated there. In the present study, the conventional pile breakwater model is modified by widening the cross-sectional area of the piles at the surface level in a conical shape termed as conical pile head breakwater (CPHB). The influence of the dimensionless structural parameters such as relative diameter (D/H_{max}), relative height (Y/H_{max}), relative clear spacing (b/D) and relative clear spacing between rows of CPHB (B/D) on the hydraulic performance is comprehensively explored through physical model studies. The hydraulic performance of the model includes wave transmission (K_t), wave reflection (K_r) and energy dissipation (K_d) coefficients. The study is carried out under monochromatic waves of varying wave height (0.06 m to 0.16 m) and wave period (1.4 s to 2 s) at different depths of water (0.35 m, 0.40 m and 0.45 m). For single-row non-perforated CPHB, the structural configuration of $D/H_{max} = 0.4$, $Y/H_{max} = 1.5$ and $b/D = 0.1$ have emerged as the best performing model for which a smaller value of K_t of 0.66 is obtained along with K_r of 0.22 and K_d of 0.72. Further, the investigation is carried out to determine the influence of the second row of similar piles arranged in a staggered manner. For two rows of CPHB, B/D of 0.4 is the optimum spacing, which provided a minimal K_t of 0.58 with K_r of 0.24 and K_d of 0.79. The addition of a second row of piles with a similar configuration reduces the K_t by a maximum of 12.34% compared to a single row of CPHB. However, from the construction point of view, driving two rows of piles at a closer spacing in the field may give rise to technical issues and practical difficulties such as disturbance of neighbouring piles, altering soil bearing capacity, equipment manoeuvring and restricted access for construction and maintenance personnel due to the limited space.

To ward off such possibilities, an effort is made to enhance the functionality of single row of CPHB structure by introducing perforations to encourage energy dissipation. The influence of perforations on the performance of the perforated CPHB is comprehensively investigated through physical model studies. The effect of perforations and their distribution around the pile head (Pa), percentage of perforations (P) and size of perforations (S/D) on the wave attenuation characteristics are evaluated to arrive at an optimum configuration. A minimum K_t of 0.58 associated with K_r of 0.26 and K_d of 0.78 is obtained for an optimum configuration of Pa = 50%, P = 19.2% and S/D = 0.25 at a water depth of 0.45 m. This result compares exceptionally well with that of two rows of CPHB. Overall, providing the perforations is found to be effective in enhancing the wave attenuation capability by up to 12.4%. The K_t of the proposed CPHB is about 19 to 35% lesser than that of the perforated hollow pile breakwater under matching test conditions.

To ascertain the suitability of an open-source software REEF3D in CPHB modelling, selected cases of CPHB are numerically simulated and the results are validated with the experimental data. For non-perforated CPHB, the numerical results are under predicted for K_t (less than 4%) and over predicted for K_r and K_d (less than 9%). For the perforated CPHB, the variation is slightly higher (up to 12%) compared to the non-perforated structure. Validation of the numerical results with the experimental data shows that REEF3D produces reliable results with acceptable RMSE values. In addition, a set of empirical equations is derived using the data fitting technique for quick prediction of K_t and K_r of CPHB. The empirical equations estimate the K_t and K_r values quite accurately with a high coefficient of determination ($R^2 \geq 0.90$). The overall performance of the CPHB is found to be promising and therefore, may be considered as one among the host of measures for the purpose of wave energy damping necessary for various shore/nearshore applications.

Keywords: Pile breakwater, conical pile head breakwater, perforated pile head, physical model studies, numerical modelling, wave transmission, wave reflection, energy dissipation.

CONTENTS

LIST OF FIGURES

x

xi

LIST OF TABLES

NOMENCLATURE

b	Clear spacing between the CPHs in a row	K_t	Transmission coefficient
		L	Wavelength
b_0	Clear spacing between the circular piles in a row	N	Number of CPHB rows
B	Clear spacing between the rows of CPH	P	Percentage of perforations
C	Blockage coefficient	Pa	Distribution of perforations around the pile head
C_c	Contraction coefficient	R_e	Reynolds number
D	Top diameter of the conical pile head	S	Size of perforations
d	Diameter of the circular pile	T	Period of the wave
f	Head loss coefficient	T_t	Transmission function
g	Acceleration due to gravity	u_0	Velocity at the gap of piles
h	Depth of water	Y	Height of conical pile head
H	Total height of the CPHB	Y_c	Height of supporting pile
H_i	Incident wave height	β	Linearised friction coefficient
H_{max}	Maximum wave height	γ	Friction coefficient
H_r	Reflected wave height	ρ	Density of water
H_t	Transmitted wave height	l	Length of the jet flowing through the gap between the piles
K	Wave number	θ	Angle of wave attack
K_d	Energy dissipation coefficient	ϵ	Porosity
K_r	Reflection coefficient	$\bar{\epsilon}$	Spatial variation of porosity

CHAPTER 1

INTRODUCTION

1.1 BACKGROUND

The ocean is well known for its enormous power and dynamic nature. Construction of structures and facilities in the coastal areas without any protective considerations would be practically impossible. Breakwaters are constructed to safeguard the coastline infrastructures, erosion, amenities and communities from such destructive forces. One of the most common types of hard structures is rubble mounds and caisson breakwaters. Extensive studies on these conventional gravity-type breakwaters, such as rubble mounds and caissons, showed that they are effective in performance and stability against the design wave forces.

These breakwaters are ideal for harbours where maintaining tranquillity is essential for manoeuvring and mooring of ships. However, the gravity-type breakwaters are gigantic and alter the natural sediment movement (Mojtahedi et al. 2020; Suh et al. 2006; Teh et al. 2013). The width and weight of the conventional type breakwaters increase with water depth, requiring a great amount of construction material. These structures are also responsible for environmental degradation due to the quarrying and transportation of large-sized armour stones. Also, these structures block littoral drift and may cause severe erosion or accretion in neighbouring beaches. In addition, they prevent the circulation of water and so deteriorate the water quality near the coast. In some places, they obstruct the passage of fishes and bottom-dwelling organisms (Elsharnouby et al. 2012; Suh et al. 2007).

Even though the breakwaters are primarily deployed to maintain tranquillity, in a few specific coastal areas, they can be used as an energy absorbent for addressing the problems associated with coasts, such as coastal erosion, beach profile restoration and realignment. For some coastal facilities, such as fishing harbours, recreational sites, oil

jetties, and marinas, partial wave attenuation is sufficient. A certain extent of wave activity is desirable in coastal protection work to facilitate sediment motion to maintain the dynamic equilibrium of beaches. An environmentally friendly structure constructed for coastal protection without spoiling the beauty of the natural beach is always a better option. Hence, there is a need for research on environment-friendly breakwaters. Environmental friendly breakwaters are the ones that consume lesser resources, easy to construct, allow the exchange of water between the sea and lee side, facilitate unhindered movement of marine life and do not hamper the sediment movement. In such cases, pile structures may be adopted which are capable of sheltering the coastal area to a reasonable extent. These pile structures may be a viable alternative to the gravity-type breakwaters in an environmentally sensitive site where complete wave tranquillity is not essential.

1.2 PILE STRUCTURES

Pile structures can broadly be classified into pile breakwaters and pile-supported breakwaters. These pile structures are gaining momentum due to their advantages over conventional breakwaters. While offering partial protection, these pile structures allow some amount of wave energy to pass on to the lee side and allow an exchange of water and sediment, thus do not influence the environment adversely. In addition, the pile breakwaters consume lesser resources and occupy a comparatively smaller area on the sea bed and are more economical than the conventional breakwaters, specifically when constructed in deep water (Isaacson et al. 1998; Laju et al. 2005; Ramnarayan et al. 2021; Suh et al. 2006). Pile breakwaters are generally the preferred economical option when the hard stratum is absent at a nominal depth and wave climate is moderate (Laju et al. 2011; Sundar and Subbarao 2003).

1.2.1 Pile breakwater

Pile breakwaters consist of closely spaced prismatic piles and are generally constructed parallel to the shoreline. Using a circular section as a breakwater prevents significant torsional moments and corner stress concentrations induced by the wave action on the pile breakwaters. Significant cost savings may be attainable by using circular concrete

pipes due to the low manufacturing cost (Isaacson et al. 1998). In the past, many researchers have studied the performance of pile breakwaters, also called as conventional pile breakwaters (Figure 1.1a). Some of the important pile breakwaters investigated by various authors available in the literature and relevant to the present work are illustrated in Figure 1.1.
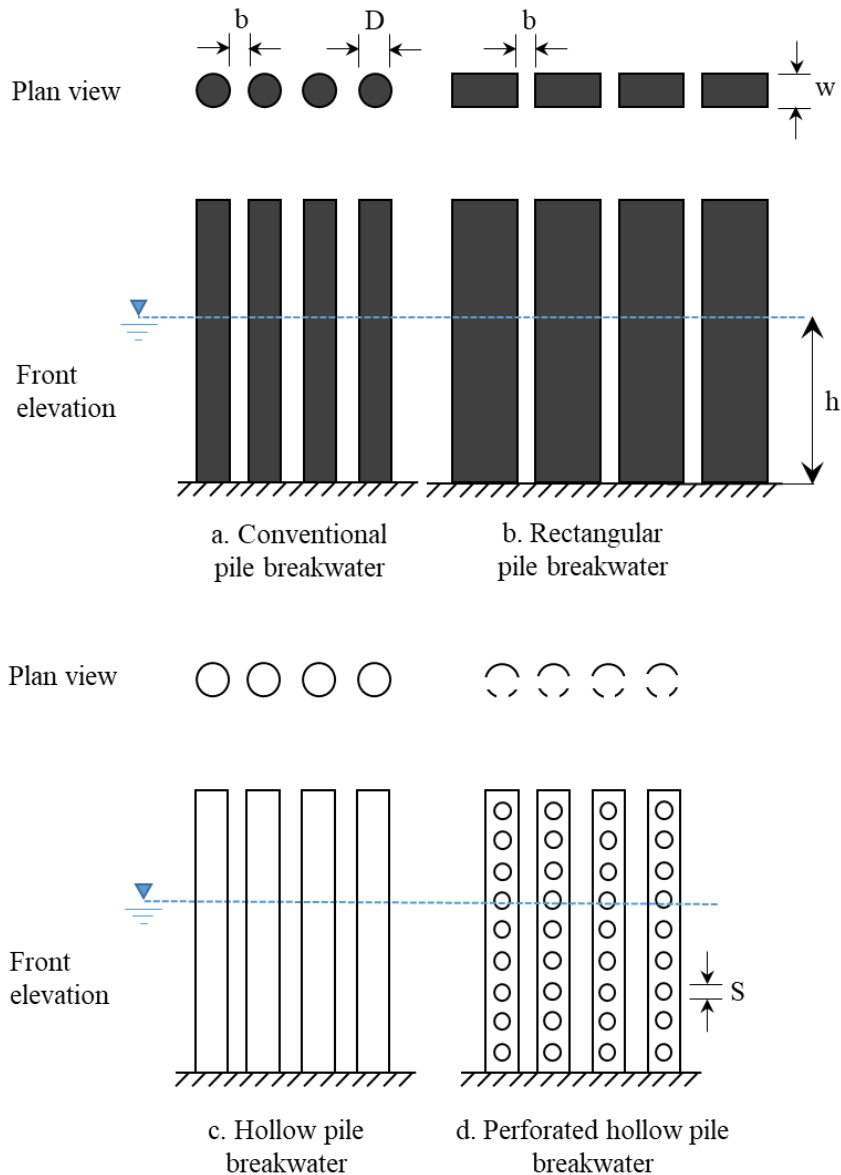
Figure 1.1 Typical representation of pile structures investigated by various researchers

In order to enhance the performance of the pile structures, perforations were introduced on the surface of the structures. The perforations were expected to increase the wave-structure interaction resulting in higher energy dissipation. The experiments carried out by Rao et al. (1999, 2002) on two rows of perforated hollow pile breakwater revealed that the wave attenuation capability of the perforated hollow pile breakwater is better than that of the non-perforated one. The performance of the two rows of perforated piles was investigated by Anuar and Sidek (2012). The study indicated that the size of perforations has a significant influence on wave attenuation characteristics. Pile breakwater structures have been constructed around the globe and are seen to be working effectively. A single row of pile breakwater constructed at Pelangi beach resort, Langkawi, Malaysia, is shown in Figure 1.2.

Figure 1.2 Front and side view of a single row pile breakwater constructed at Pelangi beach resort, Langkawi, Malaysia (Reedijk and Muttray 2009)

Some examples of existing pile breakwater structures are a reinforced concrete pile breakwater at Hanstholm, Denmark; closely spaced cylinder shells at Marsa el Brega, Libya; a steel pipe breakwater at the Port of Osaka, Japan; a concrete pipe breakwater at Pass Christian, Mississippi (Herbich and Douglas 1988); closely spaced piles at Half Moon Bay Marina, New Zealand (Hutchinson and Raudkivi 1984); a single row of pile breakwater at Pelangi Beach Resort, Malaysia (Koraim and Salem 2012; Reedijk and Muttray 2009); sheet pile breakwaters at Bay St. Louis, USA; an interlocking type pipe breakwater at the Port of Ust-Luga, Russia; a steel pipe breakwater at Tanah Merah,

Figure 1.3 Pile breakwater under construction in Zhoushan Islands, East China (Yin et al. 2021)

Singapore (Jeya et al. 2021); and Zhoushan Islands, East China (Yin et al. 2021). A Pile breakwater under construction in Zhoushan Islands, East China is illustrated in Figure 1.3.

1.2.2 Pile-supported breakwater

Even though the conventional pile breakwater is proved to be efficient, the construction of piles at closer spacing may pose practical difficulties such as pile driving or pile construction. To overcome these constraints, pile-supported breakwaters were proposed where a large barrier was provided on a series of piles located at a larger spacing. Mani and Jayakumar (1995) investigated the performance of suspended pipe breakwater, which consisted of an array of piles mounted on a frame that was suspended with the help of support piles. The construction cost of the suspended pipe breakwater was reported to be 40% cheaper than the conventional pile breakwater. Rao and Rao (2001) conducted physical modelling studies on the performance of suspended perforated pipe breakwater (Figure 1.4a) and revealed that the perforated structure enhances the wave attenuation capability of the structure with enhanced energy dissipation. A zigzag porous screen breakwater was proposed by Mani (2009) where, a zigzag porous screen was suspended between two rows of staggered piles (Figure 1.4b). Further, many studies were conducted by mounting different types of barriers/structures on the pile

supports. The various shapes considered were T-type (Neelamani and Rajendran 2002b), Ⱦ-type (Neelamani and Rajendran 2002a), U-type (Günaydin and Kabdaşli 2004) and Π-type (Günaydin and Kabdaşli 2007).
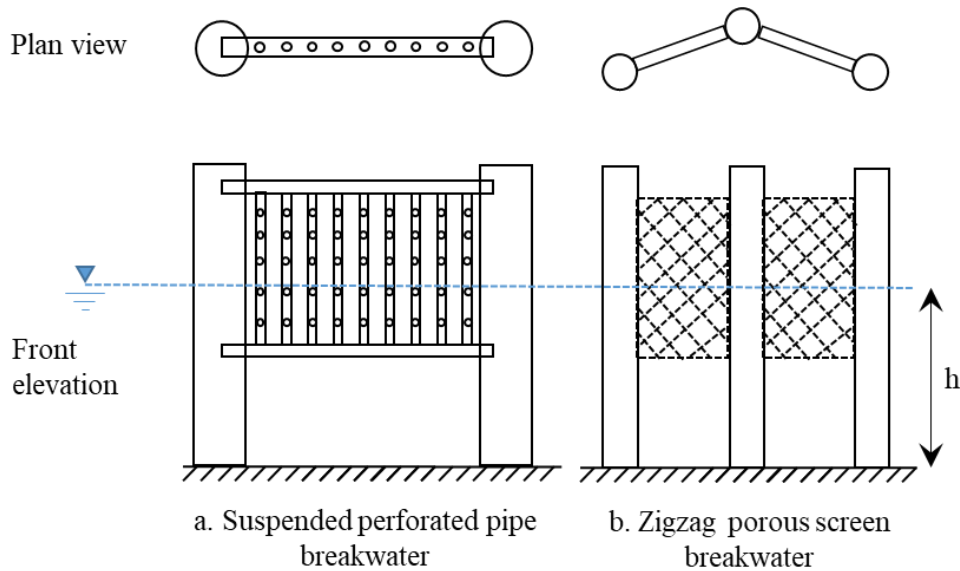
Figure 1.4 Schematic representation of different pile-supported breakwaters

Further research was carried out on pile-supported structures such as quadrant front-face pile-supported breakwater (Sundar and Subbarao 2003), pile-supported caisson breakwater (Duclos et al. 2001), curved and vertical front-face pile-supported breakwater (Ramnarayan et al. 2020, 2021, 2022) and pile-supported semi-circular breakwater (Teh et al. 2012, 2013). L-shaped and C-shaped bars were attached to the pile breakwaters to a certain depth to provide a higher obstruction area at the surface level (Koraim 2014; Koraim et al. 2014).

Pile-rock breakwater (PRBW) was constructed to protect the coast along Dongying City in China and Mekong Delta in southern Vietnam, as presented in Figure 1.5. The pile-rock breakwater mainly includes two rows of closely spaced piles connected by reinforced concrete beams and a rock core between them. Xuan et al. (2020) reported that PRBWs significantly reduced the impact of waves, and protected and rejuvenated the mangrove forest. It was also stated that PRBWs have more advantages than the

a.

b.

Figure 1.5 Double-row pile structure with rock core constructed at Dongying City, China (Xuan et al. 2020)

conventional type of breakwater due to their increased potential to combat erosion and stability. In addition, pile-supported breakwaters have been proved effective as an alternative solution for gravity-type structures at Half Moon Bay Marina in New Zealand (Hutchinson and Raudkivi 1984), Manfredonia port in Italy, Yeoho port in South Korea, Blaine harbour at Washington (Jeya et al. 2021) and the North-Western coast of Egypt (Elsharnouby et al. 2012).

1.2.3 Advantages

Pile structures offer a number of desirable characteristics that allow them to be potentially used as coastal defence structures (Teh 2013), some of which are listed below.

1. **Low construction cost**

   Pile structures require less concrete/steel per unit run as compared with the conventional breakwaters, especially when constructed at sites with relatively large water depths (Neelamani and Reddy 1992).

2. **Ease of construction**

   Compared to conventional breakwaters, pile structures can be easily installed using concrete or steel piles by cast in-situ or pile-driving technique with the help of barge-mounted cranes.

3. **Applicability in poor soil foundation and complex bathymetry**

   The construction of pile structures is hardly influenced by the bottom soil condition. The pile structures can be constructed at steep slope foreshore where the nature of the bathymetry makes the construction of the conventional breakwater to be less feasible.

4. **Eco-friendly structure**

   The methods used for pile breakwater construction reduce environmental impacts, e.g. noise and dust pollution on-site, at the quarry and in transport to the site. The breakwaters permit adequate flow exchange between the partially enclosed water body and the open sea, enabling fish migration, preservation of water quality and sediment transport activity.

5. **Reduced visual impact**

   The breakwaters have a low profile and are particularly favourable to beach users. They can sustain and preserve the natural beauty and tourist potential of the beach.

1.2.4 Applications and limitations

The pile structures offer only partial protection from the waves and their applications may be restricted to fishing harbours, tourist sites, oil jetties, marinas and coastal protection. These structures may also be employed for beach profile restoration and realignment works where, partial wave attenuation may be adequate and the sites are exposed to moderate wave action. These pile structures may be built together with the main structures, such as seawalls, jetties or even conventional breakwaters, to reduce the pressures and forces exerted on the main structures and maximise their overall hydraulic efficiency (Hsu and Wu 1999; Hu et al. 2002).

During extreme wave conditions, pile structures may not provide adequate protection to the sheltered regions and suffer from functional failures despite surviving structurally. In exceptional cases/situations, wave loadings and overtopping may also threaten its stability and integrity.

1.3 PRESENT STUDY

A pile breakwater is a permeable structure consisting of closely spaced single/multiple rows of piles. The wave attenuation in conventional pile breakwater takes place due to the combined effects of flow separation, contraction, intense flow through gaps, vortex formation, turbulence and eddy shedding. It is a well-known fact that the orbital motion of the water particles is maximum near the free surface and reduces gradually with the depth, as exhibited in Figure 1.6. To achieve the economy, it is better to increase the area of the piles near the water surface (Teh 2013) and incorporate perforations for obstructing the waves where wave activity is predominant. Therefore, the conventional pile breakwater model is modified by widening the cross-sectional area of piles at the surface level in a conical shape, termed as conical pile head breakwater (CPHB). Due to the increased area of piles in the vicinity of free surface, the proposed CPHB structure is expected to induce higher resistance against wave propagation, which contributes to increased wave attenuation. Further, during the wave-structure interaction, a certain amount of water flows in and out of the conical pile head through the perforations, contributing to additional wave attenuation by inducing additional turbulence.
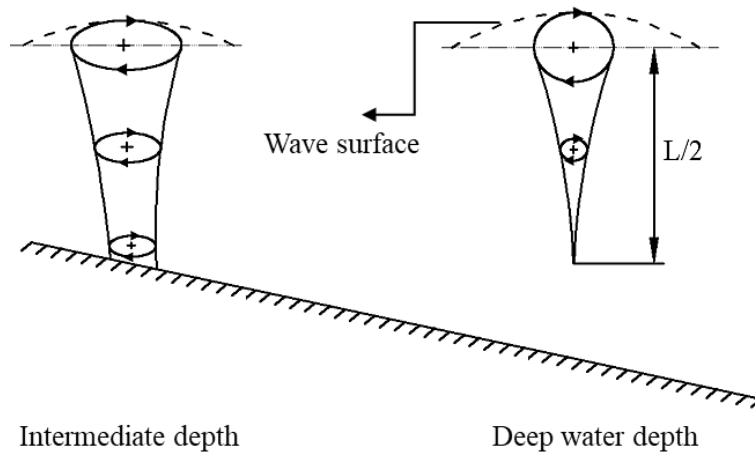
Figure 1.6 Water particle orbital motion at various depths of water (Deo 2013)

The proposed CPHB concept is an environment-friendly structure and it may overcome the difficulties due to the closer construction of conventional piles as a breakwater structure with improved efficiency. This structure gives partial protection from waves and it may be adequate for beach erosion control, small fishing harbours, marinas and recreational beach stretch. Due to the presence of gaps between the piles, the proposed structure helps to maintain the quality beaches as it does not interfere with the littoral drift and permits the passage of water and aquatic life. Hence, a detailed investigation of the hydraulic performance of pile breakwater, with the increased cross-sectional area near the free surface of the water is essential.

1.4 ORGANISATION OF THE THESIS

The research topic is introduced in Chapter 1. This includes the need for an eco-friendly mechanism for attenuating waves and scores of ideas to realise it.

Chapter 2 covers a review of relevant literature on pile/pile-supported breakwaters, including experimental, numerical and hybrid theoretical model studies. Based on the knowledge gap identified, the research problem and objectives of the present study are formulated.

The physical and numerical modelling details of the conical pile head breakwater are described in detail in Chapter 3, which includes the model scale selection, test setup and procedure, methodology and working principle of the proposed CPHB structure.

Chapter 4 discusses the results of the present investigation obtained through the physical modelling of non-perforated and perforated CPHBs. Further, validation of the numerical modelling results and empirical equations with experimental data is presented in this chapter.

The present research work is summarised and the important conclusions derived find their place in Chapter 5.

Exploring the environmental friendly options to address the wave energy attenuation solutions at the designated areas is a present day necessity. Due to the drawbacks associated with the massive structures, permeable structures may be preferred over conventional breakwaters for the attenuation of waves. A pile breakwater is one such permeable structure which can dampen the wave energy and provide partial protection. The pile breakwaters are innocuous to the environment and do not hamper the beauty of the natural beaches. Hence, a detailed study on the effectiveness of pile breakwater is necessary.

Before carrying out any research work, proper identification of a research problem is essential. For this purpose, an extensive literature review is carried out on pile structures. The literature on the experimental, numerical and hybrid theoretical investigations on the wave attenuation characteristics of pile structures are briefly discussed in the following sections.

2.1   PHYSICAL MODELLING STUDIES

One of the earliest known works on closely spaced piles was by (Costello 1952), wherein it was attempted to determine the wave transmissibility of piles. Experimental studies were conducted on wooden piles by varying the spacing between the piles in a row and multiple rows of piles. It was observed that irrespective of the density and configuration of piles, doubling the number of pile rows led to a reduction of wave transmission by up to 18%.

A mathematical equation was proposed by Weigel (1961) for the wave transmission coefficient of closely spaced piles. The equation for K_t was expressed in terms of geometry and spacing between piles only. The proposed equation was of the form,

$$K_t = \sqrt{\dfrac{b}{b+D}} \tag{2.1}$$

Where K_t is the transmission coefficient, b is the clear spacing between piles and D is the diameter of the pile. The transmitted wave height obtained through experimental work was found to be about 25% more than the theoretical prediction, and this variation was due to diffraction effects which were neglected in the equation.

Experiments conducted by Bovin (1964) on the slotted vertical wall breakwater showed that the width of the structure plays a significant role in wave energy dissipation. It was concluded that the total void ratio (ratio of the area of the opening in the wall to the area of the wall) on the seaward side was vital than individual hole characteristics and the shape of the hole had an insignificant effect on the energy dissipation characteristics of the perforated structure.

Hayashi et al. (1966) and Hayashi and Masataro (1968) studied the interaction of monochromatic waves with a single row of piles, both analytically and experimentally. An analytical solution was derived for the transmission and reflection coefficient of waves using the shallow water wave theory. The proposed equations were of the form,

$$K_t = 4\,\dfrac{h}{H_i}\,\in\left[-\in + \sqrt{\in^2 + \dfrac{H_i}{2h}}\,\right] \tag{2.2}$$

$$K_r = 1 - K_t \tag{2.3}$$

$$\in\ = \dfrac{Cb/(D+b)}{\sqrt{1-\left[b/(D+b)\right]^2}} \tag{2.4}$$

Where K_t is the transmission coefficient, K_r is the reflection coefficient, $\in$ is the porosity, h is the water depth, H_i is the incident wave height, and C is the coefficient of discharge between each spacing of the pile row. The analytical predictions were in good agreement with the experimental data. The experimental results conducted by Truitt

and Herbich (1987) using irregular waves indicated that the mathematical relationships developed for monochromatic waves might apply to irregular waves also.

Kondo and Toma (1972) investigated the effect of an idealised porous structure on wave attenuation characteristics such as transmission and reflection coefficients. The typical representation of the structure is presented in Figure 2.1. From the experiments, it was found that as the relative thickness of the structure (B/L, where, B is the thickness of perforated structure and L is the wavelength) increased, the reflection coefficient increased and the transmission coefficient exponentially decreased.
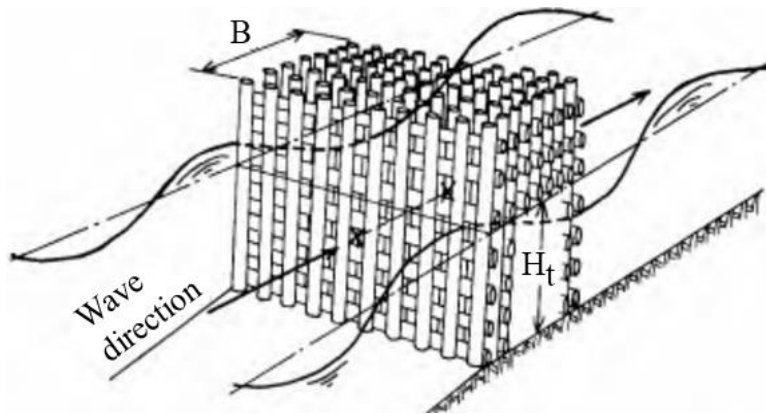
Figure 2.1 Typical representation of the porous structure (Kondo and Toma 1972)

Weele and Herbich (1972) used an experimental approach to investigate the wave transmission and reflection of four rows of piles while altering the wave wavelength and wave height. The influence of pile spacing (longitudinal and transverse direction) and pile configuration (rectangular and staggered) on wave transmission was also investigated. The results were presented in a dimensionless form to analyse the influence of pile geometry and steepness of waves on wave transmission and wave reflection. The study concluded that the reflection coefficient and transmission coefficient of a pile group reduced with the reduction of incident wave steepness. It was also reported that the reflection coefficient reduced with a reduction of spacing between the piles in both the longitudinal and transverse directions.

A case history of a constructed pile breakwater was analysed by Hutchinson and Raudkivi (1984), which was built at Half Moon Bay Marina Auckland, New Zealand in 1970. The typical cross-section of the breakwater is demonstrated in Figure 2.2.
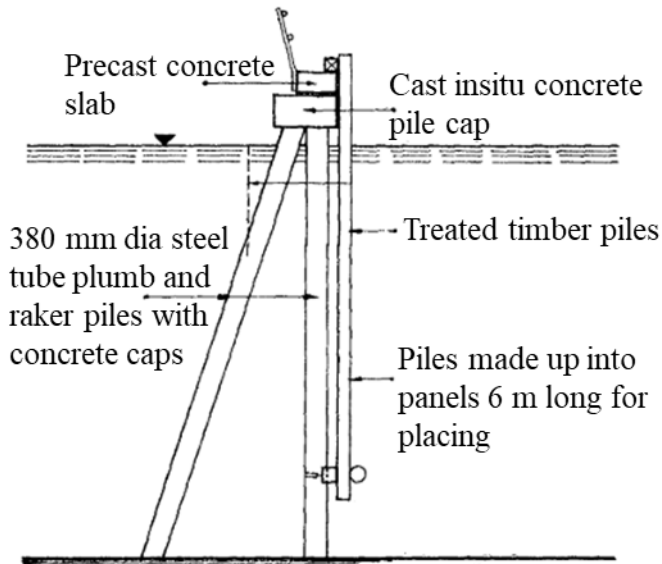
Figure 2.2 Typical cross section of the pile breakwater built at Half Moon Bay Marina Auckland, New Zealand (Hutchinson and Raudkivi 1984)

Before construction, physical tests were carried out in a wave flume which showed that about 50% reduction of wave height could be obtained by using vertical timber piles of 300 mm diameter with a clear spacing of 37 mm. Field observations showed that the breakwater had provided satisfactory shelter to 485 boats with no maintenance for the first twelve years.

Hagiwara (1984) presented an analytical solution for the reflection and transmission coefficient of vertical structures. Numerous factors which were associated with wave and physical conditions that have a major influence on wave attenuation were examined for the breakwater with perforated vertical walls provided on both landward and seaward sides. The theoretical results were compared with experimental work carried out by Kono and Tsukayama (1981) and found to be in good agreement concerning reflection and transmission coefficient. It was concluded that it was essential to find out

the relative chamber width (defined as the ratio of the spacing between the walls to the wavelength) and the opening ratio (defined as the ratio of the area of the opening to the surface area of the wall) of the pervious wall for reducing reflection and transmission coefficients.

Herbich and Douglas (1988) compared the performance of two rows of pile breakwater over a single row using experimental investigation. As predictable, the two rows of pile breakwater were found to be more efficient in wave transmission than the single row of piles. The addition of the second row of piles under similar wave conditions with a constant b/D ratio (where b is the clear spacing between piles and D is the diameter of the pile) of 0.2 resulted in the decrease of wave transmission by 15%; for a b/D ratio of 0.1, the transmission of the wave was decreased by 5 to 10%.

Herbich (1990), based on experimental studies on a single row of pile breakwater, concluded that transmission of the wave increased with an increase in the period of monochromatic waves. The wave transmission was also found to increase with an increase in the relative wave height and wave steepness. It was observed that the addition of the second row of piles under a gap ratio of 10% had decreased the wave transmissibility by 5% to 10%. For the considered range of test parameters, the diameter of the pile had a negligible influence on the transmission of waves, whereas the relative spacing had a significant influence on wave transmission.

The interaction of small amplitude waves with a group of vertical cylinders was studied experimentally and theoretically by Kakuno and Liu (1993). The flow separation and wave energy dissipation around the cylinders were modelled empirically. The energy loss coefficients (f) for square cylinders (f = 1.5) and circular cylinders (f = 0.75) were determined by comparing experimental and theoretical results. The authors stated that the research conducted was reliable to limited cases, and more laboratory experiments and field experiments are needed to determine the empirical coefficient for different geometrical shapes and wave parameters.

17
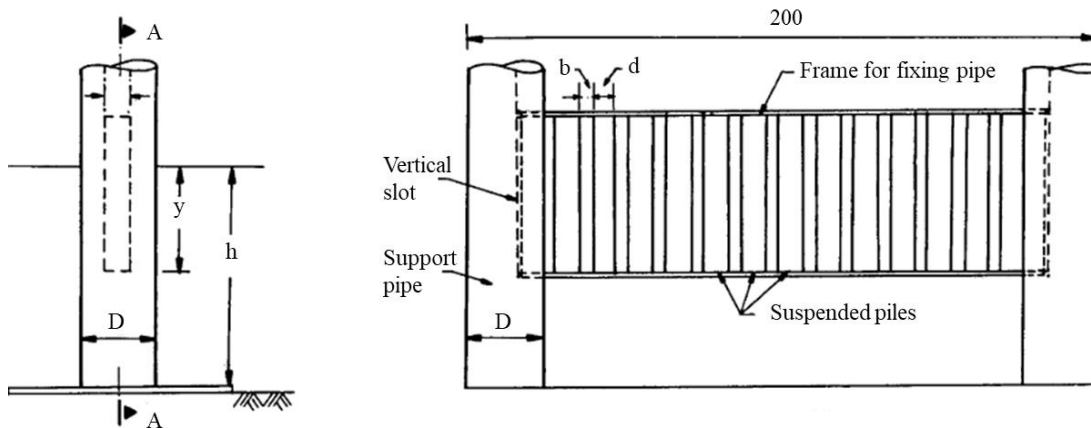
Figure 2.3 Details of suspended pipe breakwater (Mani and Jayakumar 1995)

Physical model studies were carried out on a suspended pipe breakwater by Mani and Jayakumar (1995). The suspended pipe breakwater consisted of a row of closely spaced pipes mounted onto a frame and suspended between the pile supports (Figure 2.3). The study recommended a gap to diameter ratio (b/d) of 0.22 and a draft to water depth ratio (y/h) of 0.46 to achieve a transmission coefficient of 0.5. For steep waves ($H_i/gT^2 >$ 0.008), the wave attenuation accomplished was 50%, while for gentle waves (0.005 < H_i/gT^2 < 0.008), it was 40%.

Laboratory investigations were conducted by Rao and Rao (1999) and Rao et al. (2002) on perforated hollow pipes to understand the hydraulic performance characteristics. The definition sketch and details of perforated piles are presented in Figure 2.4. The influence of water depth, incident wave steepness, arrangement of piles, clear relative spacing between the piles and number of pile rows on transmission and reflection coefficient was investigated. Introducing perforations on the piles proved to be more efficient in reducing both wave energy and wave reflection than non-perforated piles. It was found that as the incident wave steepness increased, the transmissibility of wave decreased and wave reflection increased for both perforated and non-perforated piles. The staggered arrangement of piles had reduced reflection to a considerable extent, whereas, no significant improvement was observed in the transmission of waves. The relative spacing of piles proved to be one of the important parameters in attenuating the wave energy, and the study recommended a relative spacing of 1 to 1.5 between the

pile rows for better attenuation. Similar findings have been reported earlier by Hayashi and Masataro (1968) and Weele and Herbich (1972).
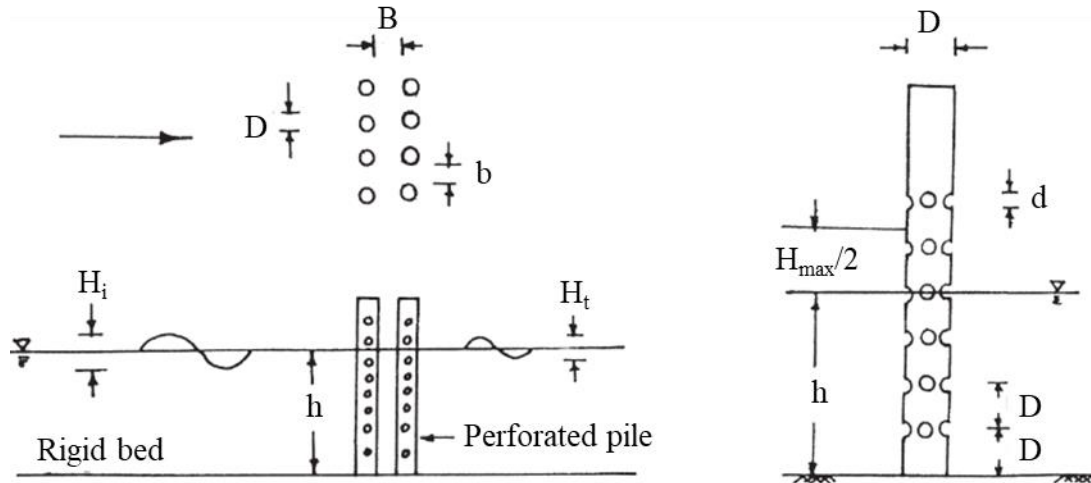
Figure 2.4 Definition sketch and details of perforated piles (Rao and Rao 1999)

The performance of suspended pipe breakwater was further investigated by Rao and Rao (1999, 2001) by imparting porosity on the surface of the pipes. The typical arrangement of the perforated pipes is illustrated in Figure 2.5. The influence of incident wave steepness, size of perforations, submergence depth, diameter of pipes, percentage area of perforations and depth of water on hydraulic characteristics have been investigated. The study revealed that as the submergence depth increased, the transmission coefficient reduced and reflection increased, but beyond 50% of the depth of submergence, the refinement was negligible. Pipes with a 25% area of perforations were found to attenuate about 10% to 14% more wave energy than non-perforated pipes and the perforated pipes reflected less wave energy when compared to non-perforated pipes. The size of perforations did not exert a significant influence on the transmission under a constant percentage of perforations. For the water depths considered, the effect of water depth on transmission and reflection was negligible. The influence of the wave period on wave transmission and reflection has not been identified.

Physical model studies were carried out by Neelamani and Vedagiri (2001) to determine the performance characteristics of the twin vertical barriers. The schematic perspective view of a partially immersed twin wall breakwater is presented in Figure
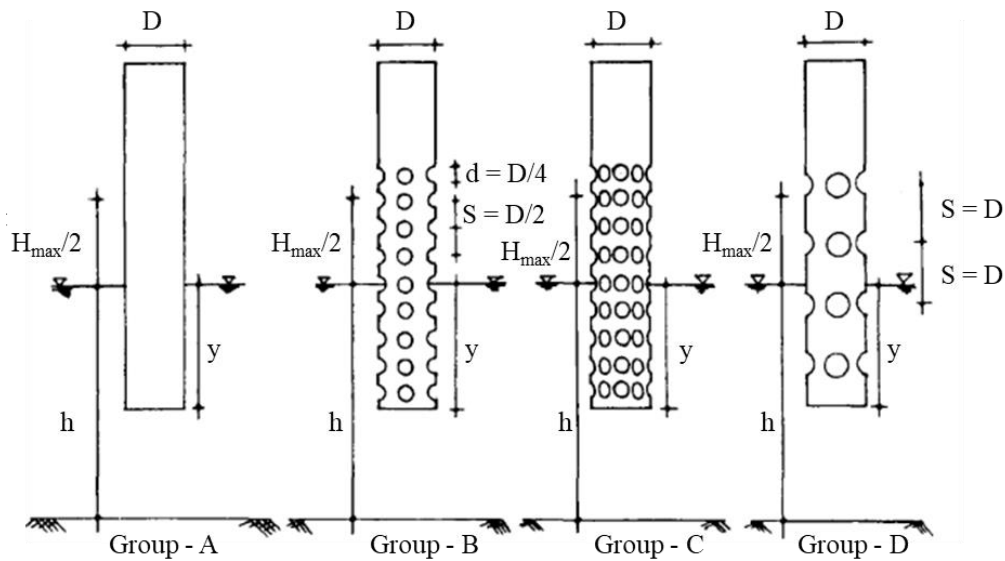
Figure 2.5 Details of perforated pipes (Rao and Rao 2001)

2.6. The wave transmission under irregular waves was lower than the monochromatic waves whereas, wave reflection was higher. The K_t value ranged from 0.60 to 0.8 for monochromatic waves and 0.37 to 0.50 for irregular waves. The average wave energy dissipation was lower for monochromatic waves ($K_d = 0.55$) than for irregular waves ($K_d = 0.80$). It was noted that the performance of the structure was better for the waves with higher input energy levels than the lower input energy level. The results also demonstrated that the test conducted for monochromatic waves exhibited conservative results compared to those for irregular waves.

Neelamani and Rajendran (2002a) carried out an experimental investigation on a partially submerged T-type breakwater (Figure 2.7) under monochromatic and irregular waves. A comparison between the monochromatic and irregular wave test results showed that the K_t of the studied structure was about 20% lower under irregular waves than monochromatic waves indicating conservative results for monochromatic waves. When the T-type breakwater was immersed about 7% of the total water depth, the K_t was less than 0.35 under normal and high wave energy input. It was reported that the tested breakwater was up to 65% effective in dissipating the incident wave energy.

20
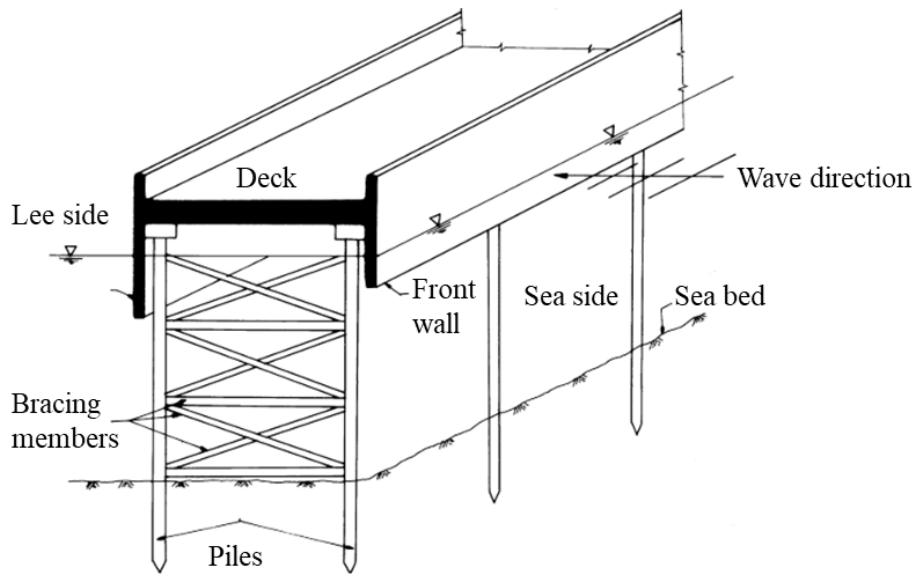
Figure 2.6 Schematic perspective view of a partially immersed twin wall breakwater (Neelamani and Vedagiri 2001)
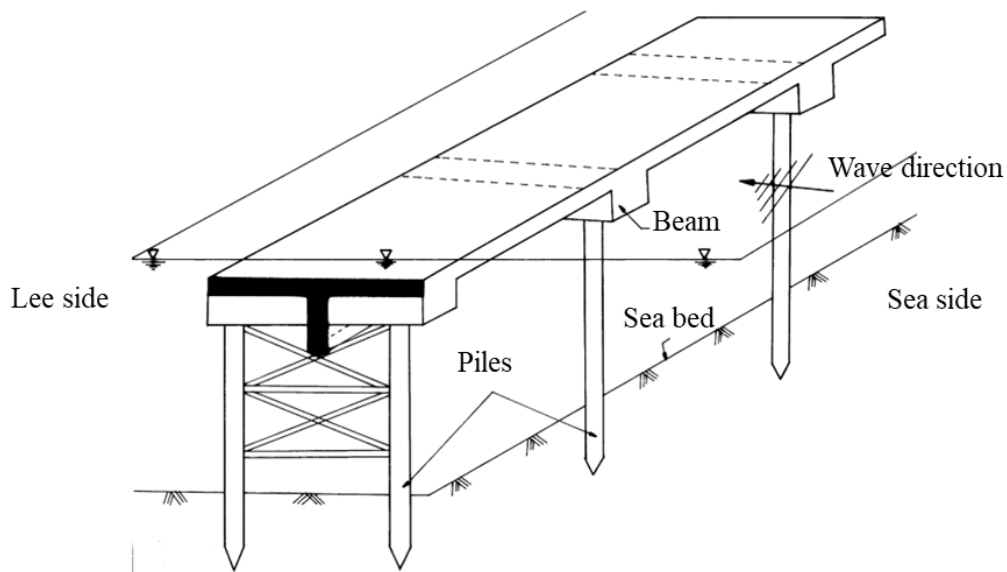
Figure 2.7 Schematic view of the T-type breakwater (Neelamani and Rajendran 2002a)

The wave transmission, reflection and dissipation characteristics of L-type breakwater were investigated by Neelamani and Rajendran (2002b). The schematic view of the
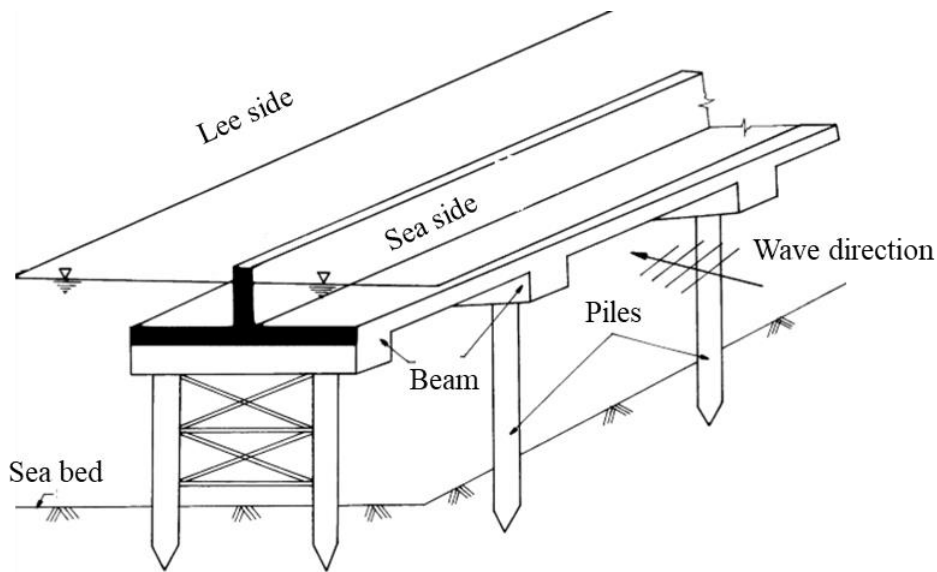
Figure 2.8 Schematic view of the L-type breakwater (Neelamani and Rajendran 2002b)

breakwater is illustrated in Figure 2.8. The range of K_t values obtained was 0.05 to 0.74 and 0.10 to 0.50 under monochromatic and irregular waves, respectively. The overall performance of the breakwater was found to be conservative under monochromatic waves than irregular waves. A comparison between the hydraulic performance of L-type and T-type breakwaters showed that latter was better than the former by about 20 to 30% under identical test conditions.

Sundar and Subbarao (2003) performed experiments for determining hydrodynamic characteristics of an innovative type of pile-supported breakwater. As seen in Figure 2.9, the breakwater had a quadrant-circle front face that was supported by piles. The variation of the reflection and transmission coefficients with the gap ratio (spacing between the piles/pile diameter) and relative water depth (water depth/pile height) were determined by subjecting to both monochromatic and irregular waves. Also, the dynamic pressures acting on the seaside as well as the total forces acting on the entire breakwater model was investigated. It was observed that under a constant gap ratio, the transmission coefficient was more at a lower water depth. K_t was found to vary from 0.1 to 0.55 for both monochromatic and irregular waves. The K_t due to irregular waves
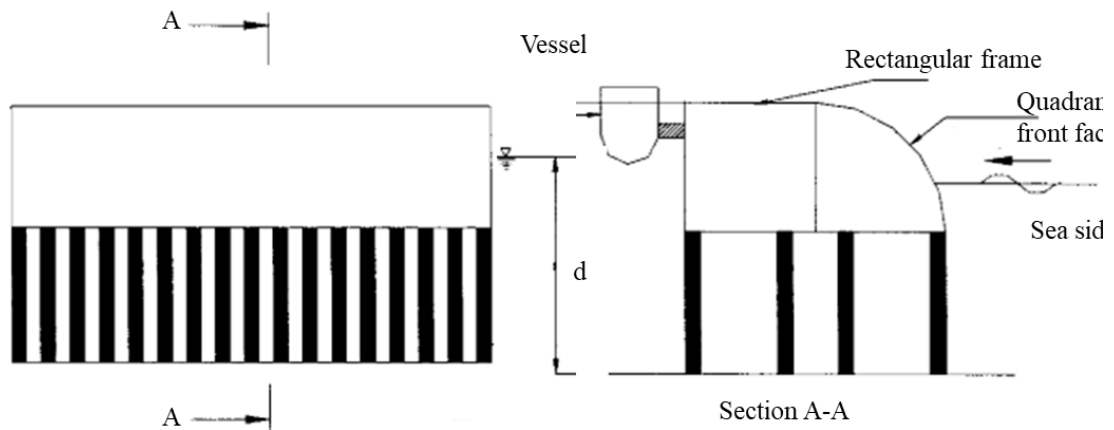
Figure 2.9 Details of quadrant front-face pile-supported breakwater model (Sundar and Subbarao 2003)

was found to be about 5% more than that due to monochromatic waves. For a constant gap ratio, as water depth increased, the reflection coefficient (K_r) was found to be increased. The study on the influence of pile spacing revealed that the gap ratio has a negligible effect on K_r. The range of variation of K_r was 0.25 to 0.85 for monochromatic waves and 0.3 to 0.7 in case of irregular waves.

Günaydin and Kabdaşli (2004) carried out physical modelling studies on pile-supported perforated U-type breakwater under monochromatic and irregular waves. The typical view of the structure is presented in Figure 2.10. The test results indicated that the K_t decreased with an increase in immersion depth. The performance of the breakwater in irregular wave conditions was up to 30% better than that of monochromatic waves. Under the monochromatic wave conditions, the structure with perforations exhibited an average of 12% reduction in K_t, 18% reduction in K_r, and 4% increase in K_d compared to non-perforated model. Whereas, under irregular waves, 4% reduction in K_t, 20% reduction in K_r and 4% increase in K_d was observed.

Analytical and experimental studies on single and two rows of pile-supported skirt breakwater (Figure 2.11) were conducted by Laju et al. (2005). The performance of double skirt breakwater was found to be better than single skirt breakwater in attenuating the waves. The results showed that the wave transmissibility was dependent
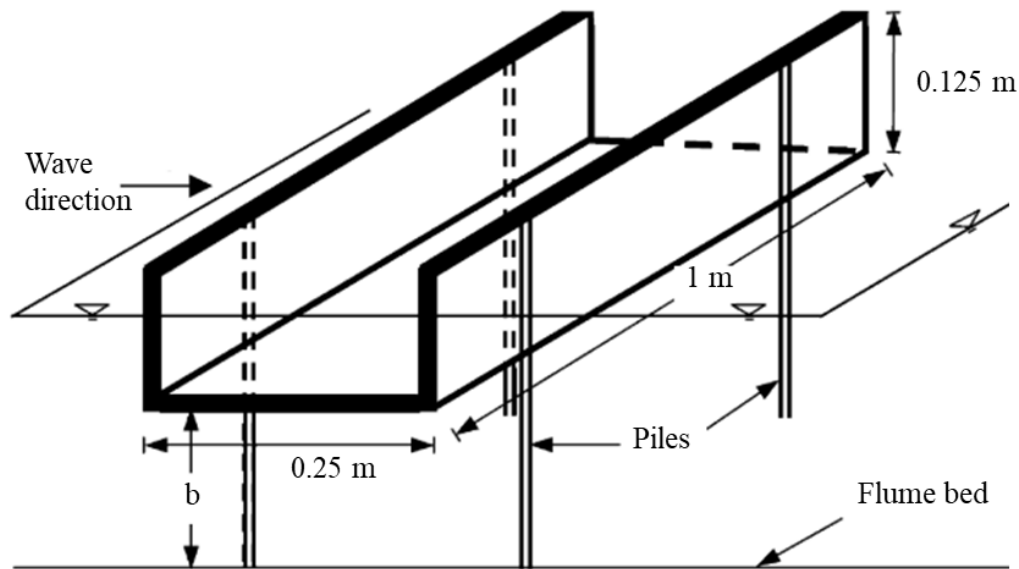
Figure 2.10 Definition sketch of U-type breakwater (Günaydin and Kabdaşli 2004)

on the maximum submergence of either the front or rear skirt, whereas, the reflection was found to depend on the submergence of the front skirt. The study recommended a relative spacing (B/h, where B was spacing between pile rows and h was the depth of water) of one for better performance.

A mathematical model was developed by Suh et al. (2006) to determine the wave transmission, reflection, wave force and run-up on a pile-supported vertical wall breakwater using the Eigenfunction expansion method. Laboratory tests were conducted on a vertical wall which was mounted on a single row of square-shaped piles against monochromatic waves. The mathematical model efficiently reproduced most of the essential features of the experimental outcomes. Later, Suh et al. (2007) modified the mathematical model to be used for circular piles instead of rectangular piles. Ji and Suh (2010) extended the study to multiple-row curtainwall-pile breakwater to compute its hydrodynamic characteristics. The extended mathematical model was validated using experimental data for two and three rows of pile breakwater with multiple combinations of drafts of curtain walls, perforations and spacing between the pile rows. The research concluded that wave transmission was significantly reduced by double-
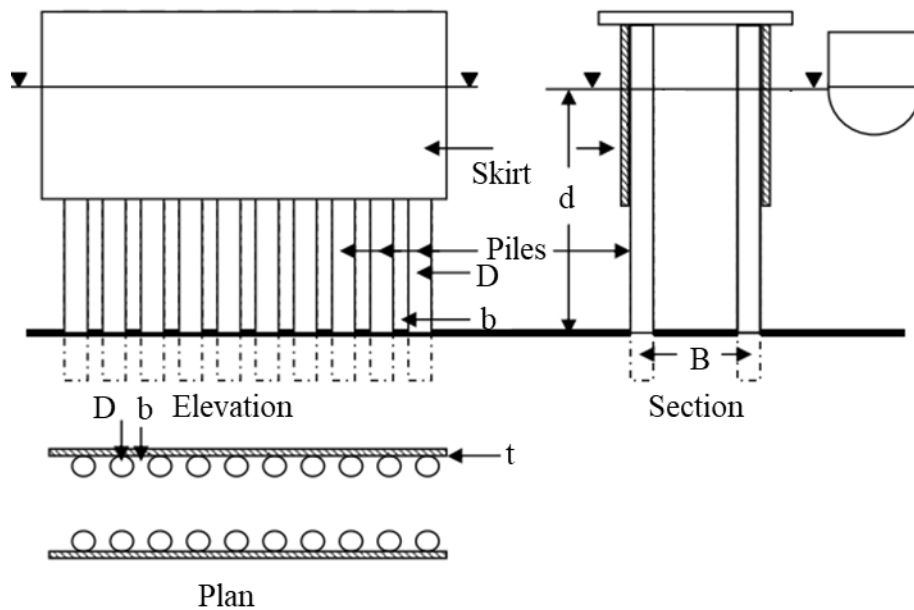
Figure 2.11 Pile-supported skirt breakwater (Laju et al. 2005)

row breakwater compared with a single-row breakwater, while the difference between double-row and triple-row breakwaters was marginal. They also observed that the transmission coefficient was highest when the distance between the pile rows was about one-half of the wavelength.

Huang (2007) conducted laboratory investigations on closely spaced single and two rows of rectangular piles (Figure 2.12). The study reported that with an increase in still water level and wave height, the K_t was found to be decreased, and K_r was found to be increased. The study concluded that for two rows, K_t was marginally affected by the width of the chamber (spacing between the piles). Further, Huang (2007) developed a linear wave solution for the preliminary design of single or double slotted breakwaters and validated it with the experimental results.

Experimental and numerical examinations on pile-supported zigzag porous screen breakwater by Mani (2009) indicated that a K_t of 0.5 could be attained at 50% submergence for steep waves ($H_i/gT^2 > 0.008$). The reflection coefficient was drastically reduced (about 70%) in comparison with the other similar breakwaters (suspended pipe breakwater and pile breakwaters). Force exerted by the zigzag porous breakwater was
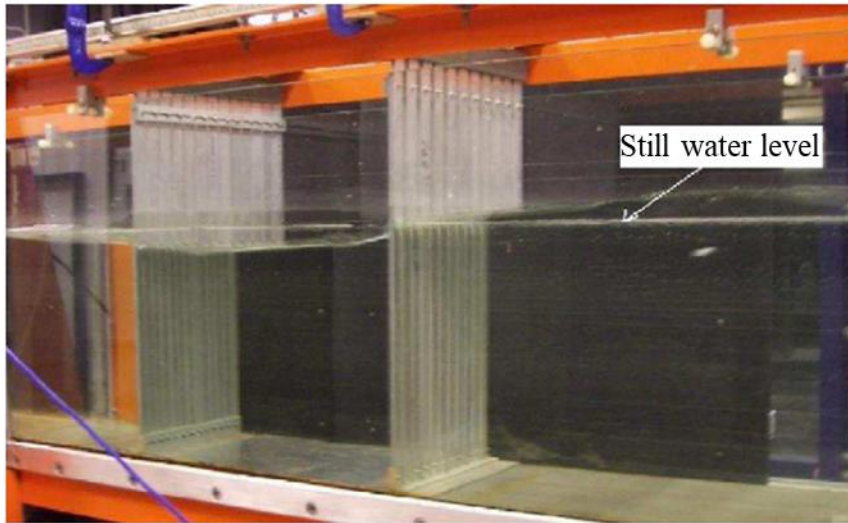
Figure 2.12 Monochromatic waves interacting with double slotted thin walls (Huang 2007)

of the order of 50% less in comparison with an equivalent straight solid breakwater. Numerical model results on the transmission coefficient underestimated the transmission characteristics by about 20%.

Zhu (2011) formulated the interaction problem of monochromatic waves with a single row of rectangular-shaped piles by neglecting the wall thickness and the width of the slot. The fluid was assumed to be inviscid, incompressible and the motion as irrotational away from the row of piles. Explicit equations were derived for wave transmission, reflection, energy loss and wave forces for a single-row pile breakwater. Later, Zhu (2013) modified the proposed equations by considering the influence of both the nonlinear convective acceleration terms for the liquid flowing through the gaps and the thickness of the structure. Further, the proposed equations were refined by Zhu and Xie (2015) by considering the effect of the thickness of the structure and fluid viscosity on the hydrodynamic behaviour of the model. The wave transmission and reflection coefficients predicted by the mathematical model agreed with the experimental results of Isaacson et al. (1998), Hagiwara (1984) and Kakuno and Liu (1993). The study revealed that when the critical value (ratio of the distance between adjacent gaps to half of the wavelength, i.e., 2b/L) exceeds one, the effect of the thickness of the structure on

the hydrodynamic characteristics can be ignored. Whereas, if the critical value was less than unity, the increase of the thickness can lead to wave resonance in these gaps and significantly enhance the wave transmission.

The hydrodynamic performance of horizontal L-shaped bars suspending on vertical piles was theoretically and experimentally analysed by Koraim (2014) under monochromatic waves. A schematic diagram of the breakwater structure is shown in Figure 2.13. A transmission coefficient of 0.38 and a reflection coefficient of 0.72 was achieved when the L-shaped bars were provided throughout the total water depth and for c/w = 0.2 and G/d = 0.33 (Where c is the distance between L-shaped bars, w is the height of L-shaped bar, G is a clear distance between piles and d is pile diameter). Comparison between experiments and theoretical results showed that the theoretical model provided a reasonable estimate of the wave transmission, reflection and energy dissipation coefficients.
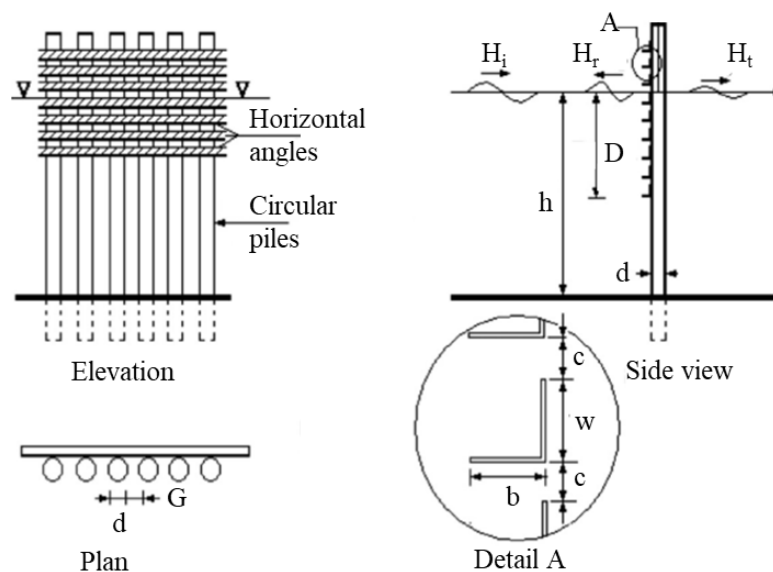
Figure 2.13 Schematic diagram of the pile breakwater with suspending horizontal L-shaped bars (Koraim 2014)

Theoretical and experimental model studies were conducted by Koraim et al. (2014) to assess the performance of double rows of piles with suspended horizontal C-shaped
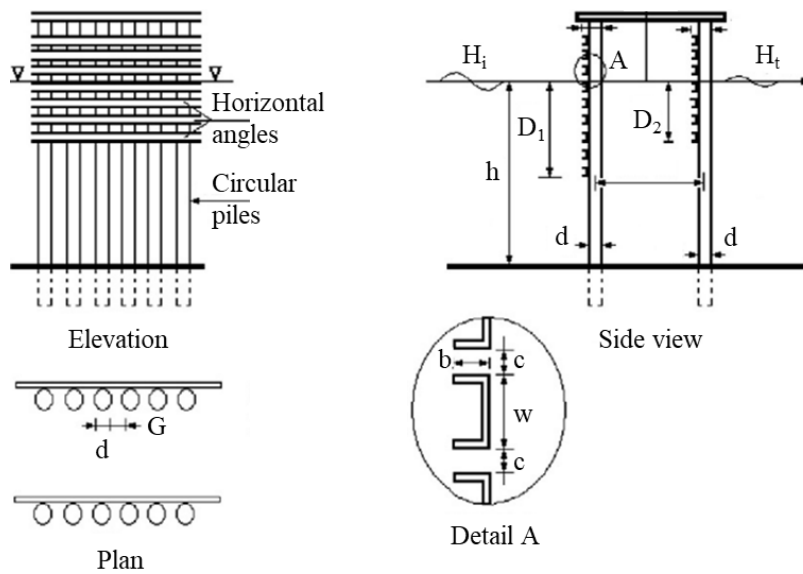
Figure 2.14 Schematic diagram of the pile breakwater with suspending horizontal C-shaped bars (Koraim et al. 2014)
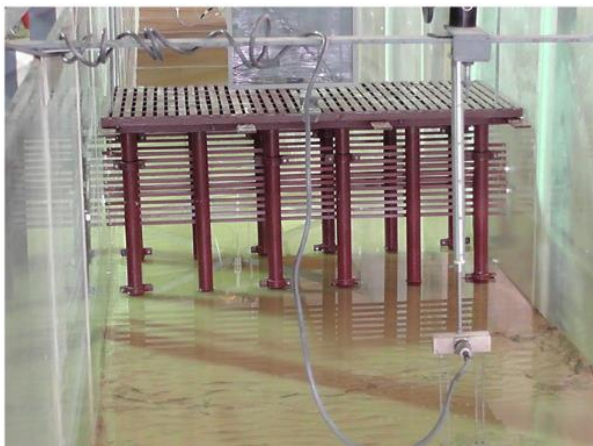
Figure 2.15 Physical model of the pile breakwater with suspending horizontal C-shaped bars (Koraim et al. 2014)

bars under monochromatic waves. The schematic diagram of the structure and physical model are presented in Figure 2.14 and Figure 2.15, respectively. The influence of the ratio of water depth to the wavelength (h/L), pile diameter to the water depth (D/h) and row distance to the water depth (B/h) was investigated.

The theoretical model over predicted the K_t and under predicted the K_r with an accuracy of $\pm 10\%$ compared to that of experimental results. As the porosity of the C shaped bar (ε_s) increased from 0 to 0.5, K_t increased from 0.2 to 0.5 and the reflection coefficient decreased from 0.76 to 0.52. When $\varepsilon_s = 0.5$, $Y/h = 0.5$, $B/h = 1.25$ and $D/h = 0.125$, increasing the d/h (0.078 to 0.156) resulted in a reduction of K_t (0.6 to 0.4) and increase in K_r (0.4 to 0.6).

Wave damping performance of the pile-supported arc and horizontal plate type breakwater was assessed through physical experiments by Wang et al. (2016) under monochromatic waves. The typical arrangement of the breakwater is shown in Figure 2.16. The study confirmed that the performance of arc plate type breakwater was better than the horizontal type of breakwater. The K_t of arc type plate breakwater was about 15% to 50% lower than the horizontal type plate breakwater. Similarly, the K_r for arc type plate breakwater was about 5% to 60% lower than the horizontal type plate breakwater. The study also stated that relative width, height, gap and amount of arc in the plate were the important parameters influencing the K_t and K_r of the structure.
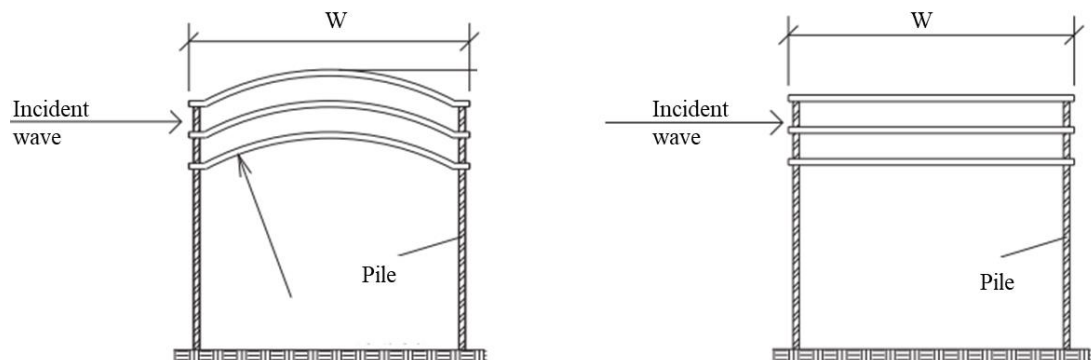
Figure 2.16 Details of arc plate and horizontal plate breakwater models (Wang et al. 2016)

Pile-rock breakwater (PRBW) was constructed to protect the coast along Mekong Delta in southern Vietnam, as shown in Figure 2.17. The efficiency of PRBWs was tested by physical model studies and results were verified through field study. It was reported that the experimental investigation results were well matching with the field

observations. Xuan et al. (2020) reported that even after a decade of installation, PRBWs showed a significant performance in reducing the impact of waves and protected and rejuvenated the mangrove forest. The K_t of the PRBW was in the range of 0.3 to 0.4 and reflection was noticeably high (K_r = 0.45 to 0.6). It was also stated that PRBWs have more advantages than the conventional type of breakwater due to their increased potential to combat erosion and stability.
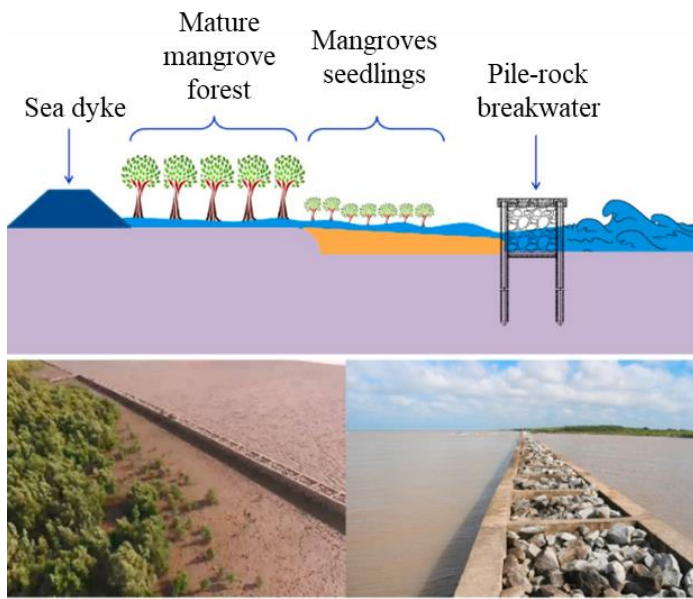
Figure 2.17 Pile-rock breakwater in Phu Tan, Ca Mau province (Xuan et al. 2020)

Hydrodynamic characteristics of the curved and vertical front face pile-supported breakwaters (PSB) were investigated by Ramnarayan et al. (2020) under monochromatic waves. The schematic sketch of the PSB models is presented in Figure 2.18. Two different curved profiles, such as Galveston wall shape (GS-PSB) and circular-cum parabola shape (CPS-PSB) were considered in the study. The hydrodynamic performance of the structures was evaluated by comparing them with the vertical face type (VW-PSB) structure. The K_t of the GS-PSB (0.05 to 0.62) and CPS-PSB (0.04 to 0.53) structures were found to be lower than that of the VW-PSB (0.03 to 0.72). The K_r was found to be the least for CPS-PSB (0.17 to 0.72) and comparable for GS-PSB (0.40 to 0.98) with that of VW-PSB (0.44 to 0.92). Whereas, a maximum K_d was observed for CPS-PSB (0.7 to 0.95) than the other two cases.
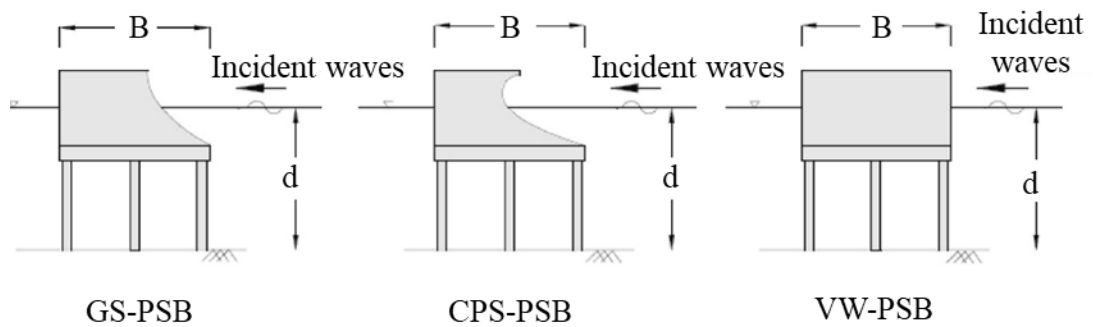
Figure 2.18 Schematic sketch of the pile-supported breakwater models (Ramnarayan et al. 2020)

The impact of incident wave direction on the hydrodynamic characteristics of the quadrant face pile-supported breakwater (QPSB) and vertical face pile-supported breakwater (VPSB) was investigated by Jeya et al. (2021) through experiments. The schematic representation of VPSB and QPSB is illustrated in Figure 2.19. The study was conducted at different water depths by exposing the structure to three different oblique wave attacks (0°, 15° and 30° to the incoming wave). The K_t, K_r and K_d of the structure were compared as a function of relative water depth. The study showed that the K_t and K_r would be lower, and the K_d would be higher when the wave attacking angle is oblique to the structure.
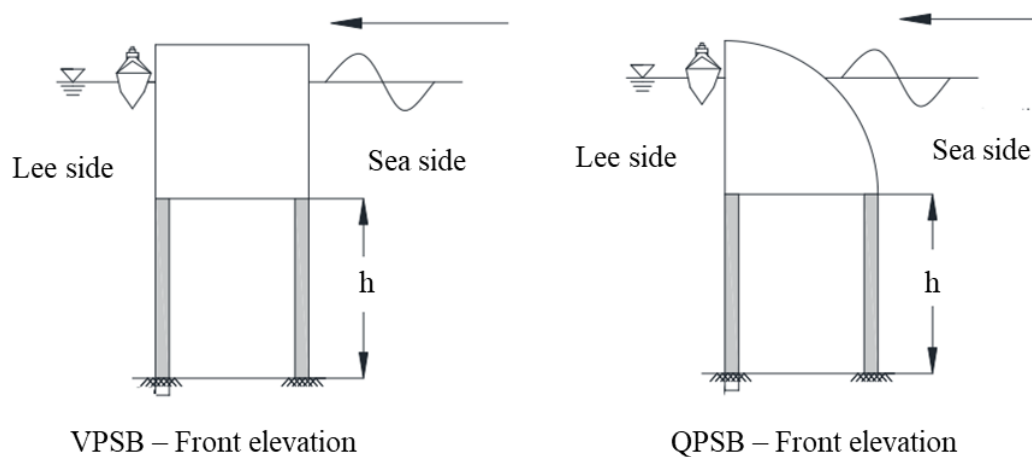
Figure 2.19 Schematic representation of vertical face pile-supported breakwater and quadrant face pile-supported breakwater (Jeya et al. 2021)

2.2 NUMERICAL MODELLING STUDIES

OpenFOAM, REEF3D, FLOW-3D and SWASH are some of the numerical modelling tools which can be employed for the simulation of pile/pile-supported structures. The relevant literature on the numerical modelling of pile structures and their key findings are discussed below.

Afshar (2010) worked on numerical wave generation using OpenFOAM software to examine the capability of the software in numerical wave generation. For wave generation, the relaxation technique was used. From the experiments, it was observed that the outgoing waves got absorbed efficiently by the relaxation zone with a distance of three wavelengths and wave generation zone of one wavelength. The study also showed that grid resolution was highly dependent on the wave steepness and the steeper the wave, the higher the number of grids required per wavelength.

Elsharnouby et al. (2012) proposed a double porous curtain wall breakwater made of horizontal steel plate attached to the pile (Figure 2.20) for the North-Western Coast of Egypt. The suitability of the proposed breakwater was analysed using a FLOW-3D numerical model for the actual wave and bathymetry condition of the region. Results showed that the proposed model could protect the shoreline without any adverse effects.

Liu et al. (2011) numerically investigated the interactions between a solitary wave and a pile breakwater made of circular-shaped piles. The depth-averaged shallow water equations were resolved by using the Bhatnagar-Gross-Krook (BGK) model-based finite volume method. The numerically obtained results were in line with the experimental results, particularly when the ratio of wave height to water depth was small (< 0.25). When the ratio exceeded 0.25, a noticeable deviation of numerical data from experimental results was observed. Both physical and numerical data indicated that for solitary waves, as the spacing between the cylinders in a row reduced, the transmission decreased and the reflection increased.

The potential of the OpenFOAM software in realistic wave generation and active wave absorption was explored by Higuera et al. (2013a). Wave generation comprised of all
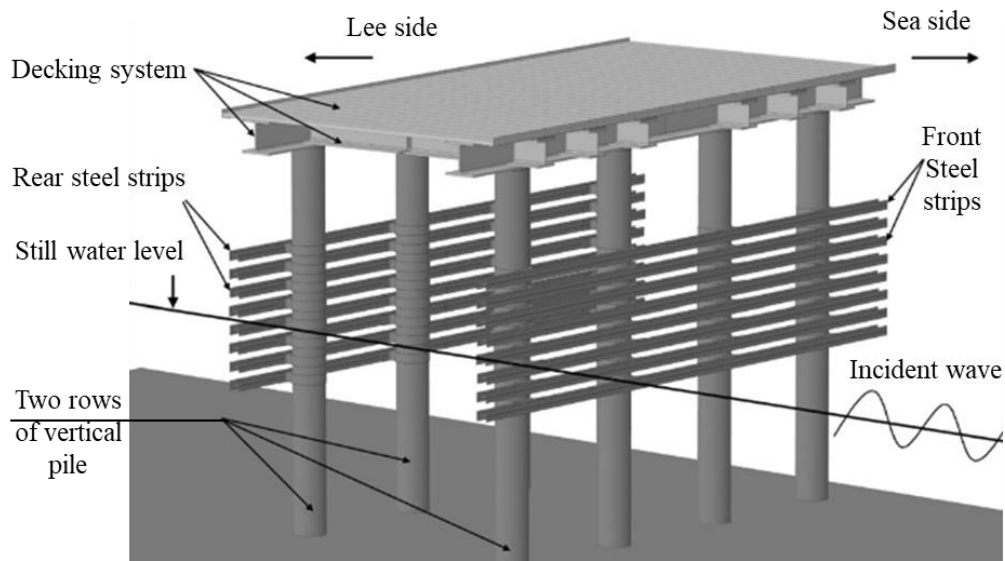
Figure 2.20 Porous suspended breakwater proposed for the Egyptian North-Western Coast by Elsharnouby et al. (2012)

the widely used theories, including specific piston-type wavemaker replication. Active wave absorption was found to improve stability by reducing the energy of the system and by correcting the increasing water level on long simulations. The numerical study was extended by Higuera et al. (2013b) by simulating some of the complex coastal processes in ocean engineering, such as wave breaking, wave run-up, and rip current with OpenFOAM. Comparisons with similar experimental benchmark cases have shown good agreement between experimental and numerical results.

Kamath et al. (2015) investigated wave forces and the flow field around cylinders placed in a monochromatic wave field. Reynolds-averaged Navier-Stokes equation-based open-source CFD model REEF3D was used for the investigation. The numerical model was validated by comparing the numerical results with experimental data from a large scale experiment performed by Mo et al. (2007). Further, the wave interaction with a single large cylinder and a pair of large cylinders placed in tandem for different incident wave steepnesses was studied. The numerically calculated forces were compared with predictions using potential theory. The computed wave forces matched the analytically predicted wave forces for lower wave steepness, whereas, for higher

wave steepness, the numerically computed results were lower than the analytically predicted wave forces by about 35%.

The wave reflections in a numerical wave tank (NWT) were analysed by Miquel et al. (2018) for different simulation scenarios using the open-source model REEF3D with different combinations of the relaxation method, Dirichlet method and active wave absorption techniques. The wave reflections without any structures in the NWT were studied for six different incident monochromatic waves considering linear, second and fifth-order Stokes waves, solitary waves, cnoidal waves and irregular waves. Further, wave breaking over a sloping bed and wave forces on a vertical cylinder were calculated, and the influence of the reflections on the wave breaking location and the wave forces on the cylinder were investigated. Also, a comparison with another open-source CFD code OpenFOAM was carried out based on published results. The active wave absorption method was found to be more efficient for long waves, whereas the relaxation method performed better for shorter waves. The relaxation method-based numerical beach generally resulted in lower reflected waves in the wave tank for most of the cases simulated in the study. The comparably better performance of the relaxation method was achieved at the cost of higher computational requirements due to the relaxation zones that need to be included in the domain.

Aggarwal et al. (2018) investigated the capability of the REEF3D software on free surface reconstruction by using theoretical and experimental data. The free surface was reconstructed by spectrally decomposing the irregular wave train as a summation of the harmonic components in coupling with the Dirichlet inlet boundary condition at wave generation. The applicability of the proposed approach to generate irregular waves by reconstructing the free surface was investigated for different coastal and ocean engineering problems. The wave parameters such as amplitude, wave frequency and wave phases were modelled with good accuracy in the time domain. The proposed approach on irregular wave generation was also employed to model them in deep water. Further, the irregular wave forces on a monopile were also investigated and found that the amplitudes and phases of the wave force signal under irregular waves were

accurately modelled in the time domain. The proposed approach on reproducing the free surface elevation numerically using REEF3D provided accurate results for all the benchmark cases studied.

The hydrodynamics of the flow within permeable pile groin fields on a beach slope was studied using the phase resolving wave-flow model SWASH (Simulating WAves till SHore) by Zhang and Stive (2019). Initially, a uniform coast without groins was simulated to calibrate model parameters and validated with the laboratory observations. To investigate the interactions between permeable pile groins and combined wave current flow, the pile groins were introduced in the calibrated model. These simulations showed that the longshore current velocities were retarded substantially by the pile groins. The retarded flow by pile groins resulted in weakening the ability to transport sediment alongshore. Within the groin fields, the retardation of longshore currents by a three groin system with a 55% permeability was up to 33%, while a larger reduction degree of 43% was obtained within the groin embayment of a five groin system with a 50% permeability. The overall consistence of the calculated results to the experimental measurements revealed a robust capacity of the SWASH model in simulating and investigating the flow fields affected by permeable pile groins.

The numerical performance of the different wave modelling techniques in the REEF3D software was analysed by Wang et al. (2020) to educate the choice of wave models for different coastal engineering scenarios. The different techniques available were Fully Nonlinear Potential Flow (FNPF) model, Computational Fluid Dynamic (CFD) model and non-hydrostatic shallow water model (SFLOW). CFD model solves the incompressible Navier–Stokes equations with a RANS turbulence model. SFLOW model reduces the computational costs significantly by solving the depth-averaged shallow water equations with a non-hydrostatic extension based on a quadratic vertical pressure profile. Whereas, FNPF solves the Laplace equation with fully nonlinear boundary conditions. The performances of the different modules were validated and compared using several benchmark cases, such as simple wave propagation, two-dimensional wave breaking over a mild slope, three-dimensional wave breaking over a

flat-tipped reef and wave propagation over a submerged bar. The comparison of results for monochromatic waves indicated that all three approaches were capable of computing the wave propagation. The submerged bar case showed high accuracy with CFD and FNPF models, whereas, the SFLOW model failed due to its theoretical limitations. The two-dimensional wave breaking case revealed that all three models were able to represent wave energy dissipation accurately during the breaking of a wave. For the case of three-dimensional wave breaking, the CFD model perfectly mimicked the physics of wave propagation, including the complex overturning of the wave during the breaking process with high computational time.

2.3 HYBRID THEORETICAL MODELS

From an engineering perspective, it would be advantageous to be able to predict the hydraulic performance of the pile breakwater quickly using simple equations. In this regard, Mei (1989) and Kriebel (1992) devised theoretical equations to evaluate the hydraulic performance of non-perforated pile breakwaters. Further, to improve the accuracy of these equations, Suh et al. (2011) and Suvarna et al. (2020, 2021) modified the theoretical solutions by incorporating empirical coefficients. These empirical parameters were obtained based on the extensive experiments conducted on the pile breakwater. These modified equations are known as hybrid theoretical models. The background of these theoretical and hybrid equations is described briefly below.

Mei (1989) derived the solutions for K_t and K_r of non-perforated pile breakwater based on continuity equations for shallow water depth. The K_t and K_r for the monochromatic waves propagating at a water depth (h) with the angular frequency (ω) are given by,

$$K_t = \frac{U_0}{\sqrt{gh\dfrac{\left(H_i/2\right)}{h}}} \tag{2.5}$$

$$K_r = 1 - \frac{\omega U_0}{gK\left(\dfrac{H_i}{2}\right)} \tag{2.6}$$

Where, $U_0 = \dfrac{\left(H_i/2\right)}{h}\sqrt{gk}\,\dfrac{\sqrt{1+2\alpha}-1}{\alpha}$, $\alpha = \dfrac{4}{3\pi}\dfrac{f\left(f\,H_i/2\right)}{h}$ and $f = \left[\dfrac{1}{\bar{\in}\,C_c} - 1\right]^2$

$\in$ is the porosity $\left(\in\,\boxminus\,\dfrac{a}{A}\right)$ and $\bar{\in}$ is the spatial variation of porosity $\left(\bar{\in} = \dfrac{1}{D}\right)$.

C_c is the contraction coefficient given by, $C_c = 0.6 + 0.4\in^2$

Kriebel (1992) proposed similar equations based on the conditions of subjective water depths as follows:

$$K_t = \frac{\sqrt{1+4T_t}-1}{2T_t} \tag{2.7}$$

$$K_r = 1 - \frac{\sqrt{1+4T_t}-1}{2T_t} \tag{2.8}$$

Where, transmission function (T_t) is equal to $T_t = \dfrac{f}{6}\dfrac{H_i}{\left(2\pi/K\right)}\dfrac{\sinh(2kh)+2kh}{\sinh^2(kh)}$

The equations for K_t and K_r for the monochromatic waves flowing through non-perforated pile breakwater at a depth of water of h with an angular frequency of ω is given by Suh et al. (2011)

$$K_t = \frac{2(R+2)}{(R+2)^2+Q^2} + i\,\frac{2Q}{(R+2)^2+Q^2} \tag{2.9}$$

$$K_r = \frac{R(R+2)+Q^2}{(R+2)^2+Q^2} - i\,\frac{2Q}{(R+2)^2+Q^2} \tag{2.10}$$

Where, $Q = lK$ and $R = \dfrac{\beta K}{\omega}$

l = length of jet flowing between the piles given by $l = 2C$ and K is the wave number.

C is the blockage coefficient given by $C = \dfrac{\pi}{4}A(1-\in)^2\,\dfrac{1}{(1-\xi)}$ where, $\xi = \dfrac{\pi^2}{12}(1-\in)^2$

β = coefficient of linearised friction given by $\beta = \dfrac{\omega D \gamma_P}{\overline{\in}}$

γ is the friction coefficient, which is obtained empirically as $\gamma = 0.0584 \left[\dfrac{\overline{\in} b}{h} \right]^{-0.7}$

To make the equations suitable for both non-perforated and perforated hollow pile breakwater, Suvarna et al. (2020, 2021) redefined the above defined friction coefficient (γ) using empirical method as,

$$\gamma_P = \gamma - X_R \tag{2.11}$$

γ is the friction coefficient given by, $\gamma = 1.569 \left[\dfrac{\overline{\in} \left(\dfrac{H_i}{h} \right) f}{\overline{\in}^{\overline{\in}}} \right]^{0.433}$

Where, $X_R \begin{cases} = 0 \ \text{...................................... For non}-\text{perforated hollow pile breakwater} \\ \\ = X_P + \dfrac{6.931 * 10^{-4}}{S - 0.0181} + \dfrac{H_i}{h} \ \text{....... For perforated hollow pile breakwater} \end{cases}$

Where X_P is given by, $X_P = 0.0117\, P' + \dfrac{0.027}{P' - 3.24} + \dfrac{0.0282}{6.79 - P'} - \dfrac{0.0473}{P' - 10.12}$

P' is given by, $P' = \dfrac{P}{100}$

2.4 SUMMARY

The need for developing innovative structures for protecting the coastline has led to the development of various kinds of breakwaters. With the improvement in technology, different types of breakwaters were developed in different parts of the world. The selection of a breakwater depends on a few specific criteria, such as hydraulic performance of the structure and its environmental impact, construction cost and maintenance. Hence, to optimise the construction and to provide an eco-friendly

solution to wave attenuation requirements, alternative types of breakwater, such as pile breakwater concept was introduced.

Many studies have been carried out to analyse the hydraulic performance of pile breakwaters since their conceptualisation. These investigations have included experimental, numerical and hybrid theoretical methods. To further optimise the construction of pile breakwater and its performance, new ideas were developed, such as perforated piles, pile-supported vertical wall breakwater, zigzag porous screen breakwater and suspended pipe breakwater.

Based on the review of literature, it can be inferred that the pile diameter, spacing between the piles, number of pile rows and their configuration, and perforation characteristics such as percentage, size and distribution of perforations are the governing factors in the design and performance of pile breakwater. For multiple rows of piles, the performance of the pile breakwater is better with the staggered arrangement than the regular one. Physical model tests conducted on pile breakwater with monochromatic waves demonstrated conservative results compared to those for irregular waves. The literature survey stressed that the perforated structures perform better than non-perforated and may be preferred. In addition, the shape of perforations showed an insignificant influence on the performance of pile structures.

2.5   KNOWLEDGE GAP

The literature review shed light on the various studies conducted on transmission, reflection and dissipation characteristics of pile breakwater of different sizes, shapes, and arrangements. Many studies have been conducted to optimise the construction and performance of the pile breakwater with various types of pile and pile-supported structures. The primary goal was to increase the wave attenuation on the lee side of the structure. However, from the available literature, it is found that minimal studies have been carried out by varying the cross-sectional area of piles in the vicinity of free surface.

2.6 PROBLEM FORMULATION

Wave attenuation near the shore is essential for many applications. This can be achieved through various hard and other eco-friendly structures. While, hard solutions help achieving this goal have their own disadvantages such as interfering with the sediment movement, water quality issues on the lee side, cost of construction, etc. While, eco-friendly measures, such as pile breakwaters are more efficient in terms of ease of construction and have a wide range of applications that can be further optimised. These objectives can be realised by increasing the cross-sectional area of the piles in the conical shape near the vicinity of free surface. In this context, conical pile head breakwater (CPHB) seems to fulfil the need in the search of an eco-friendly structure to attenuate the waves. Further, this CPHB can be refined with perforations to improve its performance.

2.7 OBJECTIVES

Based on the research gaps identified, the primary aim of the research is to explore the hydraulic response of CPHB structure of varying configurations to the wave propagation past the structure.

The objectives of the proposed study are:

1. To investigate different structural configurations of non-perforated CPHB against varying wave climates to obtain the best hydraulic performance.
2. To evaluate the influence of perforation characteristics on the pile head to arrive at the best configuration.
3. To prove the suitability of an open-source software REEF3D to simulate CPHB and validate its results with the experimental data.
4. To evolve the optimum configuration of CPHB.

2.8 METHODOLOGY

The general methodology adopted for the present research work to achieve the objectives is explained and the flow chart of the methodology is depicted in Figure 2.21.

Literature survey

A comprehensive review of the pile type of breakwaters is carried out based on the available knowledge to understand the effectiveness and the current state of knowledge of pile breakwaters in wave attenuation.

Problem identification

The literature survey indicated a knowledge gap whereby minimal studies have been carried out by varying the cross-sectional area of the piles near the water surface. In this context, the present study aims to bridge the existing knowledge gap that is achieved through experimental and numerical investigations by proposing innovative conical pile head breakwater.

Physical modelling

The main objectives of the present study are to investigate the hydraulic performance of the CPHB structure with and without perforations. Froude scaling is adopted, which allows for the correct facsimile of gravitational and fluid inertial forces. A maximum possible model scale of 1:30 is employed to describe the model dimensions and the wave climate. The proposed model is subjected to monochromatic waves of various wave heights and periods generated at different depths of water. The influence of the proposed perforated and non-perforated CPHB model on K_t, K_r and K_d is studied.

Numerical modelling

The selected cases of non-perforated and perforated CPHB models are numerically investigated using an open-source CFD tool REEF3D. The results obtained using numerical modelling are validated with the experimental data.

Analysis of results

The data obtained from the study are analysed to determine K_t, K_r and K_d of the proposed pile head breakwater. The significant factors influencing wave attenuation are identified and the model results are analysed and explained.

Conclusions

Based on the results of both the physical and numerical investigation, the conical pile head breakwater with the best performance is proposed.

Literature review

↓

Problem formulation

↓

Model fabrication

↓

Experimental investigation on non-perforated CPHB of varying configurations under different wave climates

↓

Analysis of results
Determining the hydraulic performance (K_t, K_r and K_d)

↓

Selection of best performing model configuration

↓

Experimental investigation on perforated CPHB for varying characteristics and wave climates

↓

Analysis of results
Determining K_t, K_r and K_d → Numerical modelling of selected cases of CPHB

↓

Validation of numerical results with experimental data

↓

Propose the best performing model

Objective 1

Objective 2

Objective 3 and Objective 4

Figure 2.21 Flow chart of the methodology

CHAPTER 3

MODELLING AND INVESTIGATION OF CONICAL PILE HEAD BREAKWATER

3.1 PHYSICAL MODELLING

3.1.1 Background

In the present study, investigations on the proposed CPHB are carried out through the traditional technique of laboratory experiments. The two-dimensional wave flume available in the Wave Mechanics Laboratory at the Department of Water Resources and Ocean Engineering, NITK Surathkal is used to conduct the physical modelling studies. The experimental setup along with the equipment used for the investigation, are explained in detail. The experimental procedure and data collection method are also enumerated in the following sections.

3.1.2 Dimensional analysis

Dimensions and dimensional units are essential components of any physical property measurement. Dimensional analysis is carried out using Buckingham's π-theorem to arrive at the dimensionless quantities which influence the hydraulic performance of CPHB.

3.1.2.1 Predominant variables

Predominant variables considered for dimensional analysis in the present investigation are listed in Table 3.1.

3.1.2.2 Details of the dimensional analysis

For deep water wave conditions, L and T are related by the equation,

$$L_0 = \frac{gT^2}{2\pi} \tag{3.1}$$

Table 3.1 Predominant variables for dimensional analysis

Predominant variables		Dimensions
Wave parameters	Incident wave height (H_i)	[L]
	Transmitted wave height (H_t)	[L]
	Reflected wave height (H_r)	[L]
	Dissipated wave height (H_d)	[L]
	Maximum wave height (H_{max})	[L]
	Water depth (h)	[L]
	Wave period (T)	[T]
	Wavelength (L)	[L]
	Wave celerity (C) or water particle velocity (u, v and w)	[LT^{-1}]
Structural parameters	Top diameter of conical pile head (D)	[L]
	Diameter of circular pile (d)	[L]
	Clear spacing between the CPHs in a row (b)	[L]
	Clear spacing between the rows of CPH (B)	[L]
	Height of CPH (Y)	[L]
	Total height of the CPHB (H)	[L]
	Distribution of perforations on the CPH surface (Pa)	[1]
	Percentage of perforations (P)	[1]
	Size of perforations (S)	[L]
Fluid parameters	Mass density (ρ)	[ML^{-3}]
	Dynamic viscosity (μ)	[ML^{-1}T^{-1}]
External effects	Acceleration due to gravity (g)	[LT^{-2}]

Where L_0 is the deep water wavelength. The term gT^2 is incorporated in equation (3.1) to represent the wave length instead of taking it directly. This is because, if L is used, it would be depth specific, while gT^2 is independent of depth and represents the deep water wave characteristics which can be easily transformed to shallow waters depending on local bathymetry.

The wave transmission coefficient (K_t) is determined using,

$$K_t = \frac{H_t}{H_i} \tag{3.2}$$

The wave reflection coefficient (K_r) is obtained by,

$$K_r = \frac{H_r}{H_i} \tag{3.3}$$

Where H_i is the incident wave height, H_t is the transmitted wave height and H_r is the reflected wave height. The K_r is calculated using the three probes method proposed by Isaacson (1991). The wave energy dissipation coefficient (K_d) is obtained using the law of energy conservation and is given by,

$$K_t^2 + K_r^2 + K_d^2 = 1 \tag{3.4}$$

$$K_d = \sqrt{1 - \left(K_t^2 + K_r^2 \right)} \tag{3.5}$$

Dimensional analysis is carried out using Buckingham's π-theorem to arrive at the dimensionless quantities which influence the hydraulic performance or performance characteristics of CPHB and they are in line with other similar pile structures (Rao and Rao 2001; Rao et al. 1999, 2002). The dimensionless quantities which influence the K_t, K_r and K_d are,

$$K_t, K_r, K_d = f \left\{ \frac{H_t}{H_i}, \frac{H_r}{H_i}, \frac{H_d}{H_i}, \frac{D}{H_{max}}, \frac{Y}{H_{max}}, \frac{H_i}{gT^2}, \frac{Y}{h}, \frac{b}{D}, \frac{B}{D}, \frac{h}{H}, N, Pa, P, \frac{S}{D}, \frac{\rho VD}{\mu} \right\} \tag{3.6}$$

Where,

D/H_{max} is the relative pile head diameter

Y/H_{max} is the relative pile head height

H_i/gT^2 is the incident wave steepness

$\dfrac{Y}{h}$ is the relative submergence of CPH denoted by Z

b/D is the relative clear spacing between the CPHs in a row

B/D is the relative clear spacing between the rows of CPHs

h/H is the relative depth of water

N is the number of CPHB rows.

Pa is the distribution of perforations around the pile head

P is the percentage of perforations, defined as the ratio of total area of perforations to the corresponding CPH area on which the perforations are provided.

$\rho VD/\mu$ is the Reynolds number (R_e)

In this present work, the Reynolds number is not considered. The reason is that the density and dynamic viscosity of water remains constant as the water quality is the same and a change in the Reynolds number will be only due to a change in horizontal particle velocity. As this does not represent the viscous effect, the term representing Reynolds number is neglected.

3.1.3 Similitude criteria and model scale selection

In the present study, as the CPHB structure deals with surface waves, the modelling is carried out on a 1:30 scale employing Froude's law. According to Froude's law, gravity serves as the primary physical force counteracting the inertial force and the influence of other physical forces is minimal. This may lead to scale effects when other forces,

such as viscous forces are dominant in the problem. However, viscous scale effects are expected to be minimal in this study as the CPHB was tested under non-breaking wave conditions and the Reynolds numbers are always in the totally turbulent flow range (Teh et al. 2012). The viscosity scale effects of the CPHB structure are evaluated by calculating the Reynolds number as described by Sarpkaya (1976). Additionally, the CPHB structure allows a portion of the waves to enter the hollow region of the pile head and generates turbulence. Hence, the potential viscous scale effect may be at the very minimum and not cognisable (Hughes 1993).

In dimensional analysis, the similitude between the model and prototype is achieved with the help of non-dimensional parameters. These non-dimensional parameters are to be in the same range for both the model and prototype. The similitude criteria in the present study are achieved by considering wave steepness (H_i/gT^2) as a non-dimensional parameter. Using the two-dimensional wave flume available at the Department of Water Resources and Ocean Engineering, monochromatic waves of heights and periods ranging from 0.03 m to 0.24 m and 1 s to 3 s, respectively can be produced. A 1:30 geometrically similar model scale is selected for the present experimental investigations. The equivalent of 1:30 geometric model that is scaled up to real field conditions. The wave parameters of the prototype and model are shown in Table 3.2.

Table 3.2 Wave parameters of the prototype and model

Wave parameters	H_i (m)	T(sec)	H_i/gT^2
Prototype	0.90 to 7.20	5.48 to 16.43	0.00034 to 0.02446
Model	0.03 to 0.24	1.0 to 3.0	0.00034 to 0.02446

3.1.4   Wave climate

The wave climate (wave height and period) chosen in the present study is in accordance with the data obtained off the Mangaluru coast, West coast of India (KREC Study Team 1994). The data exhibited a wave height of less than 1.0 m during the fair-weather

season and a maximum of 4.8 m in monsoon season, with an occasional height of 5.4 m. Predominant wave period is reported to vary between 8 and 11 s. For this coast, the significant wave height reported is about 3.44 m with an average zero-crossing period of 10.4 s. For design purposes, the KREC Study Team (1994) recommended considering a wave height of 4.8 m. Therefore, the current study considers wave heights between 1.8 and 4.8 m and wave periods between 8 and 11 s, with a maximum wave height (H_{max}) of 4.8 m. The tides at Mangaluru are mixed type with semi-diurnal components dominating. The tidal variation with respect to mean sea level is approximately ± 1.68 m.

3.1.5 Experimental setup

3.1.5.1 Test facility

The experiments are carried out in a two-dimensional fixed bed wave flume (Figure 3.1) constructed in the Department of Water Resources and Ocean Engineering, National Institute of Technology Karnataka, Surathkal, India. The flume has a length of 50 m with a cross-section of 0.71 m x 1.1 m. A bottom hinged flap-type wavemaker is installed at one end of the flume, capable of generating monochromatic waves. A smooth concrete bed is provided at the bottom of the flume for a length of 42 m. Smooth concrete lateral walls enclose the flume and a facility is made for photography and observations by providing a glass panel of length 25 m on one side. The details of the flume along with the test setup are showcased in Figure 3.2. A passive type wave absorber (spending beach) is constructed at the opposite end to dampen the incident wave energy. It is provided with a coarse gravel layer as the base, topped with irregular shaped granite stones with approximate nominal diameter (D_{n50}) of 0.052 m. The beach dissipates a large fraction of the wave energy by causing the incident waves to break, uprush and percolate through beach material and discourage reflection. The beach slope employed in the present study (1:12) is gentle than that of the recommendations by various investigators (1:10 by Hughes 1993 and 1:4 by Straub et al. 1957) and the length of the wave absorber is about three times greater than recommended (0.75L by Lean 1967) for archiving minimal reflection (less than 10%). Hence, wave reflection from the spending beach is incognisable in the present study.

Figure 3.1 Side view of the two-dimensional wave flume

An induction motor of 11 kW capacity can control the flap movement (Figure 3.3b). An inverter drive can regulate the motor with a frequency range of 0-50 Hz (Figure 3.3a). The flap is connected to the motor with the help of a flywheel using a bar chain mechanism (Figure 3.3d). By changing the eccentricity of the bar chain, the desired wave height can be generated. The period of the waves can be altered by varying the frequency through an inverter.

Before conducting the model studies, a particular combination of eccentricity and the generator frequency is determined to get the intended wave characteristics for all the set of waves in the required water depths considered in the study and the models are tested for only non-breaking waves. Depending upon the wavelength of generated waves, about 14 to 25 waves can be generated before the reflected waves between the model and wave maker cause re-reflection. However, a short burst of waves may be generated to act on the model. As a result, the problem of reflection and re-reflection is avoided. The waves are generated in a burst of eight to ten waves and the wave generator is switched off to avoid the reflection and re-reflection from the generator and the wave paddle. A sufficient interval is provided before generating the next wave burst to achieve tranquillity by dampening out all the reflected wave energy. The wave flume is calibrated before conducting the model tests to find out the generator stroke
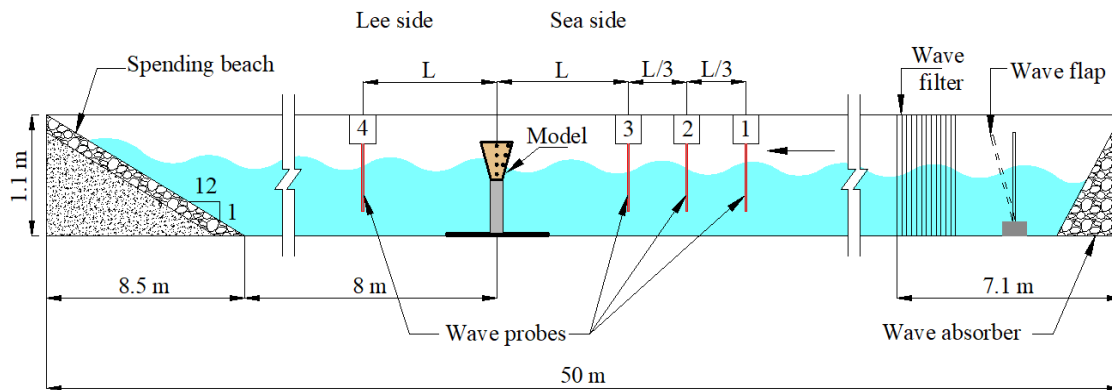
Figure 3.2 Details of the experimental setup

Figure 3.3 Wave generation system a) inverter drive, b) motor, c) wave filter and d) bottom hinged flap type wave paddle

and frequency of the inverter for generating the waves with the required combination of wave height and wave period.

3.1.5.2 Data acquisition system and analysis

The free surface elevation data is recorded using the capacitance type probes and data

acquisition system (Figure 3.4) manufactured by EMCON, Cochin, India. The surface tension errors are eliminated by applying a thin layer of Silica gel on the probe surface. Calibration of the wave probes is undertaken daily before and after conducting the experiments and the noted voltage variation is reliable (standard deviation $< 2\%$) as per Neelamani and Vedagiri (2001).

Figure 3.4 Data acquisition system

A total of four wave probes are used for logging the wave data, as displayed in Figure 3.5. Three probes are located on the seaside of the structure as per the recommendations by Isaacson (1991). The position of the probes is altered with respect to the wavelength of each wave generated. The composite wave data recorded in three probes are separated into incident and reflected wave components (H_i and H_r) by employing the three probes method proposed by Isaacson (1991) The transmitted wave height (H_t) is measured using the fourth probe placed on the lee side of the CPHB structure. Using this data, the transmitted wave height (H_t) is calculated as the difference of surface elevations between the lowest and highest levels, resulting in maximum H_t. Further, the K_t is calculated by employing this maximum H_t. Therefore, the K_t reported in the present study is conservative. The K_t, K_r and K_d are calculated by employing the

equations 3.2, 3.3 and 3.5, respectively. Each case is repeated thrice and the average values of the coefficients computed are recorded as the test data.
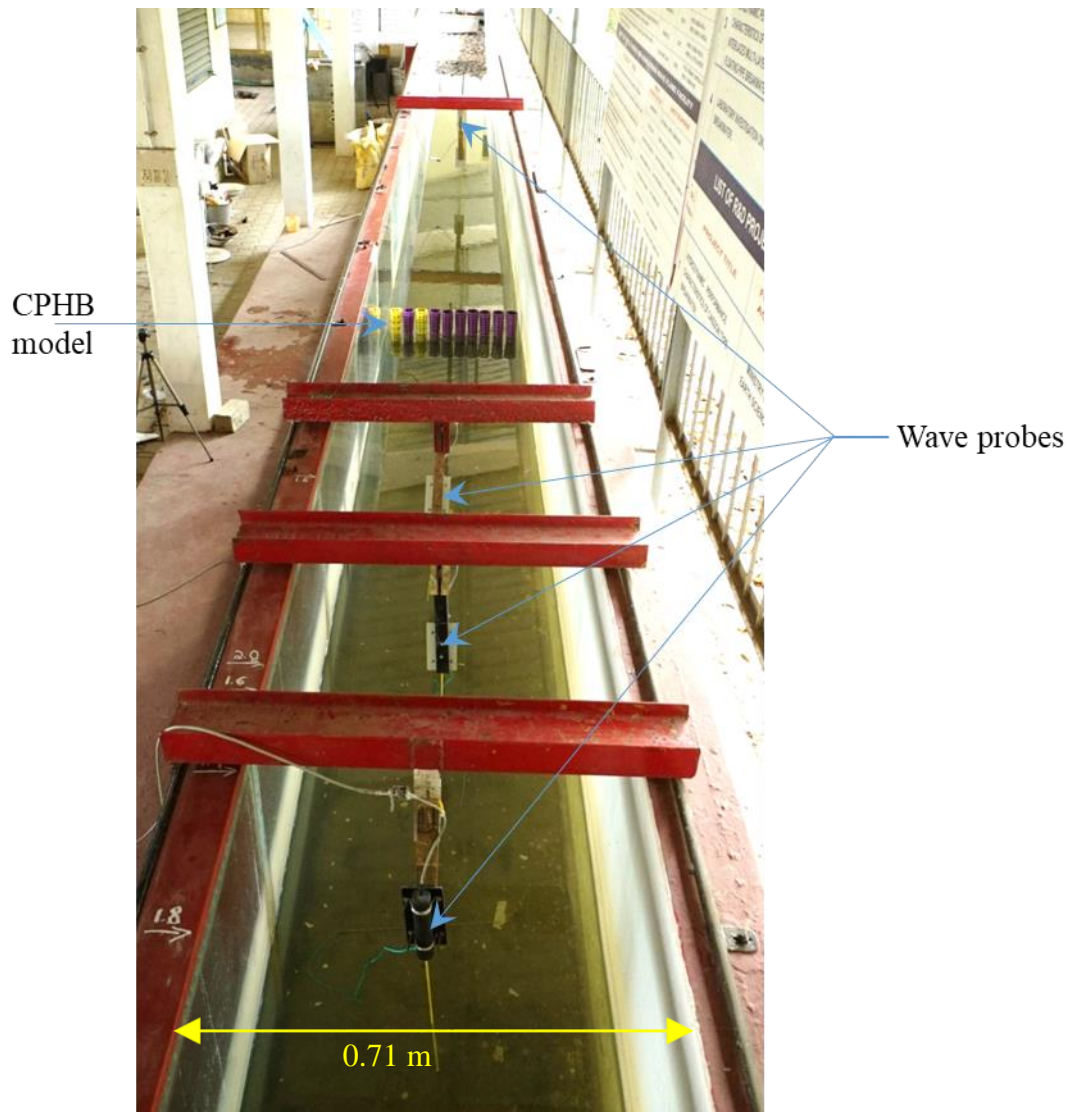
Figure 3.5 Physical modelling setup with capacitance type wave probes

3.1.6   Calibration of test facilities

To ensure the accuracy in the data collection, calibration of the experimental setup and instruments is undertaken frequently. The method of calibration of each component is given below.

3.1.6.1 Wave flume

Calibration of wave flume involves finding the crank's eccentricity, which controls the flap's movement to produce desired wave height and fix the inverter's frequency for creating the selected wave period. Eccentricity and wave height has a direct proportional relationship, while frequency and wave period have an inverse relationship. Desired wave period can be generated by changing of frequency through the inverter drive. By changing the eccentricity of a bar chain on the flywheel, wave height for a particular wave period is produced.

3.1.6.2 Wave probes

The wave probes work on the principle of electrical conductance. The primary output is in the form of voltage which varies between 0 V and 5 V. The embedded software in the wave recording system converts it to water level variations. The manufacturer initially calibrated the probes; however, the output is expected to show minor variations depending on the salinity and temperature of water used in the flume. Hence, the probes are subjected to static immersion tests and the relationship between the water level and the output voltage is determined and recorded. The probes are calibrated by lowering and raising the probe in a known depth of immersion and recording the variations in corresponding voltages. The calibration of the wave probes is undertaken daily before and at the end of experiments to find out wave height and the obtained differences are incorporated in the recorded readings.

3.1.7 Conical pile head breakwater (CPHB) model details

The physical model studies of CPHB under monochromatic waves are conducted in a two-dimensional wave flume. A schematic view of two rows of staggered hollow conical pile head breakwater is shown in Figure 3.6. Considering the existing facilities of the two-dimensional wave flume at NITK Surathkal, the CPHB and the wave parameters are modelled with the largest possible scale of 1:30, which is within the limit (1:10 to 1:50) suggested for the short-wave hydrodynamic models by Hughes (1993). Hence, the potential scale effects may be at the very minimum and not cognisable such that they may not have a noticeable effect on the results. The CPHB
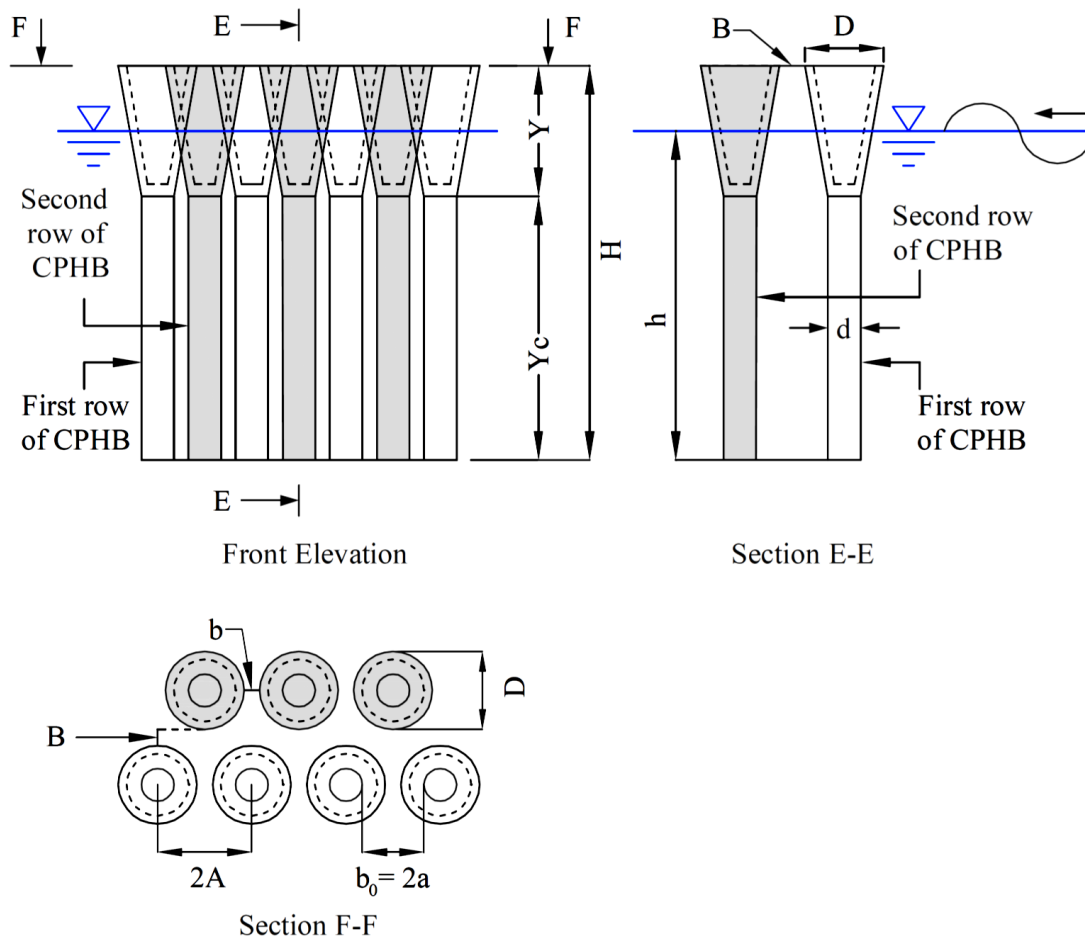
Figure 3.6 Schematic view of two rows of staggered hollow conical pile head breakwater

basically consists of two parts, namely, pile trunk and conical pile head (CPH). The CPH is connected to the pile trunk by means of bolted connections.

3.1.7.1 Pile trunk

The supporting circular piles are fabricated using hollow galvanised iron (GI) pipes with a wall thickness of 0.002 m. For the bolted connection between the CPH and the pile, a 0.005 m thick iron plate with centre threading is installed inside the upper section of the GI pipe. The GI pipe is fixed to the iron plate of 0.01 m thickness with the help of an iron collar, having 0.0015 m thickness and 0.04 m internal diameter. The collar is welded to the iron plate firmly and the horizontal connection between the collar and

plate is confirmed with the help of spirit level. Threading is provided inside the collar and the bottom of the GI pipe to strengthen the connection. The iron plate offers firm support to the CPHB structure at the base during the experimentation (Figure 3.7) and this whole arrangement makes the structure rigid.

3.1.7.2   Non-perforated conical pile head

The hollow conical pile head (CPH) is fabricated using solid wood with a 0.01 m thick sidewall and 0.015 m thick base. A perforation of 0.015 m diameter is provided at the CPH base and the CPH is connected to the circular pile by means of bolted connections. The typical arrangement of different configurations of CPHB considered in the present investigation is depicted in Figure 3.7.
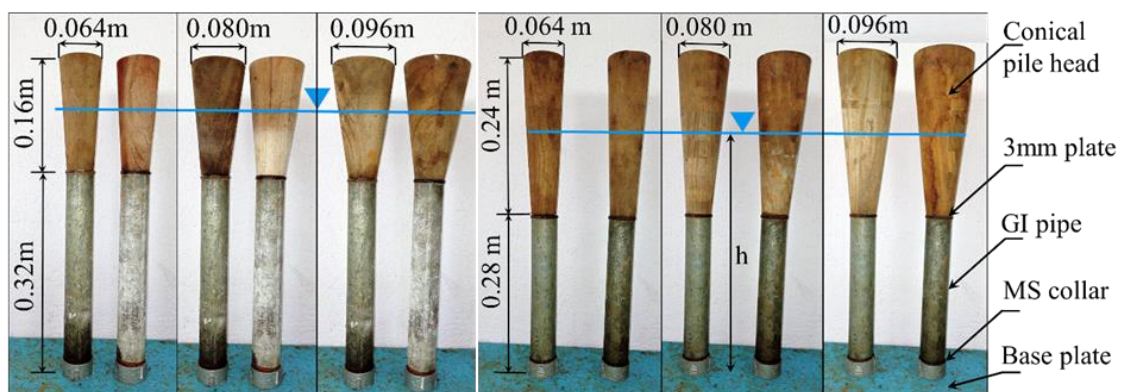
Figure 3.7 Non-perforated conical pile head breakwater test models

3.1.7.3   Perforated conical pile head

Extensive study has been carried out by varying the distribution of perforations (Pa), percentage of perforations (P) and size of perforations (S) to determine the influence of perforations on the performance of the proposed structure. As demonstrated in Figure 3.8a, the perforated CPH is 3D printed using Polylactic acid (PLA) material with an accuracy of 0.01 mm. The thickness of the CPH is 0.003 m.

It should be noted that the colour of the CPHs demonstrated in Figure 3.8b is only representative and no colour coding is adopted in the present study.
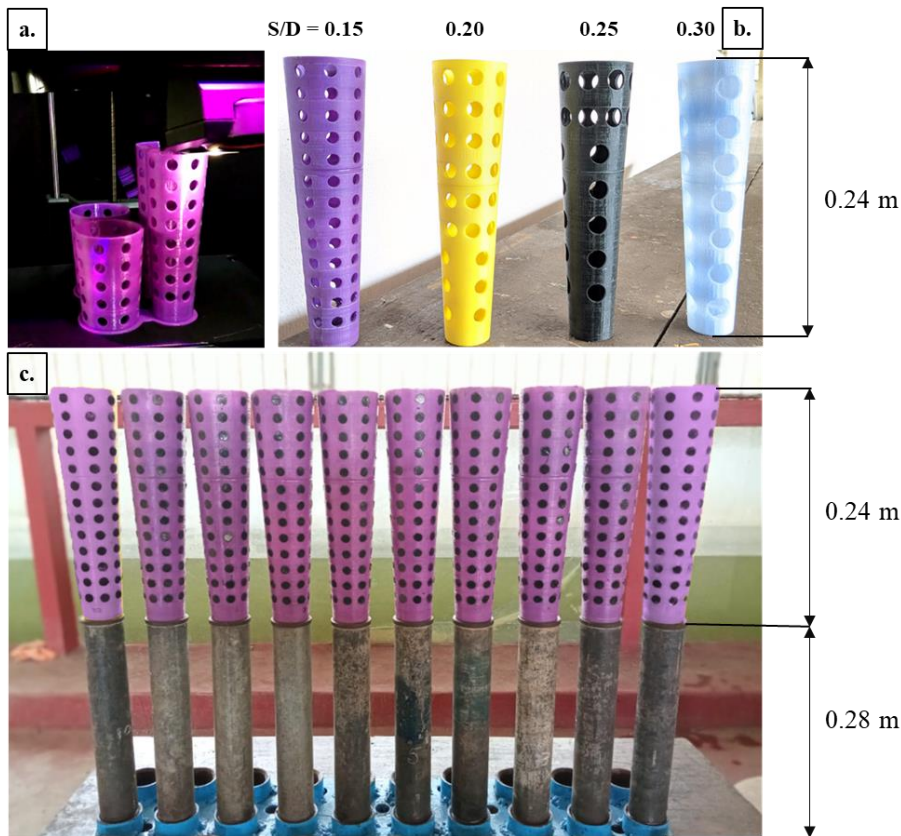
Figure 3.8 Illustration of a) 3D printing of perforated CPH, b) variation of S/D under constant Pa and P, c) experimental setup of the perforated CPHB
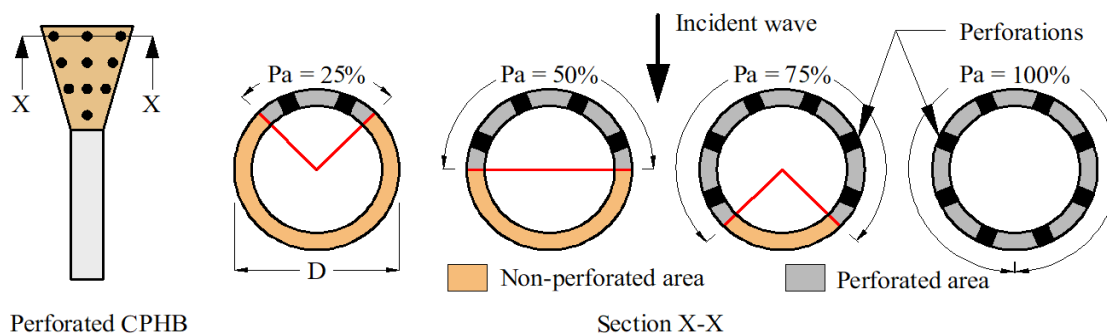
Figure 3.9 Typical tabulation of the distribution of perforations (Pa) on the CPH surface area

The colour of the CPH model is chosen based on the material available at the time of 3D printing. The calculation of the distribution of perforations (Pa) on the surface of

CPH is illustrated in Figure 3.9. The percentage of perforations is defined as the ratio of the total area of perforations to the corresponding CPH area on which the perforations are provided.

3.1.8 Range of experimental variables

The ranges for experimental variables are to be determined at the earlier stage of any experimental studies on the breakwater. The parameters related to the wave conditions and structure are portrayed in Table 3.3.

3.1.9 Test conditions

To design economical and safe structures, model test conditions must be designed and operated judiciously. In the present study, the waves are generated in a burst of eight to ten waves and the wave generator is switched off to avoid the reflection and re-reflection from the generator and the wave paddle. A sufficient interval is provided before generating the next wave burst to achieve tranquillity by dampening out all the reflected wave energy. The current experimental studies are carried out under the following assumptions.

1. The sea bed is rigid and the sediment movement does not interfere with the performance of the CPHB.
2. The waves are periodic and monochromatic.
3. Secondary waves generated during the test are not considered.
4. The density difference between freshwater and seawater is insignificant.
5. Frictional effects from the bottom and sidewalls are not accounted.
6. The CPHB structure is rigid.

Table 3.3 Governing experimental variables of CPHB structure

Governing variables	Expression	Test range
Maximum wave height (m)	H_{max}	0.16
Top diameter of CPH (m)	D	0.064, 0.080, 0.096
Diameter of supporting pile (m)	d	0.04
Height of conical pile head (m)	Y	0.16, 0.24
Height of supporting pile (m)	Y_c	0.32, 0.28
Height of the CPHB structure (m)	H	0.48, 0.52
Size of perforations (m)	S	0.0096, 0.0128, 0.016, 0.0192
Depth of water (m)	h	0.35, 0.40, 0.45
Wave period (s)	T	1.4 ,1.6, 1.8, 2.0
Incident wave height (m)	H_i	0.06, 0.08, 0.10, 0.12, 0.14, 0.16
Angle of wave attack (degrees)	θ	90
Non-dimensional parameters		
Relative pile head diameter	D/H_{max}	0.4, 0.5, 0.6
Relative pile head height	Y/H_{max}	1.0, 1.5
Relative clear spacing between the CPHs in a row	b/D	0.2, 0.1
Relative depth of water	h/H	0.729, 0.833, 0.937 0.673, 0.769, 0.865
Relative clear spacing between the rows of CPHs	B/D	0.0, 0.2, 0.4, 0.8
Incident wave steepness	H_i/gT^2	0.00152 to 0.00620
Percentage surface area of perforated pile head	Pa	25, 50, 75, 100
Relative diameter of perforations	S/D	0.15, 0.20, 0.25, 0.30
Percentage of perforations	P	9.6, 14.4, 19.2

3.1.10 Wave attenuation mechanism

3.1.10.1 Pile breakwater

In general, when the waves interact with permeable structures such as pile breakwater, a part of the wave energy gets transmitted towards the lee side of the structure with partial reflection and energy dissipation. For pile breakwater, the wave energy dissipation occurs due to wave-structure interaction associated with turbulence, eddy formation and vortex shedding. Many studies indicated that in the absence of currents under monochromatic waves, wave energy dissipation due to pile breakwater takes place by means of the following mechanism (Hildebrandt and Sriram 2014; Kakuno and Liu 1993; Liu et al. 2011; Park et al. 2000; Rao et al. 1999; Suh et al. 2006, 2011).

1. Flow separations
2. Inertia resistance
3. Contraction
4. Wave reflection
5. Turbulence
6. Vortex shedding

When a wave interacts with the structure, the flow gets separated due to inertial resistance. The separated flow gets contracted between the pile gaps with an intensified velocity, which is responsible for vortex formation and eddy shedding in the main flow direction. All these processes lead to wave energy dissipation because of turbulence. In the theoretical analysis, all these energy losses are accommodated in the form of blockage coefficient (C), contraction coefficient (C_c), linearised dissipation coefficients (β) and head loss coefficient (f).

When the flow is turbulent, the inertia force is more dominant than the viscous forces, resulting in vortex formation behind the pile structure (Davidson 2015). The typical flow behaviour for a cylinder under different Reynolds numbers (R_e) is presented in Figure 3.10.

During the wave-structure interaction, depending on the wave phase, the vortex formation may take place on the lee side or the seaside of the pile structure. The typical pattern of vortex formation and turbulence generation for circular piles under a monochromatic wave is shown in Figure 3.11.

In the process of turbulent dissipation, the energy of larger eddies gets transferred into smaller vortices by breaking, as illustrated in Figure 3.12. This process of breaking into smaller vortices continues until the inertia forces dominate. On equalisation of the inertial and viscous forces (i.e. $R_e \approx 1$), this breaking process of eddies ceases, and the remaining energy is absorbed by the viscosity of fluid (Davidson 2015).

1. $R_e < 1$

2. $5 < R_e < 40$

3. $100 < R_e < 200$

4. $R_e \approx 10^4$

5. $R_e < 10^6$
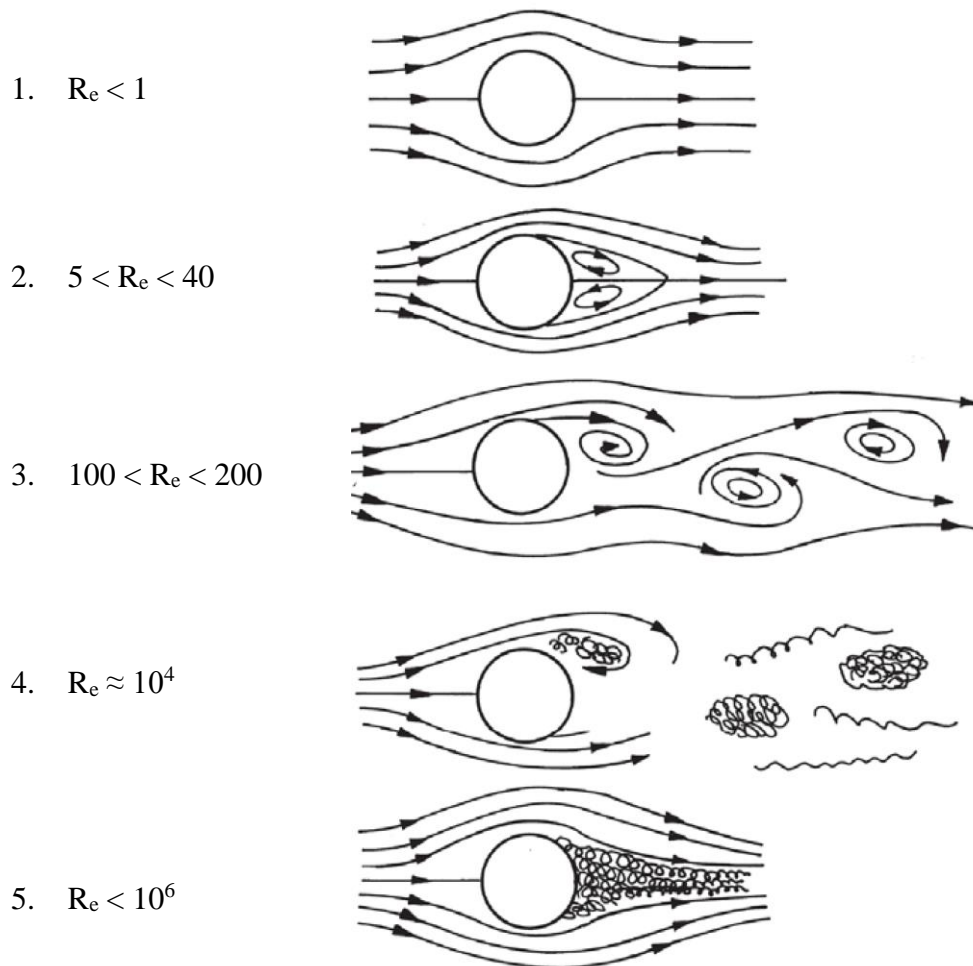
Figure 3.10 Typical flow behaviour for a cylinder under different Reynolds numbers (Davidson 2015)
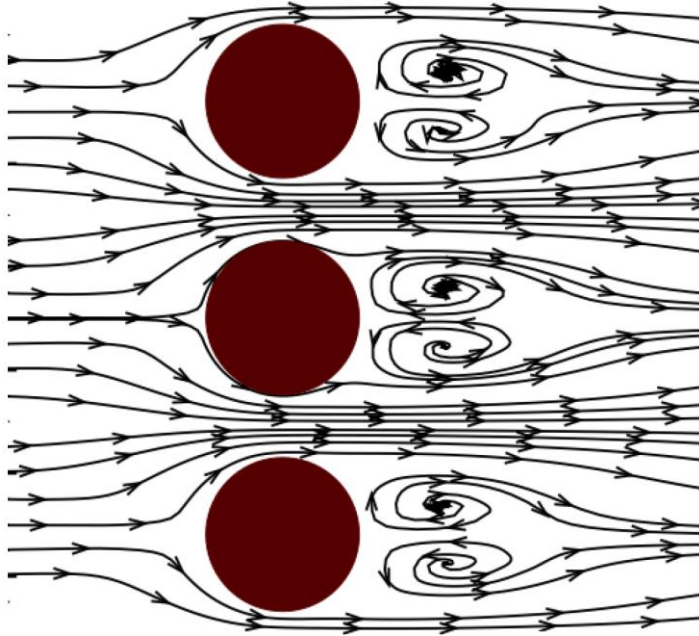
Figure 3.11 Vortex formation during the wave crest propagating through pile structure (Liu et al. 2011)
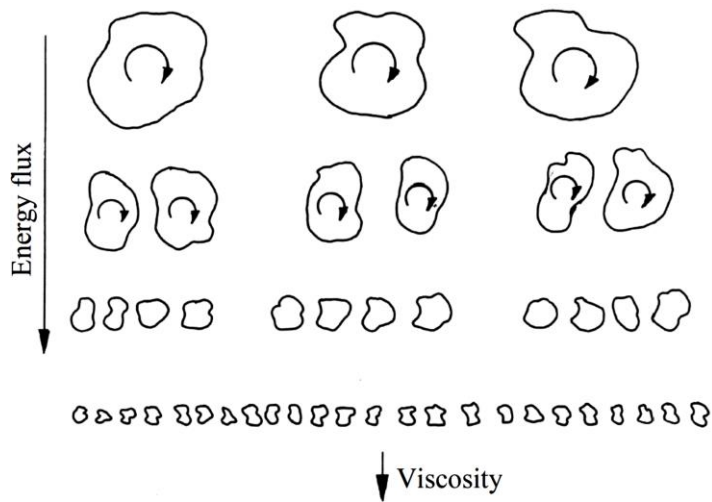
Figure 3.12 Typical cascade of energy from larger eddies to smaller eddies (Davidson 2015)
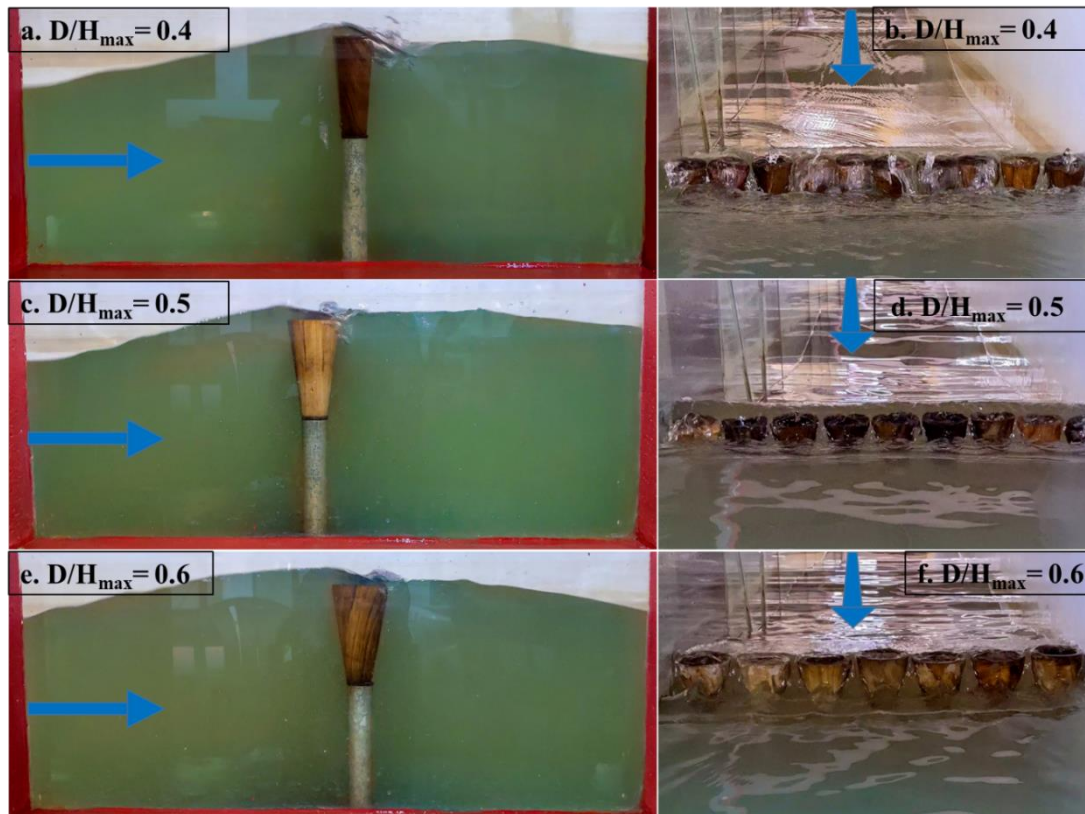
Figure 3.13 Wave interaction with non-perforated CPHs at 0.40 m water depth (h/H = 0.769) for Y/H$_{max}$ = 1.0 and b/D = 0.1 for various D/H$_{max}$

3.1.10.2 Conical pile head breakwater

To enhance the performance of the pile breakwater, many researchers (Koraim 2014; Koraim et al. 2014; Laju et al. 2011; Liu and Li 2011; Mani 2009) investigated the influence of blocking the waves at free surface where the wave energy is concentrated. It is a well-known fact that the orbital motion of the water particles is maximum near the free surface and reduces gradually with the depth, as shown in Figure 1.6. The idea behind the CPHB is to dissipate the wave energy by interrupting the orbital motion of the waves to the possible extent. With this logic, the concept of conical pile head breakwater (CPHB) is formulated, where the cross-sectional area of pile is tapered as the velocity reduces with the depth.

The wave attenuation in conventional pile breakwater takes place due to the combined effects of flow separation, contraction, intense flow through gaps, vortex formation and
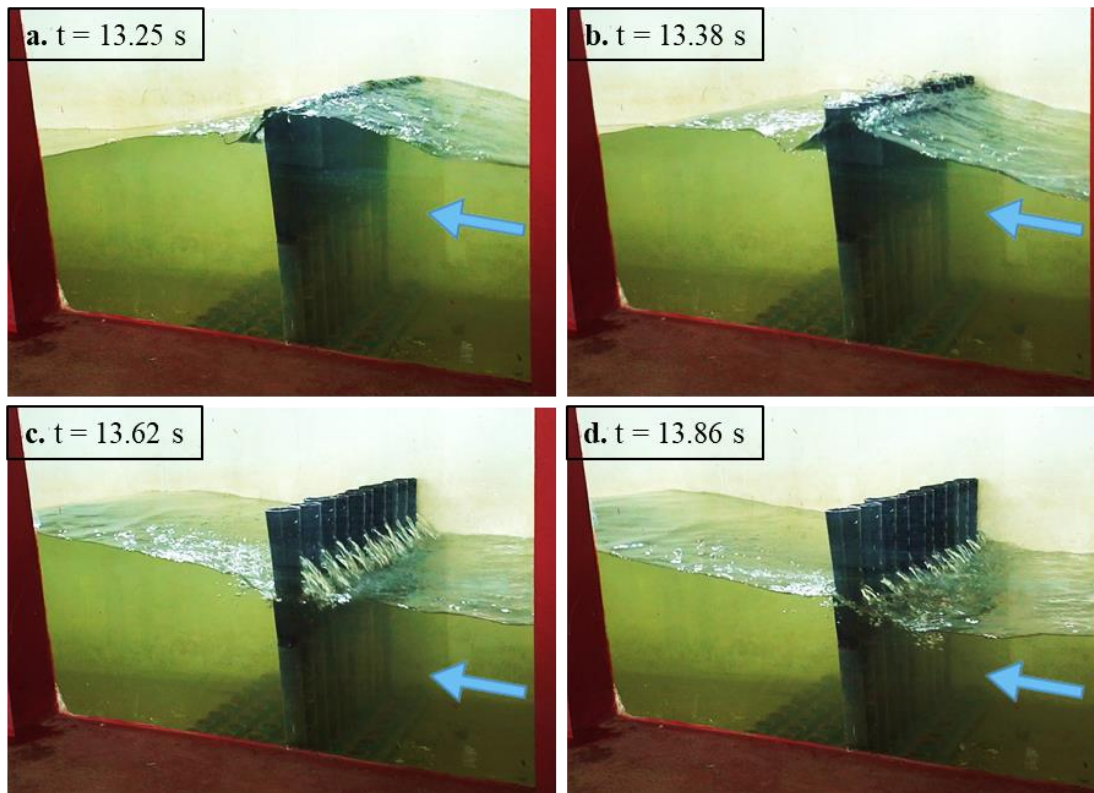
Figure 3.14 Demonstration of wave interaction with perforated CPHB (D/H$_{max}$ = 0.4, Y/H$_{max}$ = 1.5, b/D = 0.1, Pa = 50%, P = 19.2% and S/D = 0.25) at different time instances (t) for H$_i$ = 0.16 m and T = 1.8 s at h = 0.40 m (h/H = 0.769)

eddy shedding and partially due to the wave reflection. In addition to the above-stated mechanism, the increased area at the surface level provides a higher blockage area against wave propagation. As the wave crest passes through the CPH structure, some portion of the wave passes through the gaps and gets transmitted. Depending upon the wave height, the remaining portion may overtop and transmit the wave energy on the lee side and/or enter the hollow portion through the perforations (Figure 3.13 and Figure 3.14). In the case of non-perforated CPHB, this water, falls and pops up through the top of the hollow pile head and loses energy. This water that pops out from the top and perforations of CPHB may interact with the incoming wave, which may result in increased reflection or energy dissipation, thus reducing wave transmission.

Wave interaction with non-perforated CPHB for various D/H_{max} is illustrated in Figure 3.13. For further clarity, a numerically simulated wave-structure interaction is depicted in Figure 3.15. The plan-view of the particle path lines during the propagation of the wave crest over the non-perforated pile head is presented in the figure, where the formation of vortices is clearly noticed on the lee side of the structure.
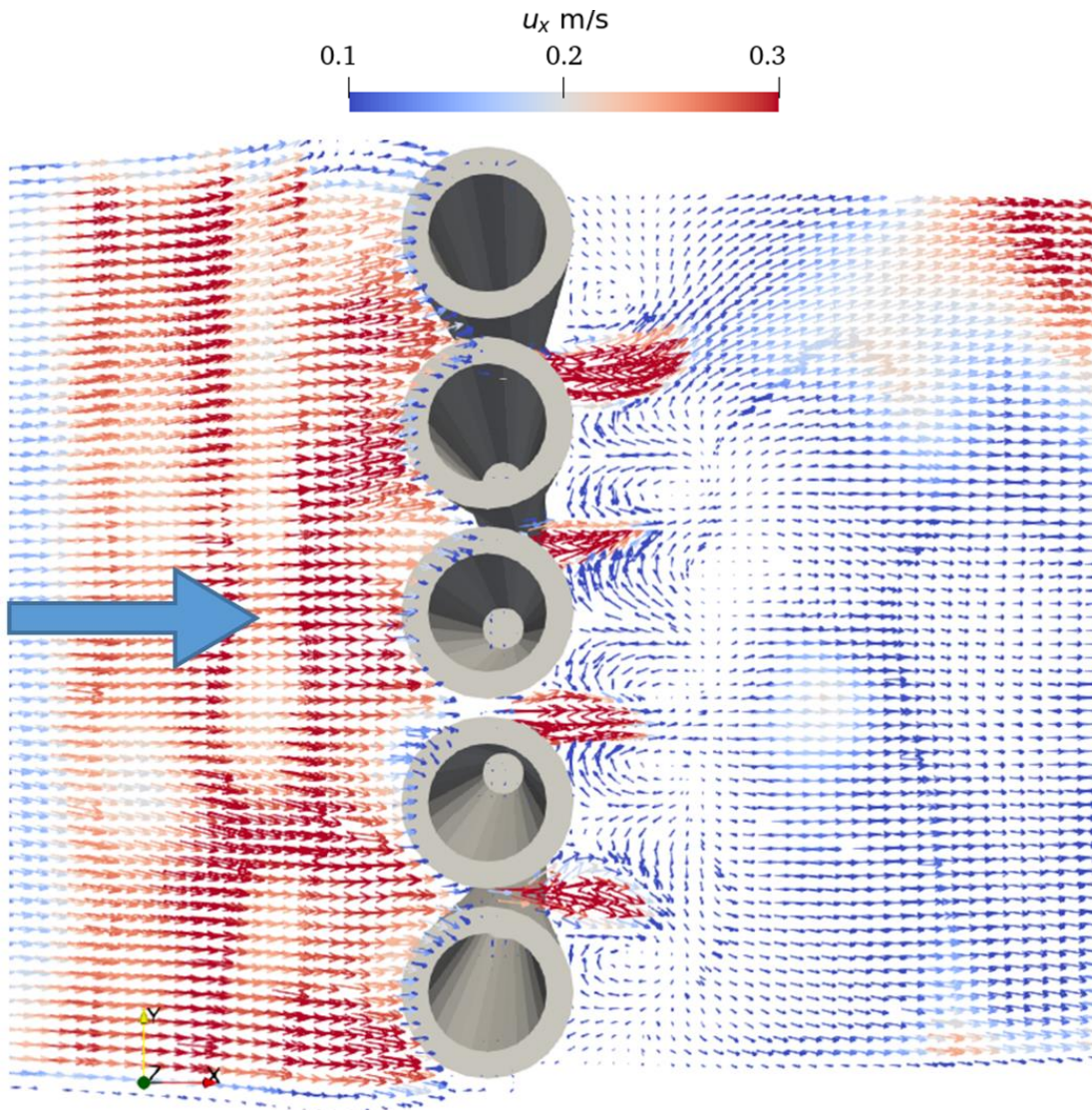
Figure 3.15 Plan-view of particle path lines during wave crest interaction (H_i = 0.16 m, T = 1.8 s and h = 0.40 m) with non-perforated CPHB (D/H_{max} = 0.4, Y/H_{max} = 1.5 and b/D = 0.1) at t = 9.10 s

3.1.11 Experimental procedure

The wave flume is cleaned and filled with ordinary tap water to the required depth. Before conducting the experiments, wave flume is calibrated for the considered combinations of wave heights and wave periods. Capacitance type wave probes are installed to measure the water surface elevation. The probes are also calibrated every time before and at the end of experiments and the obtained differences are incorporated in the recorded readings. The experimental investigation is conducted initially on a single row of non-perforated CPHB to arrive at the best performing model. The tests are conducted on different combinations of b/D, D/H_{max} and Y/H_{max}. The total number of test cases is narrowed down for two rows by omitting low performing configurations of a single row. It is reported in the literature (Weele and Herbich 1972) that the performance of the pile type of breakwater is better with the staggered arrangement than the regular one when conducted in multiple rows. Therefore, for two rows, the study is carried out only with the staggered arrangement of piles for different B/D ratios.

Further, an attempt is made to improve the performance of this best performing single row of CPHB structure by incorporating perforations. To arrive at the best performing model of perforated CPHB, the influence of perforation characteristics such as distribution of perforations (Pa), percentage of perforation (P) and size of perforation (S/D) are investigated. The list of governing variables considered in the present study is listed in Table 3.3. The accuracy and reliability of the results are ensured by repeating all the cases three times which is in accordance with the studies by Zhao and Ning (2018).

3.1.12 Sources of errors and precautions exercised

The following sources are identified, which may cause errors in the experimental investigation.

a. Liner dimension error: The model is constructed with an accuracy of linear dimensions up to ±1.0 mm, which may contribute to errors between 0.2% to 0.3%.

b. Wave height measurement error: The least count of the wave probe is 0.01 mm and this may contribute to a maximum error of 0.2% in the measurement of wave height.

c. Error due to change in water level: Error occurs due to the improper desired water level in the flume.

The following criteria were adopted to minimise the errors in the present study:

a. The model is constructed as per the standard procedure with the largest possible model with a scale of 1:30.

b. Before conducting the model studies, a particular combination of eccentricity and the generator's frequency is determined for all the sets of waves in the required depths of water considered in the study.

c. During the model studies, the wave generator is turned off after generating a burst of eight to ten waves to eliminate the reflection from the beach and wave paddle. The next wave burst is generated only after dampening the wave energy completely.

d. The depth of water in the flume is maintained precisely at the required level and is continuously monitored. An average variation of 2 mm was found after a full day of model testing. Any drop in the water level of more than 2 mm was immediately corrected.

3.2 NUMERICAL MODELLING

3.2.1 REEF3D

In the present study, a well-known and widely used open-source CFD software REEF3D (Bihs et al. 2016a) is used for simulating the complex wave-structure interaction. The REEF3D is highly useful for investigating coastal problems such as wave breaking (Aggarwal et al. 2019; Kamath et al. 2022), wave-structure interaction (Bihs et al. 2017; Kamath et al. 2016), seabed scouring (Ahmad et al. 2019), coastal structures (Sasikumar et al. 2020; Srineash et al. 2020) and structures used in mariculture (Martin et al. 2020).

REEF3D uses the incompressible Reynolds-averaged Navier-Stokes (RANS) equations together with the continuity equation to solve the fluid flow problem:

$$\frac{\partial u_i}{\partial x_i} = 0 \qquad (3.7)$$

$$\frac{\partial u_i}{\partial t} + u_j \frac{\partial u_i}{\partial x_j} = -\frac{1}{\rho}\frac{\partial p}{\partial x_i} + \frac{\partial}{\partial x_j}\left[(\nu + \nu_t)\left(\frac{\partial u_i}{\partial x_j} + \frac{\partial u_i}{\partial x_i}\right)\right] + g_i \qquad (3.8)$$

Where u_i is the averaged velocity over time t, ρ is the density of water, ν is the kinematic viscosity, ν_t is the eddy viscosity, p is the pressure and g is the acceleration due to gravity. A Cartesian grid is used in the two- phase flow model for the high-order spatial discretization schemes. A ghost cell immersed boundary method is employed in REEF3D to incorporate the irregular and non-orthogonal solid boundary conditions. The pressure terms in the RANS equation are solved by the projection method proposed by Chorin (1968). BiCGStab algorithm (Van Der Vorst 1992) is applied to solve the Poisson equation for pressure. The fifth-order weighted essentially non-oscillatory (WENO) scheme developed by Jiang and Shu (1996) is employed to discretize the convection terms of the RANS equation in the conservative finite-difference framework. Time discretization is achieved through the third-order TVD Runge–Kutta scheme (Shu and Osher 1988). According to Brackbill et al. (1992) continuum surface force (CSF) model, the material characteristics of the two phases are calculated for the numerical domain. REEF3D uses Courant-Friedrichs-Lewy (CFL) criterion, which determines the optimal time steps to maintain numerical stability throughout the simulation. MPI (Message Passing Interface) is used for parallel computation between multiple cores to maximise the efficiency of the numerical model. The k-ω model presented by Wilcox (1998) is applied for turbulence modelling in which k and ω denote turbulent kinetic energy and specific turbulence dissipation rate, respectively. The governing equations depicted in equations (3.7) and (3.8) are solved with the level set method and k−ω turbulence model in a finite difference framework.

The k and ω are determined using the following equations.

$$\frac{\partial k}{\partial t} + u_j \frac{\partial k}{\partial x_j} = \frac{\partial}{\partial x_j}\left[\left(\upsilon + \frac{\upsilon_t}{\sigma_k}\right)\frac{\partial k}{\partial x_j}\right] + P_k - \beta_k\, k\, \omega \qquad (3.9)$$

$$\frac{\partial \omega}{\partial t} + u_j \frac{\partial \omega}{\partial x_j} = \frac{\partial}{\partial x_j}\left[\left(\upsilon + \frac{\upsilon_t}{\sigma_\omega}\right)\frac{\partial \omega}{\partial x_j}\right] + \frac{\omega}{k}\alpha P_k - \beta\, \omega^2 \qquad (3.10)$$

Where, P_k denotes the rate of turbulent production and the values of the closure coefficients are $\sigma_k = 2, \sigma_\omega = 2, \alpha = 5/9, \beta_k = 9/100$ and $\beta = 3/40$ (Bihs et al. 2016b). To limit the overproduction of eddy viscosity outside the boundary layer, the eddy viscosity is regulated by the eddy viscosity limiters presented by Wilcox (1998) as:

$$\upsilon_t = \min\left(\frac{k}{\omega}, \sqrt{\frac{2}{3}}\frac{k}{|S|}\right) \qquad (3.11)$$

Where, $|S|$ is mean rate of strain.

3.2.2 Free surface

The free surface between the air and water is differentiated based on the level set method in accordance with Osher and Sethian (1988). The level set function is reinitialised after each iteration as per the procedure stated by Peng et al. (1999) by means of a partial differential equation. The level set function (Φ) gives the shortest distance from the interface between two fluid domains. The phases are distinguished based on the sign of level set function as follows:

$$\Phi\left(\vec{x}, t\right) \begin{cases} > 0, & \text{if } \vec{x} \text{ is in phase 1} \\ = 0, & \text{if } \vec{x} \text{ is at the inter face} \\ < 0, & \text{if } \vec{x} \text{ is in phase 2} \end{cases} \qquad (3.12)$$

3.2.3 Reconstruction of free surface

In the present study, the spectrum decomposition approach is used to reconstruct the free surface elevation. The reconstruction of free surface elevation is based on the coupling between Dirichlet inlet boundary conditions and input wave characteristics. The Dirichlet inlet boundary condition specifies the wave profile at the inlet boundary,

typically using a known wave theory or measured wave data. In the present study, an additional wave gauge is employed in the wave flume to collect the wave data before placing the structure. This measured data contains all the information regarding wave parameters (wave height and wave period). In numerical modelling, this measured time-domain data of experiments is used to reconstruct the waves using spectrum decomposition technique. Appendix-I presents the free surface reconstruction approach by employing the Dirichlet inlet boundary condition. Aggarwal et al. (2018) used theoretical and experimental data to evaluate the potential of REEF3D to generate waves through spectral wave components. The study was conducted using irregular waves against a few benchmark cases (wave breaking over the submerged bar, deep water wave generation and wave structure interaction with monopile) and demonstrated that the model could accurately generate free surface waves in this manner.

3.2.4 Numerical model setup

The numerical investigation of the performance characteristics of a CPHB is carried out by simulating the structure in a numerical wave tank (NWT). The numerical setup is similar to that used in the physical model study. The dimensions of the NWT are smaller compared to that of the physical wave tank to reduce the computational domain. The length of the NWT is 11 m, based on the minimum requirement to compute K_t and K_r as per Isaacson (1991). The width of the tank is truncated by half (0.71 m to 0.355 m) using the symmetric plane boundary condition applied on one side of the tank. The other side of the tank has a no-slip wall boundary condition. Similar boundary conditions are also applied at the bottom of the tank. The details of the boundary conditions of NWT are presented in Figure 3.16.

The waves are generated at one end using the Dirichlet inlet boundary condition. The active absorption method is adopted at the opposite end to absorb the transmitted waves, requiring no additional tank length. For wave absorption, the velocity of the waves to be absorbed or the reflected waves is prescribed at the end of the domain with the opposite sign, so as to cancel out the reflected wave. AWA boundary condition (Schaffer and Klopman 2000) is implemented as follows:
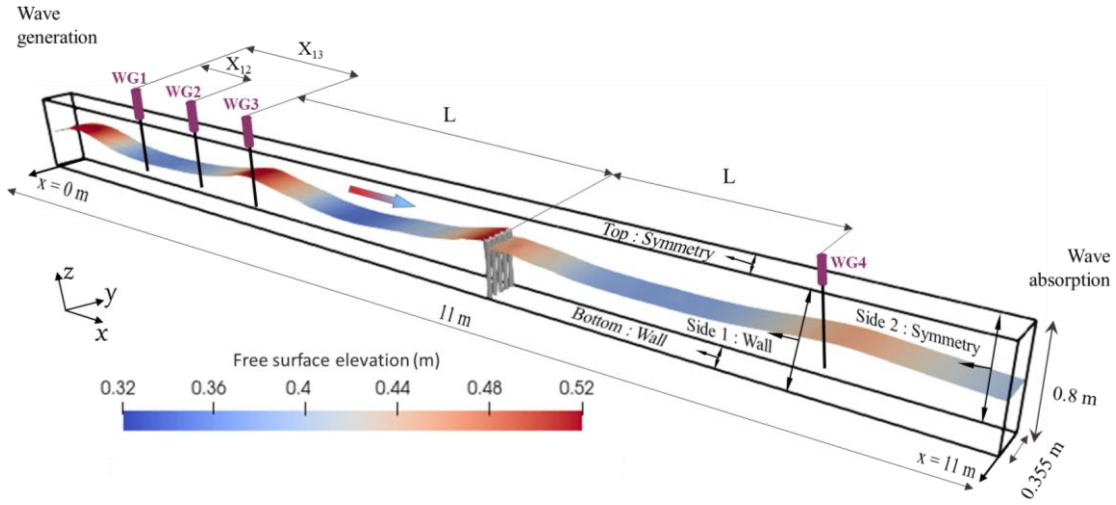
Figure 3.16 Detailed view of the numerical wave tank

$$u(t) = \sqrt{\frac{g}{h}}\, \zeta(t) \qquad (3.13) \qquad\qquad \zeta(t) = \eta(t) - h \qquad (3.14)$$

Where, $\zeta(t)$ is the free surface elevation along the outlet boundary condition and h is the depth of water.

At the top of the NWT, symmetric plane boundary condition is applied to represent the tank being open to the atmosphere. The same scale of 1:30 as that of physical modelling is adopted in NWT to define the structural and wave parameters. In REEF3D, the free surface elevation is calculated using numerical wave gauges. The K_r is calculated using the three probes approach in order to ensure consistency between physical and numerical modelling. The positioning of wave gauges is in accordance with the physical modelling (X_{12} = L/3 and X_{13} = 2L/3), as illustrated in Figure 3.16. The transmitted wave height is measured using WG4, which is positioned at a distance of L, as shown in Figure 3.16.

4.1 INVESTIGATION ON HYDRAULIC PERFORMANCE OF NON-PERFORATED CPHB

The influence of non-dimensional parameters such as relative pile head diameter (D/H_{max}), relative clear spacing between the CPHs (b/D), relative pile head height (Y/H_{max}) and relative water depth (h/H) on the performance characteristics (K_t, K_r and K_d) of non-perforated CPHB are analysed. The variation of K_t, K_r and K_d is plotted with respect to wave steepness (H_i/gT^2) by keeping the analysing parameter as a third variable. The best fit lines are drawn for the discrete data to understand the behaviour of the results. While plotting the trend lines, the logarithmic type is selected for all the graphs as it is found to be fitting better than the other types. The R^2 values obtained for different types of trend lines for a typical case of CPHB are illustrated in Appendix-II.

4.1.1 Influence of structural and wave parameters on a single row of CPHB performance

4.1.1.1 Relative pile head diameter

The geometry of conical pile head breakwater has an important role in wave attenuation, and this study investigated the effect of increased pile head area attributed by varying the height and diameter in terms of maximum wave height (H_{max}). To bring out the influence of pile head diameter on the hydraulic performance of non-perforated CPHB, the variation of K_t, K_r and K_d are plotted against H_i/gT^2 in Figure 4.1, Figure 4.2 and Figure 4.3, respectively. The experiments are carried out at different depths of water by keeping D/H_{max} as the third variable. In general, irrespective of all the considered dimensionless parameters (h/H, b/D and Y/H_{max}), the D/H_{max} is found to be directly proportional with K_t and indirectly proportional with K_r and K_d. Reducing the D/H_{max} from 0.6 to 0.4 resulted in the reduction of K_t in the range of 2.3 to 10%. A maximum reduction of 10% in K_t is observed at lower wave steepness (H_i/gT^2 =
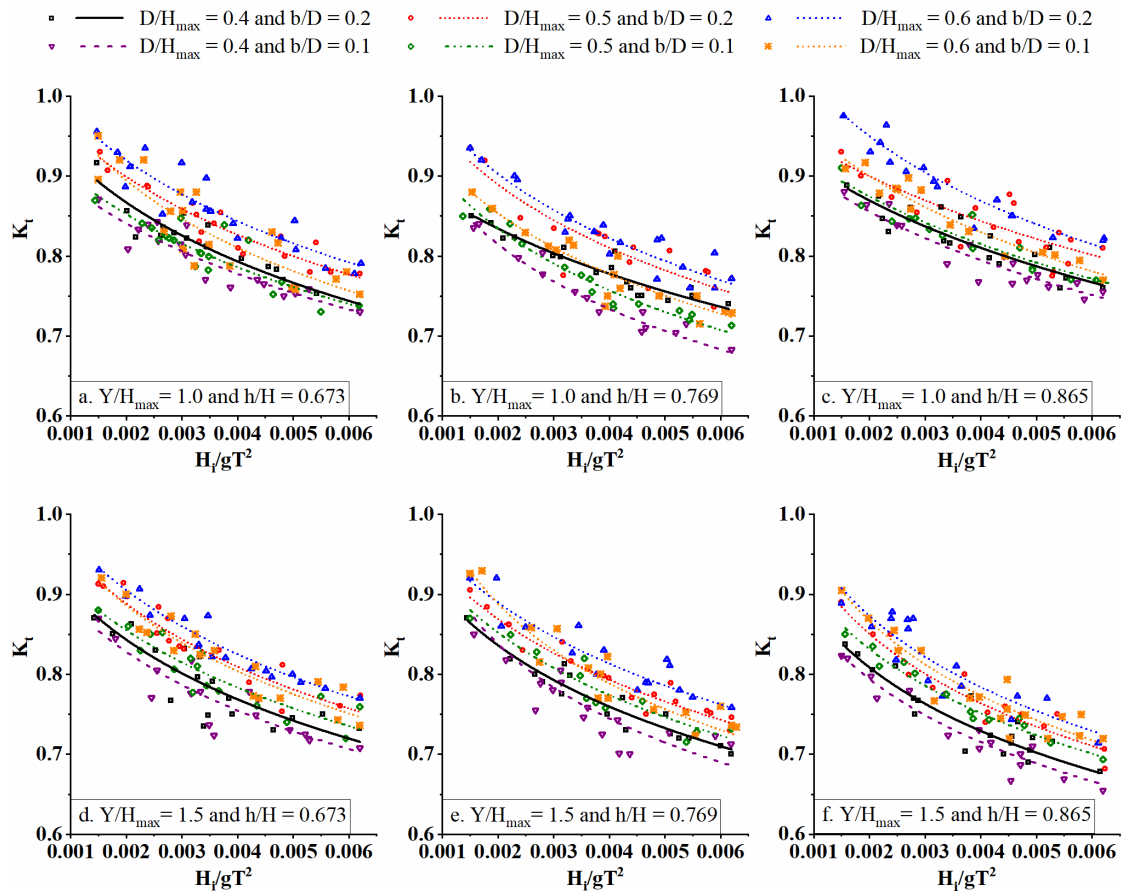
Figure 4.1 Influence of D/H$_{max}$ and b/D on K$_t$ for different Y/H$_{max}$ and relative water depths

0.00152) when D/H$_{max}$ is reduced from 0.6 to 0.4 for the case of b/D = 0.1, Y/H$_{max}$ = 1 and h = 0.40 m (h/H = 0.833).

When b/D = 0.1, Y/H$_{max}$ = 1.5 and h = 0.40 m (h/H = 0.769), reducing the D/H$_{max}$ from 0.6 to 0.4 resulted in 3 to 9% reduction in K$_t$ and 10 to 25% increase in K$_d$ with almost doubling of K$_r$. A minimum K$_t$ of 0.66 is obtained at higher wave steepness for the structural configuration of D/H$_{max}$ = 0.4, Y/H$_{max}$ = 1.5 and b/D = 0.1 at 0.45 m water depth (h/H = 0.865). The results suggest that the D/H$_{max}$ = 0.4 as the best performing CPH configuration than the other considered cases (D/H$_{max}$ = 0.6 and 0.5).

The observed behaviour may be due to the effect of total obstruction area of the structure against wave propagation. The pile heads with larger diameter have higher
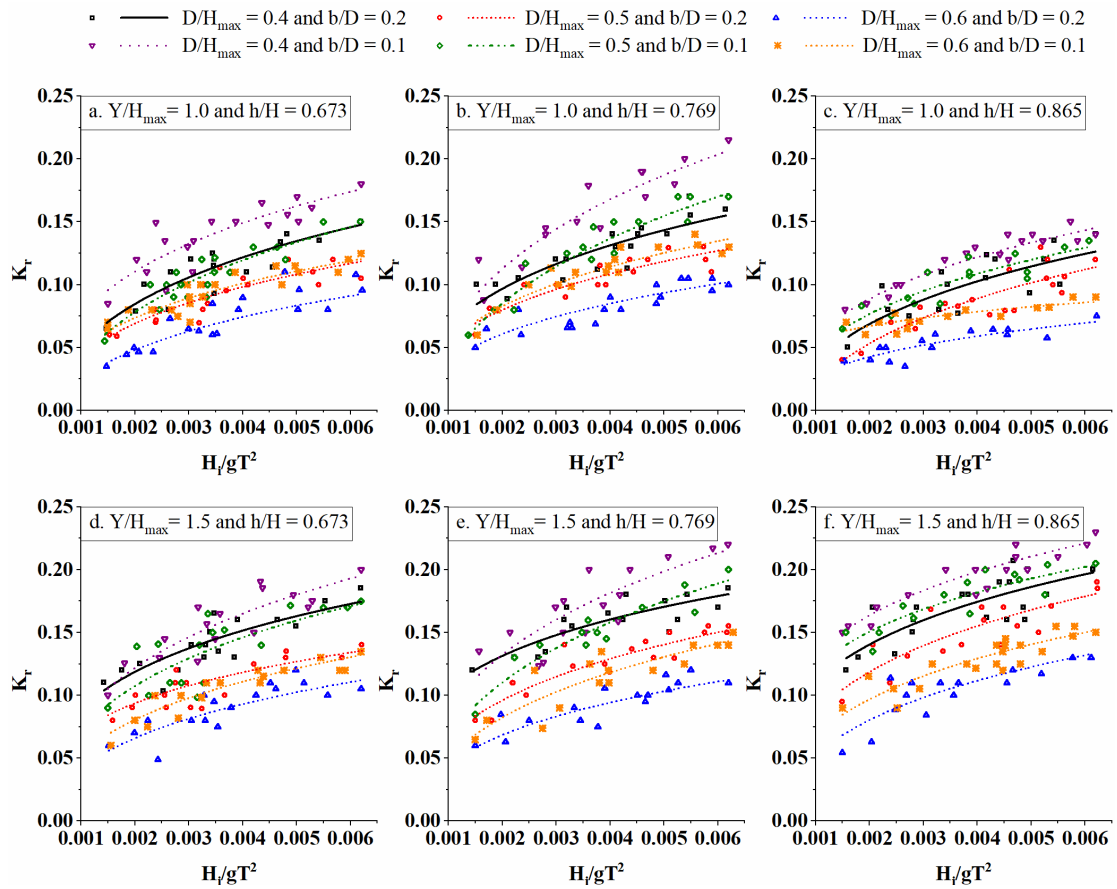
Figure 4.2 Influence of D/H$_{max}$ and b/D on K$_r$ for different Y/H$_{max}$ and relative water depths

projection area than the smaller diameter pile heads. However, to accommodate these larger-sized pile heads on supporting piles under constant spacing (b/D), the total number of conical pile heads needs to be reduced. This results in reduction of total projection area. For Y/H$_{max}$ = 1.5 and b/D = 0.1 configuration, the CPHB with D/H$_{max}$ = 0.4 case has about 15% higher projection area per unit width (per m) of the structure than D/H$_{max}$ = 0.5. Similarly, D/H$_{max}$ = 0.4 has about 30% higher projection area than D/H$_{max}$ = 0.6. Therefore, it can be stated that the pile head configuration with D/H$_{max}$ = 0.4 offers higher resistance against wave propagation than the other cases. This causes higher wave attenuation with increased wave reflection and energy dissipation.
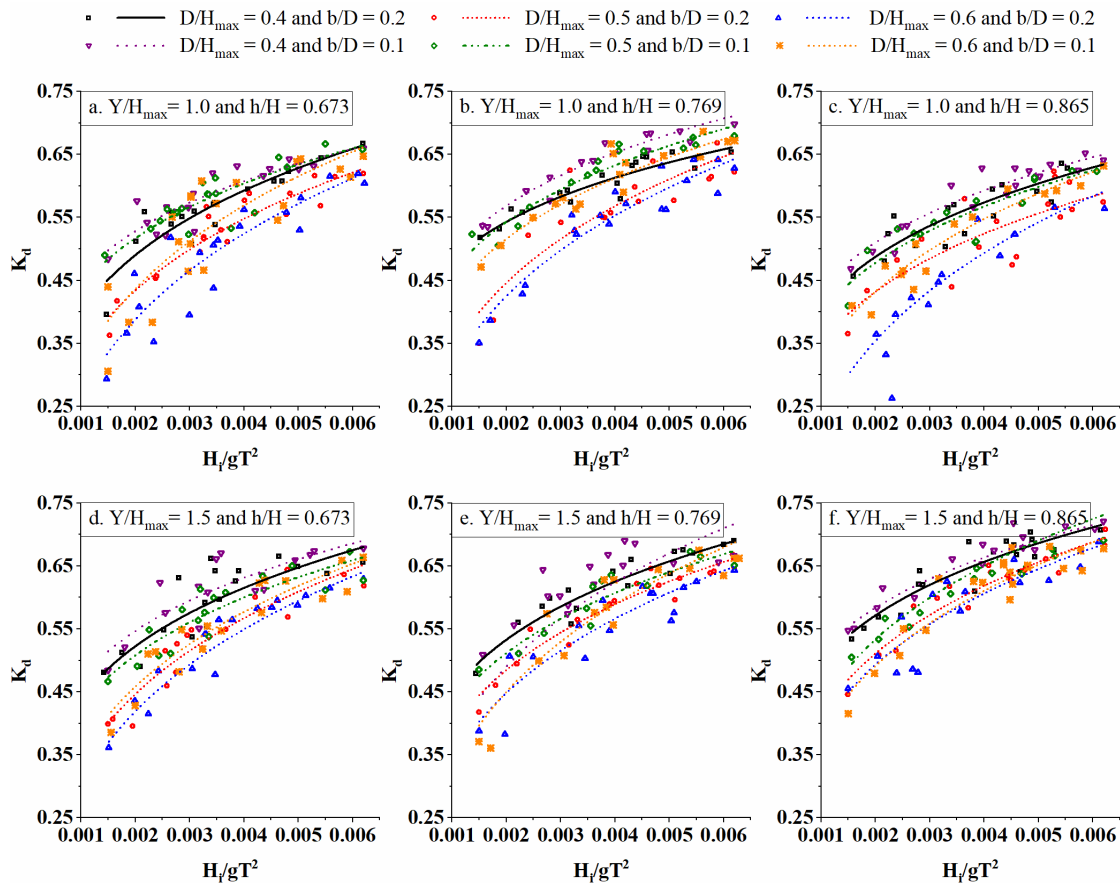
Figure 4.3 Influence of D/H$_{max}$ and b/D on K$_d$ for different Y/H$_{max}$ and relative water depths

4.1.1.2 Relative clear spacing between the CPHs

One of the advantages of the proposed structure over conventional pile breakwater is that the CPHB may be constructed at a larger spacing between the supporting piles, which overcomes the construction difficulties. In addition, the b/D is a key factor in deciding the number of pile head units. Hence, investigating the influence of relative clear spacing between the CPHs is important. The influence of b/D is analysed for only the best performing configuration of relative pile head diameter (D/H$_{max}$ = 0.4) based on the results discussed in the previous section (Section 4.1.1.1).

The variation of K$_t$, K$_r$ and K$_d$ are analysed by plotting the graphs with respect to wave steepness for different Y/H$_{max}$ and relative water depths (Figure 4.1, Figure 4.2 and

74

Figure 4.3). In general, decreasing the b/D from 0.2 to 0.1 resulted in increased wave attenuation of the CPHB structure. When $Y/H_{max} = 1$ and h = 0.35 m (h/H = 0.729), reducing the b/D from 0.2 to 0.1 resulted in reduction of K_t by 3.55% and 1.48% at lower and higher wave steepness, respectively. Similarly, for the same case with Y/H_{max} = 1.5, 2.28% and 1.8% reduction in K_t is noticed. For $Y/H_{max} = 1$ and h = 0.40 m (h/H = 0.833), 2.09% reduction is observed at lower steepness and a maximum reduction of 7.84% is obtained at higher steepness. For all the other cases considered in the present study, reduction in K_t is found to be less than 3%. Further, the K_r and K_d are found to be increasing with decreasing b/D. When $D/H_{max} = 0.4$, $Y/H_{max} = 1$ and h = 0.40 m, reducing the b/D from 0.2 to 0.1 caused an increase of K_r by about 11% and 32% at lower and higher steepness, respectively. Similarly, for the same case, varying the b/D from 0.2 to 0.1 increased the K_d by 3% and 9% at lower and higher steepness, respectively.

As the b/D increases, the clear spacing between the pile heads increases whereas, the number of pile head units decreases, and vice versa. Result of this, the CPHB with larger spaced pile heads (b/D = 0.2) offers lesser obstruction to the incident waves than the closely spaced pile heads (b/D = 0.1). With increasing spacing between pile heads, the wave energy is easily transmitted towards the lee side of the structure with lower wave reflection and energy dissipation. Whereas, for closely spaced pile heads, the waves lose a large portion of their energy in the process of wave separation, contraction, vortex shedding and wave breaking with higher reflection and energy dissipation. Overall, as it can be visualised that the CPHB with b/D of 0.1 is found to be better in wave attenuation than b/D of 0.2.

4.1.1.3 Relative pile head height

The study on the influence of Y/H_{max} is beneficial as Y/H_{max} plays a key role in deciding the pile head height for the required performance, as demonstrated in Figure 4.4, Figure 4.5 and Figure 4.6. The impact of Y/H_{max} on the attenuation capability of the CPHB is investigated at different relative water depths by varying the Y/H_{max} from 1.0 to 1.5 with a fixed b/D of 0.1. The influence of relative pile head height (Y/H_{max}) on the
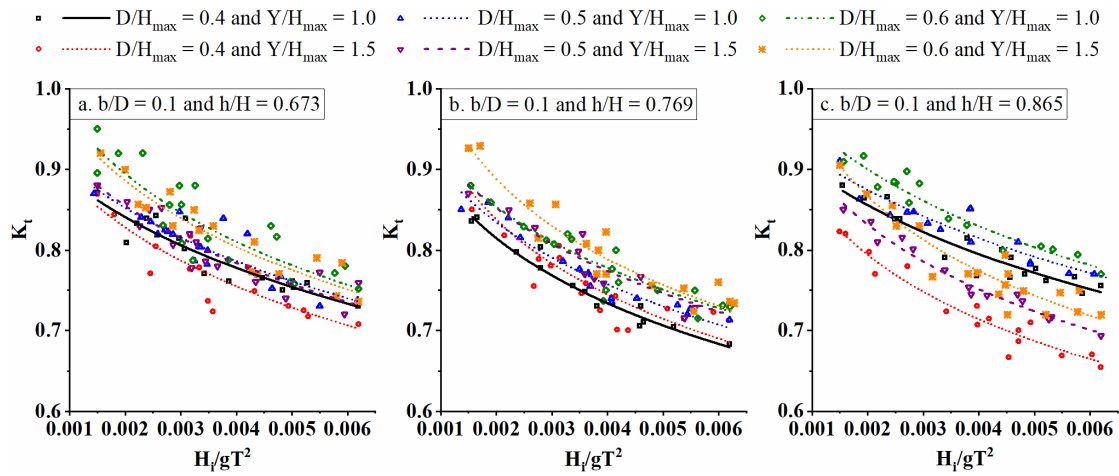
Figure 4.4 Influence of Y/H$_{max}$ on K$_t$ for different D/H$_{max}$ and relative water depths
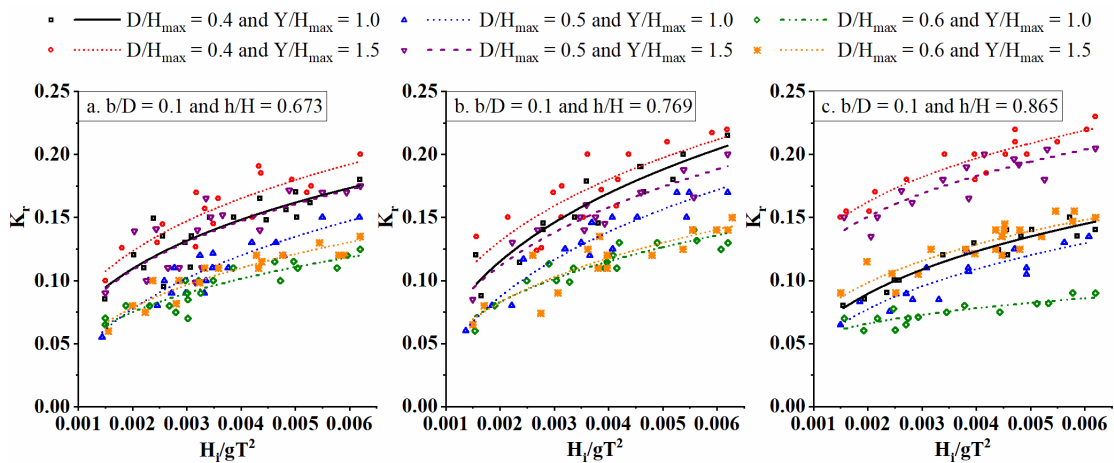
Figure 4.5 Influence of Y/H$_{max}$ on K$_r$ for different D/H$_{max}$ and relative water depths

hydraulic performance of CPHB is demonstrated by plotting K$_t$, K$_r$ and K$_d$ against wave steepness in Figure 4.4, Figure 4.5 and Figure 4.6, respectively.

At 0.35 m water depth, increasing the Y/H$_{max}$ in the considered range does not have a considerable influence on K$_t$ as the maximum reduction is within 3.5%. Whereas, for D/H$_{max}$ = 0.6 at 0.40 m water depth, Y/H$_{max}$ = 1 is found to be better performing than Y/H$_{max}$ = 1.5 with 6.24% lower K$_t$. When D/H$_{max}$ = 0.4, increasing Y/H$_{max}$ showed a significant improvement in K$_t$ at 0.45 m water depth, with a maximum reduction of

76
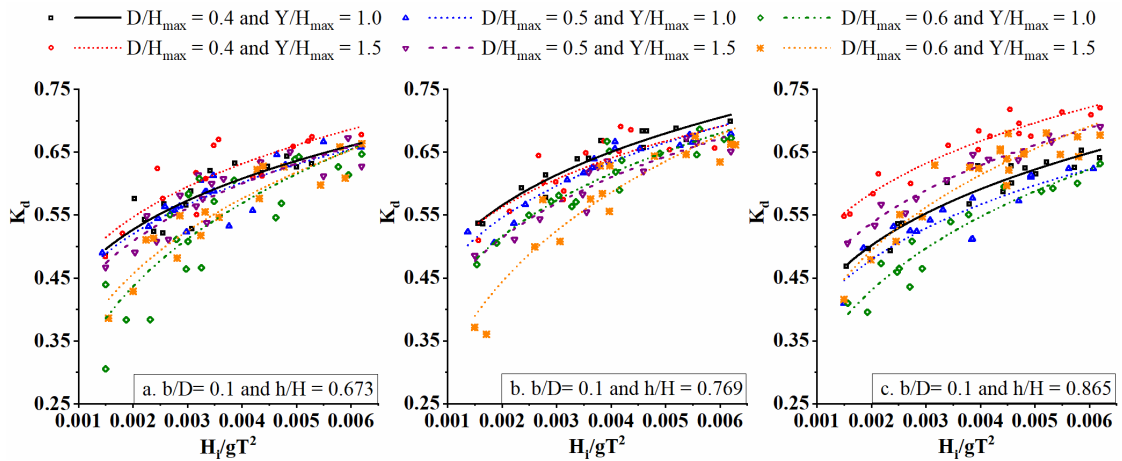
Figure 4.6 Influence of Y/H_{max} on K_d for different D/H_{max} and relative water depths

13.01% for steep waves. Overall, when the Y/H_{max} is increased from 1 to 1.5, the improvement in wave attenuation is negligible at 0.35 m water depth, but significant at 0.45 m. However, an opposite behaviour is observed at 0.40 m depth of water. At 0.35 and 0.45 m depths of water, no significant variation in K_r and K_d is observed when Y/H_{max} is varied from 1 to 1.5 under a constant D/H_{max} of 0.4. Whereas, at 0.45 m water depth, increasing the Y/H_{max} resulted in increase of K_r by about 1.5 times and the K_d is found to be increased by an average of about 14%.

The wave attenuation in conventional pile breakwater is due to the combination of flow separation, inertial resistance, contraction, turbulence, vortex shedding and wave reflection. In addition to this, the proposed CPHB structure dissipates additional wave energy through wave breaking. Also, the turbulence generated during the entry and exit of water into the hollow pile head causes additional energy losses. At 0.35 m depth of water, a larger portion of the pile head is emerged above the water surface for both cases of pile heads ($Y/H_{max} = 1$ and 1.5). Due to this, the waves fail to break and enter the hollow pile head. When $Y/H_{max} = 1$ is tested at 0.40 m water depth, the waves may easily break and enter the hollow portion of the pile head and cause additional energy losses. However, because the majority of the pile head is submerged at 0.45 m depth of water, even the gentle waves easily transmit the wave energy to the lee side without

noticeable interaction. Whereas, the CPHB with $Y/H_{max} = 1.5$ performs better at 0.45 m depth of water as the emerged portion of the pile head contributes to additional energy losses through breaking of waves, as discussed above. Considering the overall performance, $Y/H_{max} = 1.5$ is concluded as the better performing CPH than the other verified cases.

4.1.1.4 Depth of water

In the prototype conditions, the depth of water may vary due to one or a combination of tides, base erosion and storm surge. Therefore, the CPHB is tested at different water depths in order to ascertain its performance. The different depths of water considered in the present study are 0.35 m, 0.40 m and 0.45 m. For the analysis, only the best performing relative clear spacing (b/D = 0.1) case is considered. Figure 4.7, Figure 4.8 and Figure 4.9 illustrate the influence of relative water depths on the K_t, K_r and K_d for different configurations of CPHB structure.
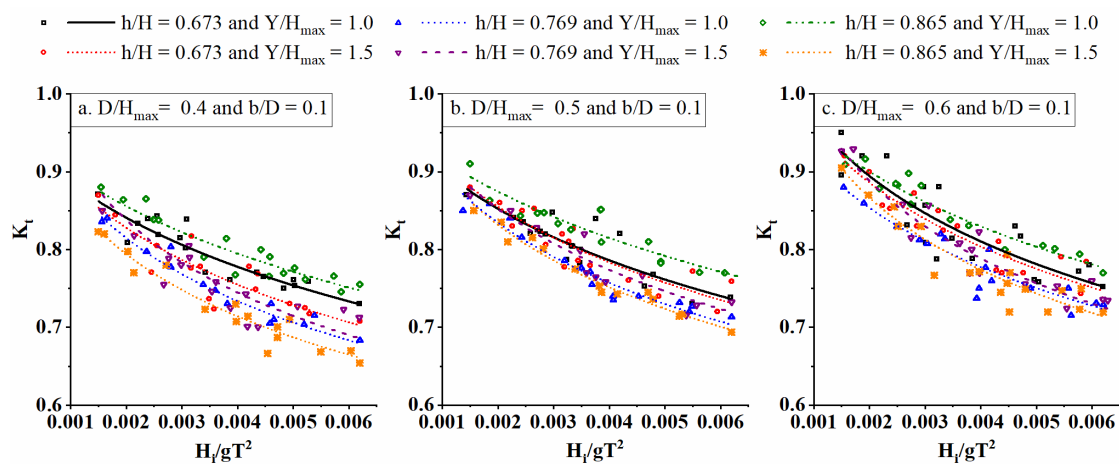
Figure 4.7 Influence of relative water depth on K_t for different configurations of CPHB at b/D = 0.1

For $Y/H_{max} = 1$, it is observed that irrespective of CPH diameter, the performance of the structure improves when the water depth increases from 0.35 m to 0.40 m. At the same time, when depth of water is further increased from 0.40 m to 0.45 m, the transmission capability reduces. Whereas, for $Y/H_{max} = 1.5$, improvement in K_t appears
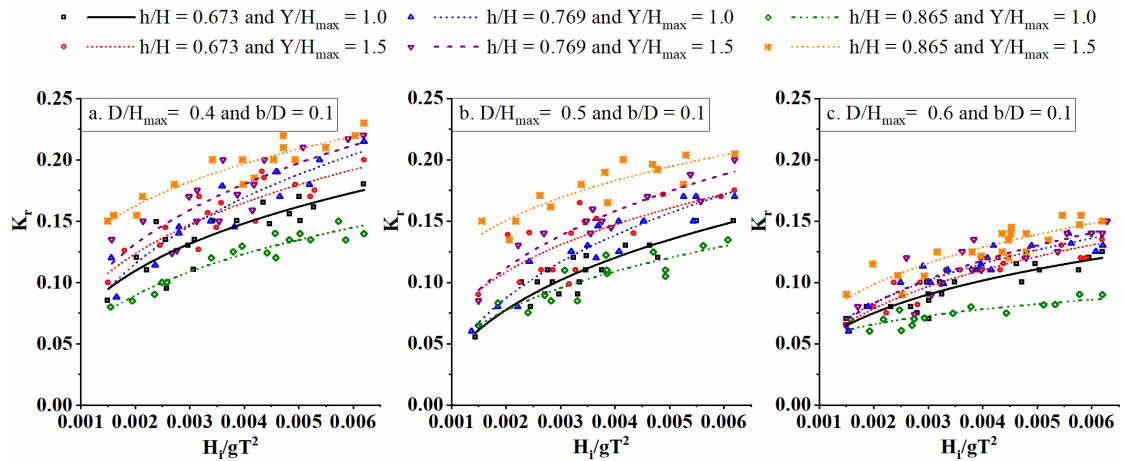
Figure 4.8 Influence of relative water depth on K_r for different configurations of CPHB at b/D = 0.1
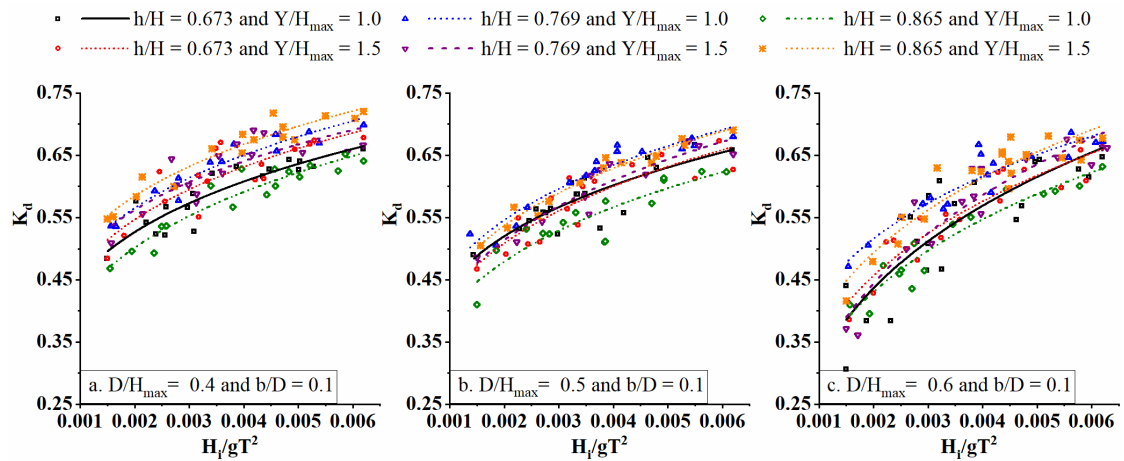
Figure 4.9 Influence of relative water depth on K_d for different configurations of CPHB at b/D = 0.1

significant (up to 11.58%) when the water depth is increased from 0.40 to 0.45 m. For $D/H_{max} = 0.4$, $Y/H_{max} = 1.5$ and $b/D = 0.1$ configurations, it is observed that changing the water depth from 0.35 m to 0.40 m leads to increase in K_r by 9.62% (0.104 to 0.114) for gentle waves and 9.18% (0.196 to 0.214) for steep waves. The identical trend is observed when the water depth is again increased from 0.40 m to 0.45 m, with 33.33% (0.114 to 0.152) for gentle waves and 5.14% (0.214 to 0.225) for steep waves.

79

Based on these observations, it can be postulated that the $Y/H_{max} = 1$ performs better at 0.40 m water depth (h/H = 0.833), and $Y/H_{max} = 1.5$ at 0.45 m (h/H = 0.865) due to the auxiliary energy losses by the phenomenon of wave overtopping and unique wave-structure interaction. Considering the prototype conditions, the CPH with $Y/H_{max} = 1.5$ is proposed as an efficient structure over $Y/H_{max} = 1.0$ since the wave damping performance is steady in all the examined water depths.

4.1.1.5 Wave steepness

The CPHB structure is subjected to different combinations of wave height and wave period to understand the performance of the structure at different wave climates. The wave steepness parameter (H_i/gT^2) accounts for both the effects of wave height and wave period. The wave attenuation capability of the CPHB is more pronounced for steep incident waves than for gentle waves. It is noticed from Figure 4.1 to Figure 4.9 that as the H_i/gT^2 increases, the K_t decreases. Whereas, K_r and K_d follow the opposite trend. For the case of $Y/H_{max} = 1.5$, $D/H_{max} = 0.4$, b/D = 0.1 and h = 0.40 m, the K_t obtained for the steep wave ($H_i/gT^2 = 0.0062$) is about 18.5% lower than that of the gentle wave ($H_i/gT^2 = 0.0015$). Similarly, the K_r and K_d calculated at steep waves are about 83% (0.12 to 0.22) and 30% higher than that of gentle waves.

The probable reason for the above behaviour is that the steep waves tend to be unstable and the slightest provocation triggers wave breaking and loss of energy with minimal obstruction against propagation, while the gentle waves are comparatively stable. Also, when the conical pile head breakwater obstructs the steep waves against propagation, some part of the wave plunge into the hollow pile head and causes turbulence. The gentle wave propagates across the structure without noticeable confrontation. Similar behaviour is also reported in the literature for pile breakwater (Rao et al. 1999, 2002; Truitt and Herbich 1987; Weele and Herbich 1972) and suspended pipe breakwater (Mani and Jayakumar, 1995; Rao and Rao, 1999).

Overall, the influence relative pile head diameter (D/H_{max}), relative clear spacing between the CPHs (b/D), relative pile head height (Y/H_{max}) and relative water depth (h/H) on the hydraulic performance of non-perforated CPHB are comprehensibly

investigated against varying wave climate. From the above discussion, it can be inferred that the CPHB with the configuration of $Y/H_{max} = 1.5$, $D/H_{max} = 0.4$ and $b/D = 0.1$ is the best performing model configuration among the considered cases in the present study with the least K_t of 0.66 associated with a K_r of 0.22 and K_d of 0.72.

4.1.2 Two rows of CPHB

To further enhance the performance of the CPHB structure, an additional row of CPHB is introduced in a staggered manner. The influence of clear spacing between the two rows of pile heads (B/D) on the performance of CPHB is investigated through physical modelling studies. The B/D considered in the present study are 0.0, 0.2, 0.4 and 0.8. Only the best-performing configuration of CPHB ($Y/H_{max} = 1.5$, $D/H_{max} = 0.4$ and $b/D = 0.1$) selected in the previous section (Section 4.1.1) is taken into consideration for this analysis. The laboratory investigations are conducted at 0.35 m (h/H = 0.673), 0.40 m (h/H = 0.769) and 0.45 m (h/H = 0.865) water depths against varying wave parameters.

The performance comparison of the single row and two rows of CPHB with various B/D configurations is shown in Figure 4.10. The inclusion of the second row of CPHB in staggered order is proved to increase the wave attenuation of the structure. Due to the closer spacing of the pile head rows, the structure may perform similarly to a single unit when B/D is 0.0 and 0.2, resulting in higher reflection and lower dissipation. Also, the gap between the pile head rows may be insufficient to fully interfere in the wave propagation as two independent structural components because the waves transmitted through the first row of the structure encounter the second row immediately. As the B/D is increased to 0.4, due to the mutual influence of two rows of pile heads, both rows increasingly contribute to the energy losses through effective interaction. Increasing the B/D to 0.8 is not very effective in further increasing the energy dissipation and reducing the wave transmission, as waves are already attenuated by the first row of pile heads.

It is observed from Figure 4.10 that as the B/D is increased from 0.0 to 0.4, the K_t is decreased by up to 7%. Further increasing the B/D from 0.4 to 0.8 resulted in increase of K_t by up to 5.5%. Varying the B/D from 0.0 to 0.4 reduced the K_r by about 20%.

81
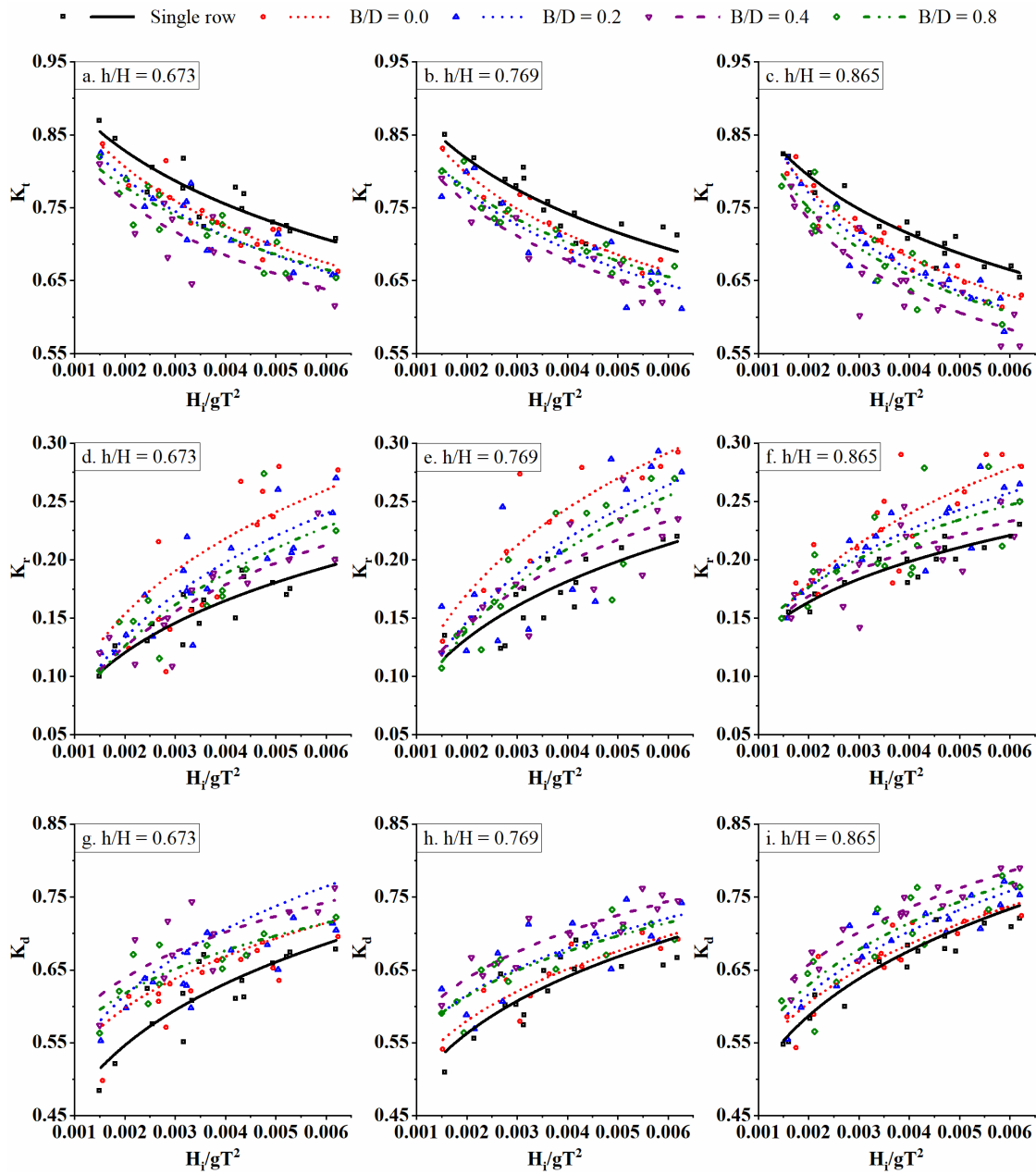
Figure 4.10 Comparison of performance of CPHB in single and two rows at b/D = 0.1 and various B/D

Similarly, altering the B/D from 0.0 to 0.4 increased K_d by about 12.8%. The addition of the second row of CPHB with $D/H_{max} = 0.4$, $Y/H_{max} = 1.5$ b/D = 0.1 and B/D = 0.4 configuration in staggered arrangement reduces the K_t by a maximum of 12.34% compared to a single row.

From the above discussion, it can be concluded that B/D has a significant influence on the performance characteristics of two rows of CPHB. The findings are similar to the research results reported by Weele and Herbich (1972), Herbich and Douglas (1988), Herbich (1990) and Rao et al. (1999) for the conventional pile breakwater. Overall, it appears from the above analysis that the B/D of 0.4 is the optimum spacing between two rows of pile heads for which the least K_t of 0.58 is obtained associated K_r and K_d of 0.24 and 0.79, respectively.

4.1.3 Key findings

Based on the extensive experiments conducted on non-perforated CPHB, the following observations are drawn.

1. The hydraulic performance of the CPHB is significantly influenced by the structural parameters of the CPH, such as height (Y/H_{max}), diameter (D/H_{max}), and clear spacing of CPHs in a row (b/D) and rows of pile heads (B/D).

2. In general, the transmission coefficient (K_t) decreases with an increase in wave steepness (H_i/gT^2) whereas, reflection (K_r) and energy dissipation coefficients (K_d) follow the opposite trend.

3. In a single row of CPHB, as the relative clear spacing between the conical pile heads (b/D) decreases, the wave transmission of the structures reduces with increased K_r and K_d.

4. K_t is directly proportional to the relative pile head diameter of the CPHB (D/H_{max}) and inversely proportional to reflection and energy dissipation coefficients.

5. The wave attenuation capability of the non-perforated CPHB enhances with increase in relative pile head height of the structure (Y/H_{max}) with higher reflection and energy dissipation.

6. The wave attenuation, wave reflection and energy dissipation of the CPHB are more pronounced for steep waves than for gentle waves.

7. The structural configuration of $D/H_{max} = 0.4$, $Y/H_{max} = 1.5$ and b/D = 0.1 is the best performing model configuration for single row of CPHB with the least K_t of 0.66 along with K_r of 0.22 and K_d of 0.72.

8. For two rows of CPHB with staggered arrangement, the B/D of 0.4 is the optimum spacing, which provided a minimal K_t of 0.58 with K_r of 0.24 and K_d of 0.79.

9. The addition of the second row of CPHB with $D/H_{max} = 0.4$, $Y/H_{max} = 1.5$, $b/D = 0.1$ and $B/D = 0.4$ configuration in staggered arrangement reduces the K_t by a maximum of 12.34% compared to a single row. However, from the practical point of view, providing whether single or double row structure to achieve an extra 12.34% reduction in K_t is a matter of judgement considering site conditions. Therefore, efforts are made to introduce perforations on pile heads and achieve improved performance.

4.2 INVESTIGATION ON HYDRAULIC PERFORMANCE OF PERFORATED CPHB

4.2.1 Influence of perforation characteristics and wave parameters on hydraulic performance of CPHB

4.2.1.1 Selection of pile head configuration

The influence of D/H_{max}, Y/H_{max} and b/D of the non-perforated CPHB is investigated comprehensively in the previous section (Section 4.1) and the best performing structural configuration is evolved ($D/H_{max} = 0.4$, $Y/H_{max} = 1.5$ and $b/D = 0.1$). Considering the conservative performance of non-perforated CPHB, a water depth of 0.40 m is selected, and the corresponding best performing pile head configuration is further tested with perforations to explore the improvement in structure performance. To arrive at the best performing model of perforated CPHB, the influence of perforation characteristics such as distribution of perforations (Pa), percentage of perforation (P) and size of perforation (S/D) are investigated. Initially, the study is conducted at 0.40 m depth of water to arrive at the best performing configuration of Pa, P and S/D. Once after finalising the configuration, the depth of water is varied to determine the influence of depth of water. All the results (K_t, K_r and K_d) are analysed by plotting the data with respect to the wave steepness (H_i/gT^2). The best fit lines are drawn for the discrete data to understand the behaviour of the results. To evaluate the uncertainty of present test results, 95% confidence and prediction bands are plotted for the typical cases of CPHB. The details of the same are presented for typical cases in Appendix-III. The details of the perforations provided on the pile head are enumerated in the following sections.

4.2.1.2 Distribution of perforations

To bring out the influence of distribution of perforation on the surface of CPH, graphs are plotted for various combinations of P and S by fixing Pa as the third parameter in Figure 4.11. In general, providing the perforations on 50% of the surface area of CPH is found to be optimum. Where, increasing or decreasing Pa from 50% resulted in the higher K_t values. A minimum K_t of 0.61 is obtained at higher wave steepness ($H_i/gT^2 = 0.0062$) for the structural configuration of P = 19.2% and S/D = 0.25 with Pa = 50%.
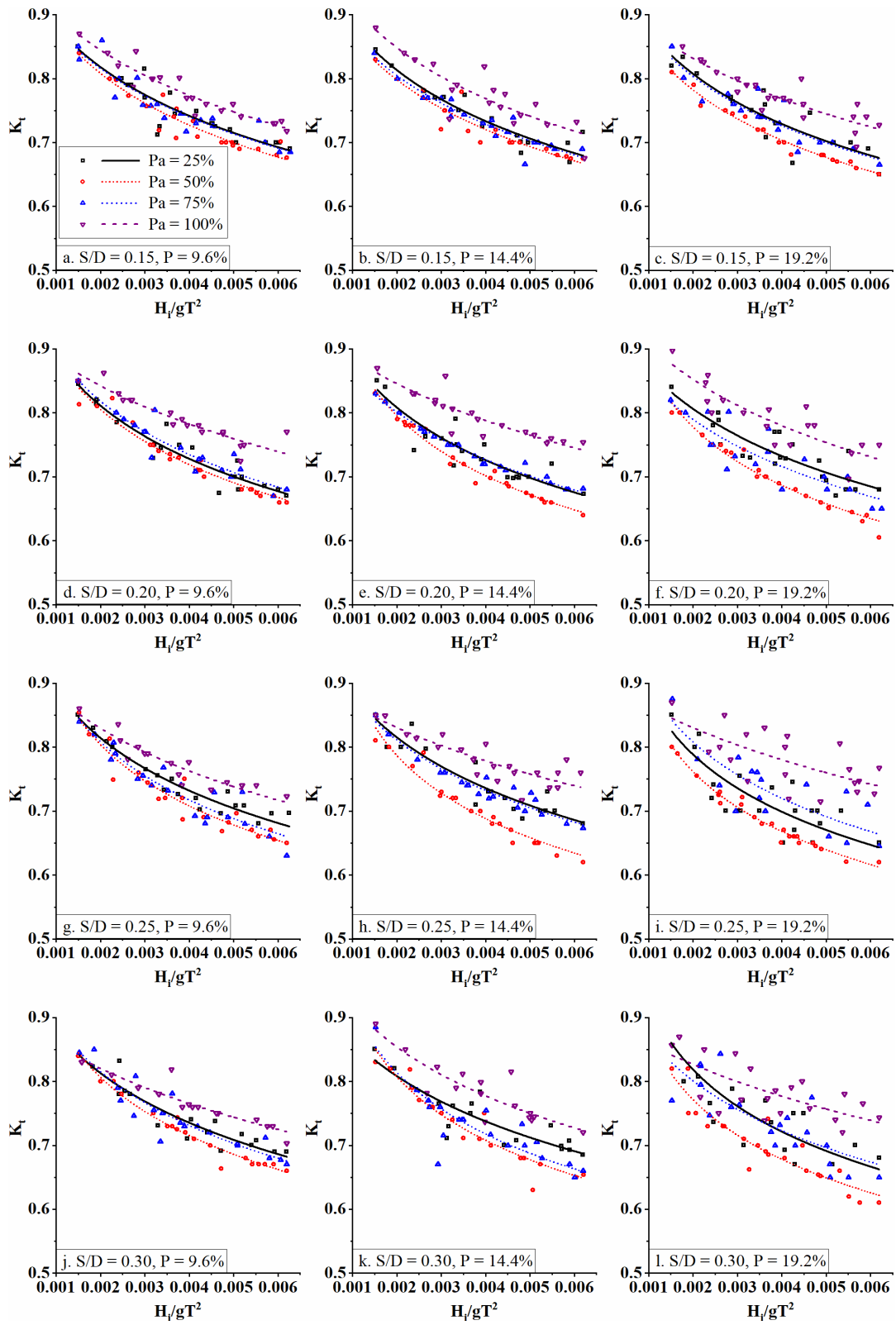
Figure 4.11 Influence of Pa on K$_t$ for various P and S/D at h = 0.40 m (h/H = 0.769)
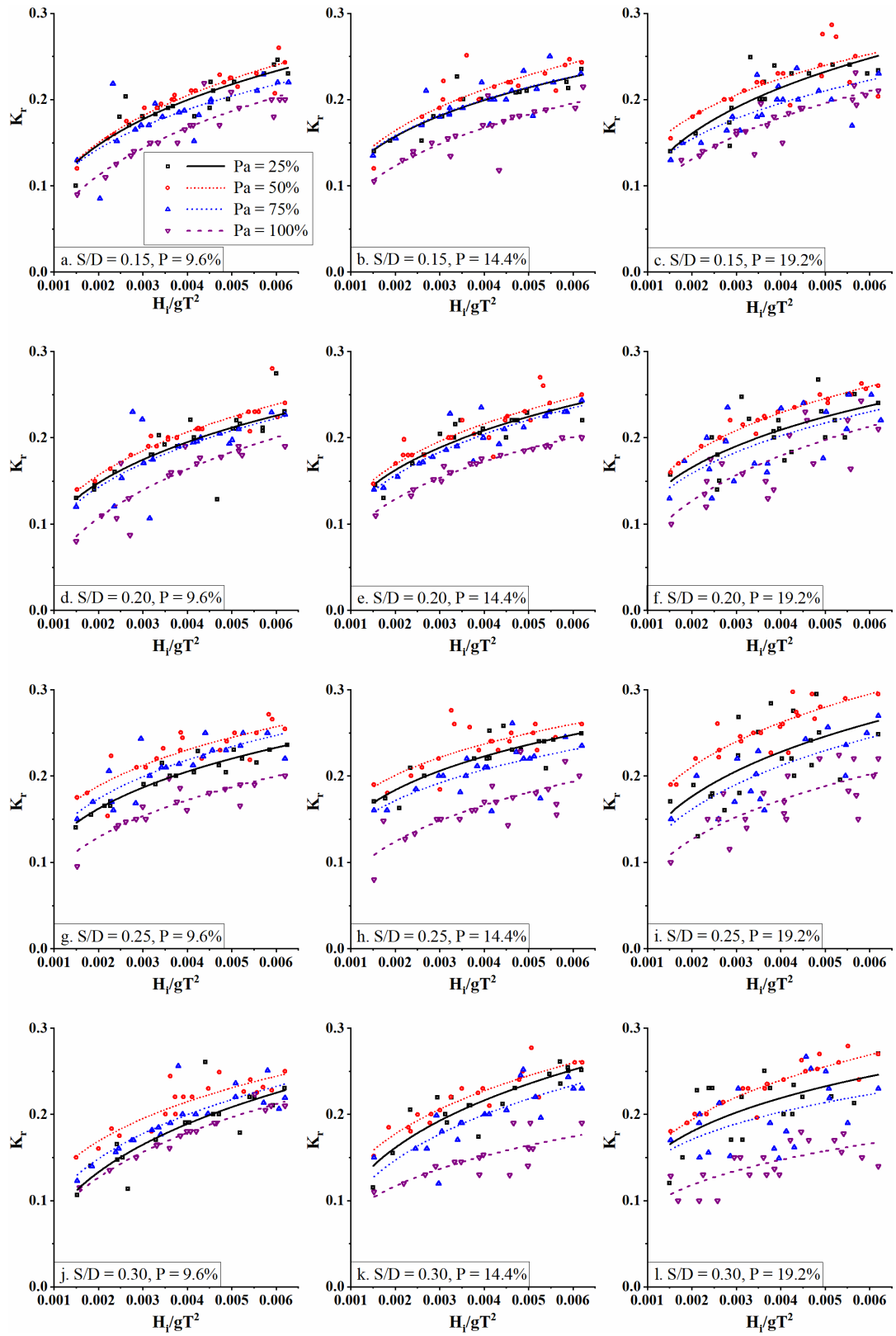
Figure 4.12 Influence of Pa on K_r for various P and S/D at h = 0.40 m (h/H = 0.769)
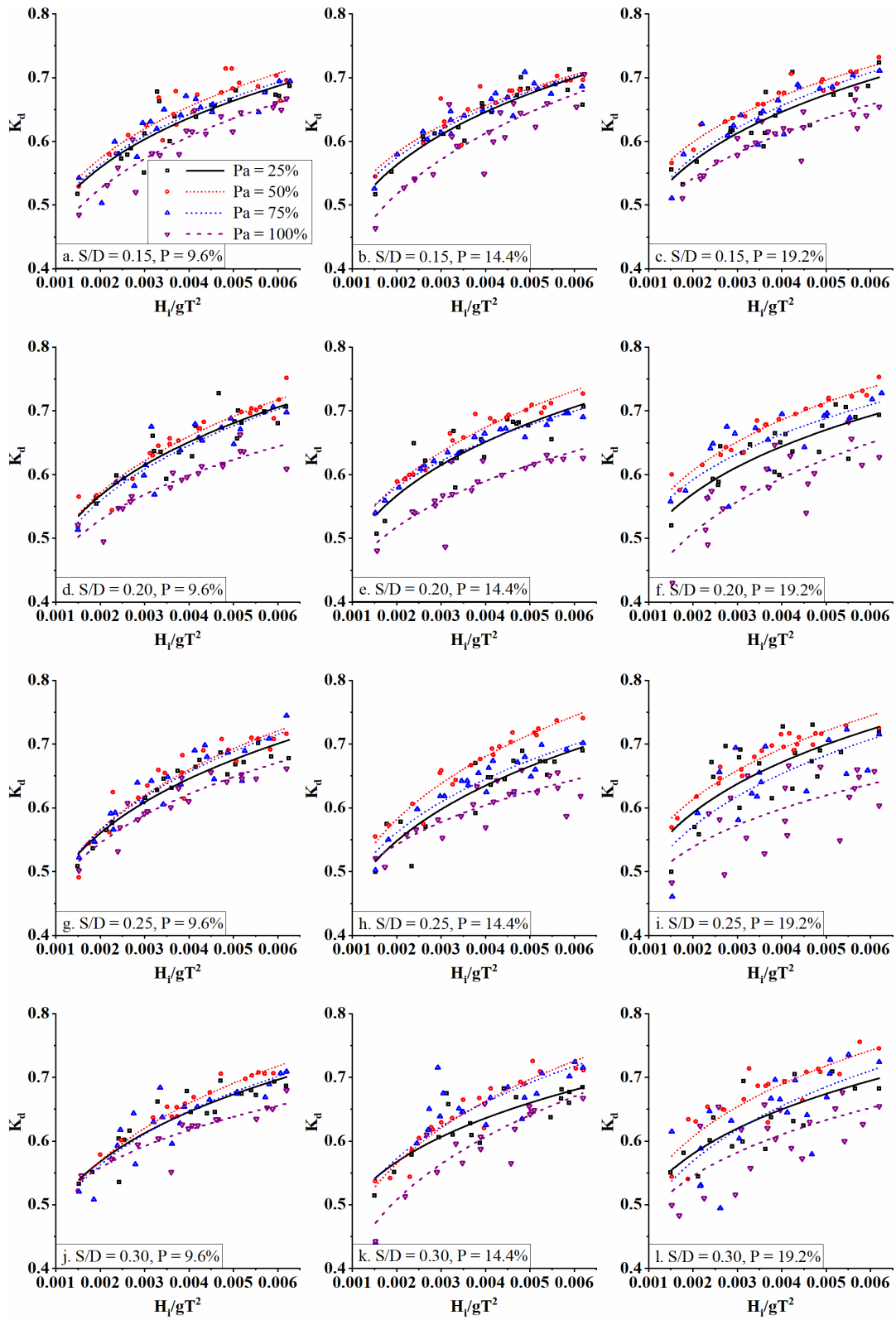
Figure 4.13. Influence of Pa on K_d for various P and S/D at h = 0.40 m (h/H = 0.769)

At lower wave steepness ($H_i/gT^2 = 0.0015$), the K_t obtained for the Pa = 50% case (Figure 4.11) is about 3.2%, 5.7% and 6.6% lower than that of Pa = 25%, 75% and 100%, respectively. For the same case, about 4.4%, 8.5% and 20.9% lower K_t values are noted at higher wave steepness.

The idea behind providing the perforation is to add an additional mechanism to diffuse more energy and attenuate a larger amount of waves. During the interaction between the wave crest and the CPH, a certain amount of water gets trapped inside the CPH. The trapped water flows out through the perforations in the form of smaller jets and further interacts with the incident waves causing additional turbulence. As illustrated in Figure 3.14, the blockage area of CPH against the wave propagation decreases with an increase in Pa. The amount of water entering the CPH is restricted due to the reduced opening in the case of Pa = 25%. Even though this amount is higher for Pa = 75% or 100%, the water easily propagates towards the lee side of the structure through the perforations without getting trapped. When the perforations are provided on 50% of the surface area (Pa = 50%), comparatively more water flows into the CPH and gets captured. This water escapes through the seaside perforations and distorts the orbital motion of incident waves, resulting in higher turbulence and energy dissipation.

The reflection and dissipation characteristics of the perforated CPHB are plotted with respect to the wave steepness (H_i/gT^2). Figure 4.12 and Figure 4.13 illustrate the variation of K_r and K_d at a depth of water of 0.40 m for the corresponding cases of K_t discussed in Figure 4.11. In general, both the K_r and K_d are found to be increasing with the increasing wave steepness. A higher value of K_r of 0.30 is obtained for the perforation configuration of Pa of 50%, P of 19.2% and S/D of 0.25, along with a maximum K_d of 0.75. The maximum variation observed in K_r is 26%, 42% and 80% when Pa is varied from 25 to 50%, 50 to 75%, and 50 to 100%, respectively. In a similar way, a maximum of 7%, 11% and 21% higher K_d is recorded for Pa = 50% in comparison with 25%, 75% and 100%, respectively. When the perforation distribution (Pa) is 75% or 100%, part of the outflowing water from CPH passes to the structure's lee side, posing lower reflection and dissipation. Since the lee side of the CPH is

blocked in the case of Pa = 25% and 50%, the water escapes through seaside perforations. The escaping water disturbs the orbital motion of the upcoming incident waves causing higher turbulence and energy dissipation. In this context, providing perforations on 50% of CPH is optimum in terms of wave attenuation.

4.2.1.3 Percentage of perforations

While studying the effect of percentage of perforations on the performance of CPHB, only the best performing Pa (i.e. 50%) is considered by eliminating the other cases of Pa (25%, 75% and 100%). The variation of K_t, K_r and K_d against the wave steepness for different cases of S/D is presented in Figure 4.14, Figure 4.15 and Figure 4.16, respectively.
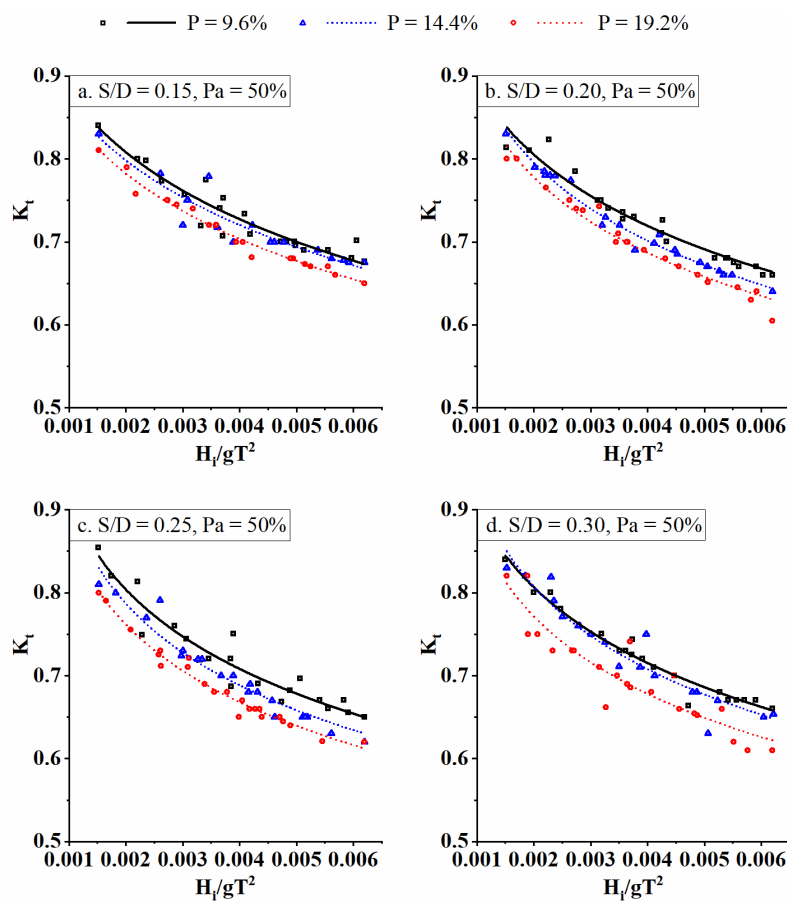
Figure 4.14. Influence of P on K_t for different S/D when Pa = 50% and h= 0.40 m (h/H = 0.769)
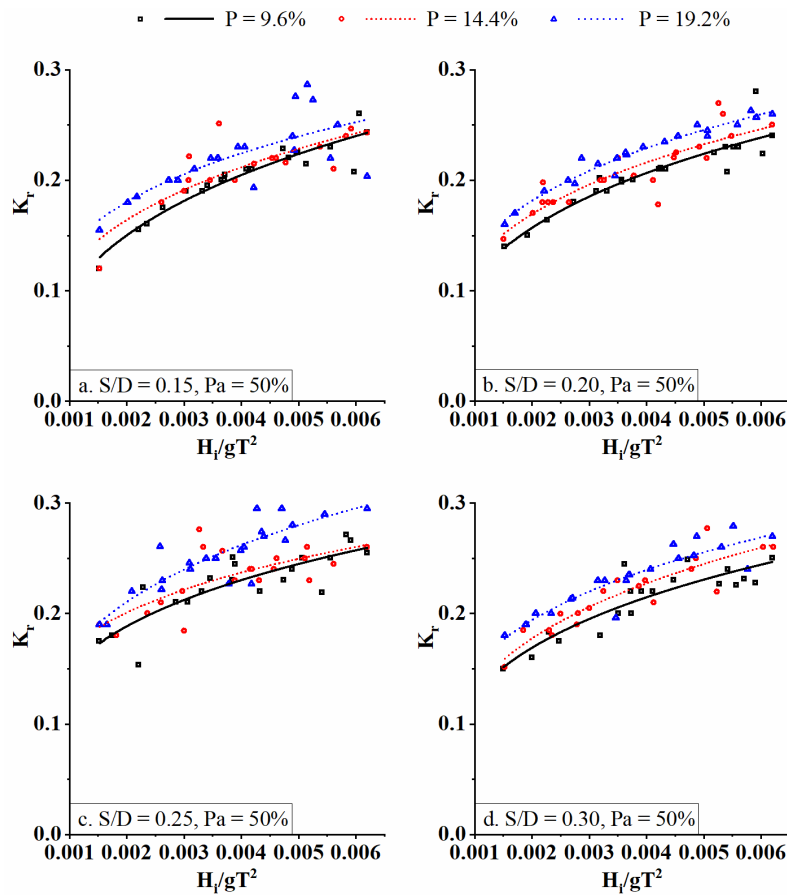
Figure 4.15 Influence of P on K_r for different S/D when Pa = 50% and h= 0.40 m (h/H = 0.769)

In general, it is observed that irrespective of the size of perforations, increasing the percentage of perforation resulted in the reduction of K_t, and increase of K_r and K_d. When S/D = 0.25, the K_t obtained for 19.2% is about 5.7% lesser than P = 9.6%, and 4.6% lesser than P = 14.4%. For the same case (S/D = 0.25), the K_r calculated for P = 19.2% is 11.5 to 14.7% higher than P = 9.6%, and 3.7 to 16% higher than P = 14.4%. Similarly, the K_d noted for P = 19.2% is 2.8 to 9.2% higher than P = 9.6%, and 1.8 to 7.4% higher than P = 14.4%.

Overall, a maximum reduction of 10.8% in K_t is achieved for P = 19.2% in comparison with P = 9.6%. As the percentage of perforation increases, the amount of water entering the pile head also increases. The observed behaviour may be due to higher turbulence

91
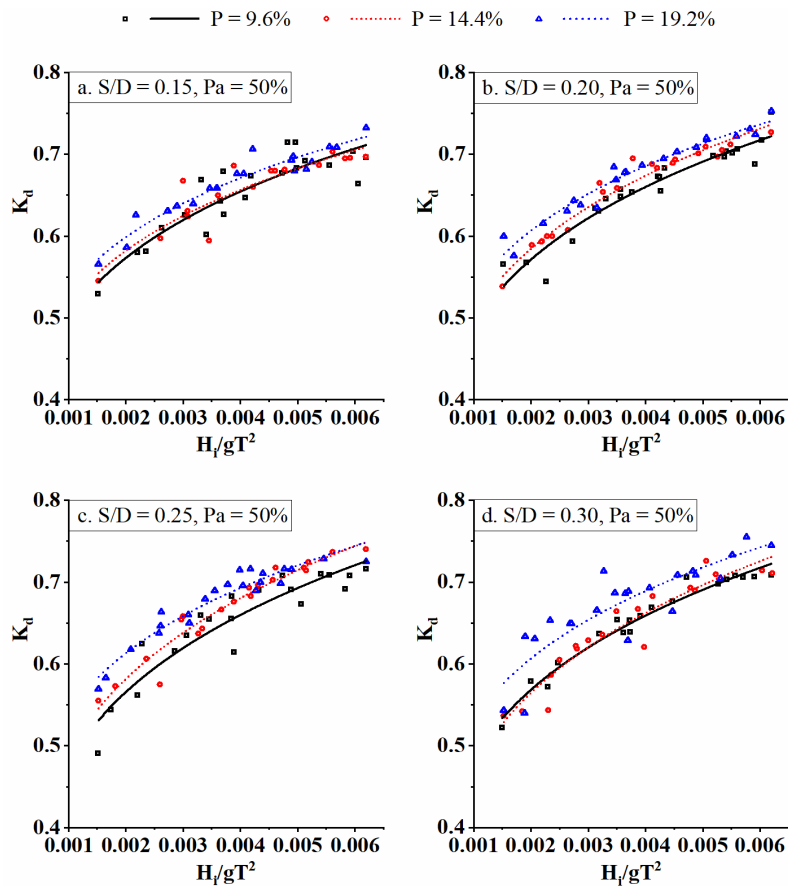
Figure 4.16 Influence of P on K_d for different S/D when Pa = 50% and h= 0.40 m (h/H = 0.769)

caused by the larger movement amount of water into CPH when P = 19.2% than the other cases (P = 9.6% and 14.4%).

In the perforated CPHB structure, water enters the hollow part of the pile head through both the perforations and top. This phenomenon induces turbulence, which contributes to additional energy losses. The number of perforations on the CPH surface increases with the increasing percentage of perforations (P) under constant Pa and S/D. As the percentage of perforation increases, the amount of water entering the CPH through perforations also increases. This results in higher turbulence and energy losses leading to enhanced wave attenuation. Therefore, it can be concluded that among the considered cases of percentage of perforations, P = 19.2% is more efficient in wave attenuation.

4.2.1.4 Size of perforations

The attenuation characteristics of the perforated CPHB are evaluated under four different sizes of perforations and the same is exhibited in Figure 4.17a. The different sizes of perforations studied are 0.0096 m, 0.0128 m, 0.016 m and 0.0192 m, which correspond to S/D ratios of 0.15, 0.20, 0.25 and 0.30, respectively. While analysing the effect of S/D, only the optimum cases of Pa and P (50% and 19.2%) are considered. Referring to Figure 4.17a, it is noted that irrespective of the size of perforations, the K_t values converge at lower wave steepness with a maximum variation of 2.5%. At higher wave steepness, the least K_t of 0.61 is noticed for the optimum relative pore size of 0.25. The K_t obtained for S/D = 0.25 is about 6.2%, 1.8% and 1.9% less than that of S/D = 0.15, 0.20 and 0.30, respectively. The K_r calculated for S/D = 0.25 is about 16%, 18.9% and 10.4% higher than S/D = 0.15, 0.20 and 0.30, respectively. For the same case (S/D = 0.25), the K_d is 3.6%, 0.3% and 0.6% higher than 0.15, 0.20 and 0.30, respectively. Hence, it can be stated that the perforations provided using an S/D of 0.25 are optimum compared to the other cases studied (S/D = 0.15, 0.20 and 0.30).
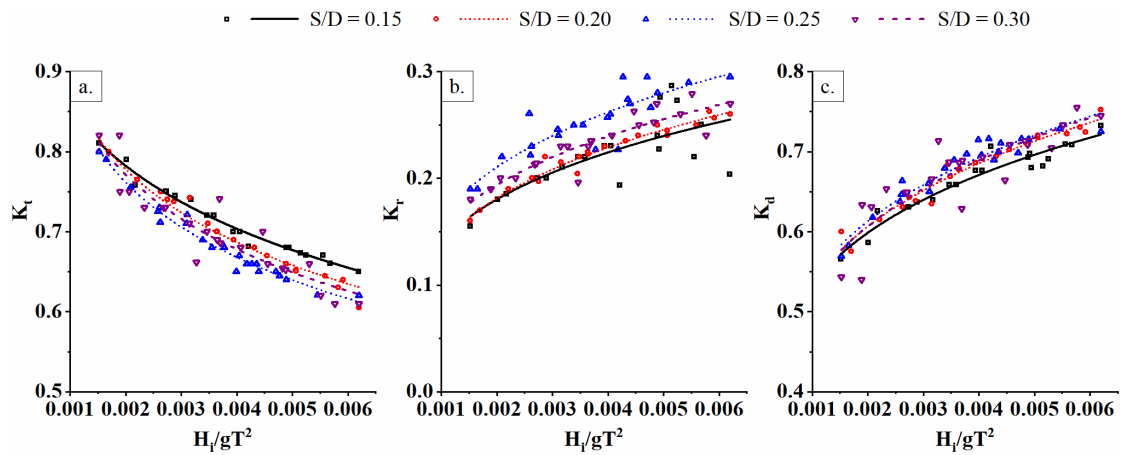
Figure 4.17 Influence of S/D on the performance of CPHB when Pa = 50%, P = 19.2% and h= 0.40 m (h/H = 0.769)

Perforations with a certain percentage of perforation can be configured on CPH, either using larger pores with a smaller number or vice versa. In the case of the smaller size of pores, the total quantity of water entering the CPH may be limited since the water

needs to get contracted and enter the CPH under high pressure. During the water discharge from CPH, the smaller perforations may take a longer duration with small-sized water jets. At the same time, larger perforations empty the CPH immediately after crossing of wave crest without any cognisable jet formations. The optimum size of perforation is the one that can balance both the entry and exit mechanism of water with the optimal rate to make the structure efficient. The perforations provided with the relative size (S/D) of 0.25 may be the optimum diameter because of which lower values of K_t with higher K_d are achieved. Overall, Pa = 50%, P = 19.2% with S/D = 0.25 can be inferred as the best performing configuration of CPH perforation, which resulted in a minimal K_t of 0.61 at higher wave steepness when the depth of water is 0.40 m (h/H = 0.769).

4.2.1.5 Depth of water

Examining the coastal protection structures at different water depths is essential because the structure may encounter different depths of water in actual sea conditions, which may arise due to base erosion, tide, and storm surge. In the present study, the best performing configuration of the perforated CPHB arrived in the previous section (section 4.2.1.4) is further investigated at 0.35 m (h/H = 0.673) and 0.45 m (h/H = 0.865) and the results are illustrated in Figure 4.18. Concerning Figure 4.18a, it is identifiable that reducing the depth of water by 0.05 m (0.40 m to 0.35 m) leads to an increase of K_t by about 6.2% at the gentle side and 9.6% at the steep side of the wave. However, increasing the depth of the water by 0.05 m (0.40 m to 0.45 m) enhanced the wave attenuation capability by 4.6% at higher wave steepness. Similarly, reducing the depth of water from 0.40 m to 0.35 m resulted in an average reduction of 3% in K_r and 7% reduction in K_d values. Further, increasing the depth of water from 0.40 m to 0.45 m resulted in an average reduction of 14.5% in K_r and 13.6% increase in K_d.

In the present work, wave attenuation occurs due to the combined resistance offered by the pile head and supporting circular pile. The maximum interaction between CPHB and the wave takes place when the wave crest propagates against the pile structure. The interaction of the pile head with waves is relatively higher and significant when
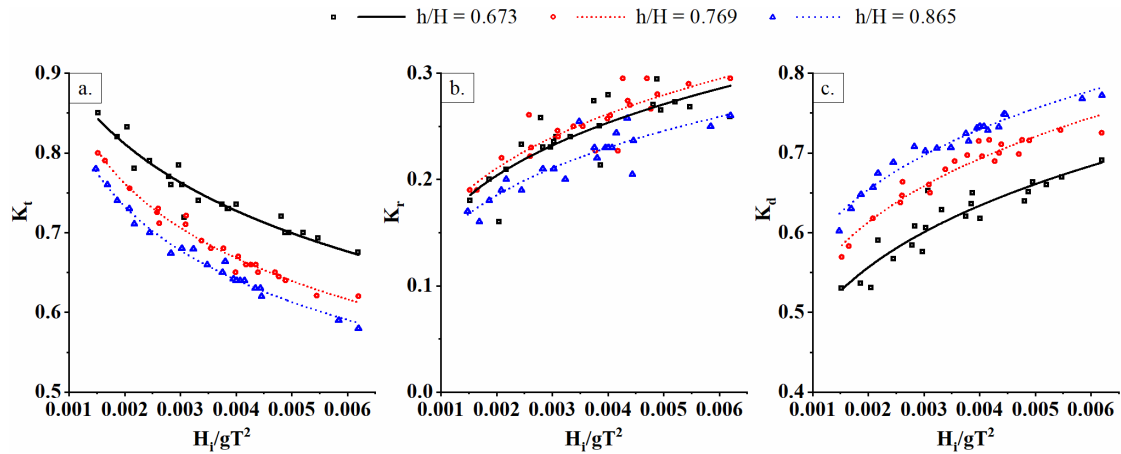
Figure 4.18 Influence of depth of water on the performance of CPHB when Pa = 50%, P = 19.2% and S/D = 0.25

compared to the supporting pile of the structure and also increases with the depth of water. The remaining portion of the pile structure interacts with the balanced portion of the wave phenomenon. Also, as the depth of water increases, the resistance offered by the CPH against wave propagation increases due to the conical shape offering increased areas of obstruction, bringing more and more perforations on CPH into action. In this context, the following scenarios in the wave structure interaction are explained.

For a minimum water depth of 0.35 m, a maximum of 41.6 to 65% of the pile head interacts with the wave for varying wave climates. Whereas, for a maximum water depth of 0.45 m, a maximum of 83.3 to 100% of the pile head interacts with the wave under varying wave climates. Further, when h = 0.35 m, about 70.8% of the CPH emerges with respect to the reference depth, which reduces to 50% at 0.40 m and 29.2% at 0.45 m. One of the unique wave attenuation features of the CPH is the plunging of larger waves inside the hollow CPH. Wherein at 0.35 m depth of water, the plunging mechanism does not occur even for larger waves due to the higher emergence of CPH. At 0.45 m, even the gentle waves plunge into the CPH, leading to higher wave attenuation with improved energy dissipation. In brief, a minimum K_t of 0.58 is recorded at higher wave steepness for the perforated CPHB with the structural configuration of $D/H_{max} = 0.4$, $Y/H_{max} = 1.5$ and $b/D = 0.1$ and perforation characteristics of Pa = 50%, P = 19.2% with S/D = 0.25 at a depth of water of 0.45 m.

95

4.2.1.6   Wave steepness

At coastal sites, the structure may be subjected to incident waves of different wave heights (H_i) and wave period (T). Therefore, studying the effect of wave steepness (H_i/gT^2) on the performance of the CPHB structure is beneficial in understanding the attenuation behaviour. From Figure 4.11 to Figure 4.18, it can be identified that the wave attenuation capability of the structure is more pronounced for the steep waves than the gentle waves by about 11.2% to 24.5%. For the optimum configuration, the K_t is reduced from 0.79 to 0.61 (22.8% reduction), where the smaller K_t corresponds to higher wave steepness and the larger K_t corresponds to lower wave steepness. In general, both the K_r and K_d are found to be increasing with the increasing wave steepness. For the same configuration, the K_r increased from 0.19 to 0.29 and K_d increased from 0.58 to 0.75.

The wave steepness parameter (H_i/gT^2) accounts for both wave height and wave period. The wave steepness parameter attains higher values when the wave height is larger with a shorter wavelength (smaller T) and vice versa. The probable reason for the aforementioned behaviour of CPHB is that steep waves have a tendency to be unstable, breaking at the smallest provocation and losing energy with minimal resistance to propagation, whereas gentle waves are quite stable. Additionally, a portion of the wave may plunge into the hollow conical pile head when it prevents steep waves from propagating, creating turbulence. While the gentle waves propagate around the structure without much noticeable resistance. The findings of the present study are in line with the results reported in the literature for conventional pile breakwater (Rao et al. 2002; Weele and Herbich 1972), suspended pipe breakwater (Mani and Jayakumar 1995) and pile breakwater with C-shaped suspended bars (Koraim et al. 2014).

Overall, the influence of perforation characteristics such as distribution of perforations (Pa), percentage of perforation (P) and size of perforation (S/D) are investigated by incorporating perforation on the surface of CPH through physical modelling studies. The wave attenuation capability of perforated CPHB appears to be maximum when Pa = 50%, P = 19.2%, and S/D = 0.25.

4.2.2 Comparison of hydraulic performance between non-perforated and perforated CPHB

The wave interaction between the non-perforated and the perforated CPHB with the optimum configuration is demonstrated in Figure 4.19. Comparatively lower transmitted waves can be observed for the perforated case than the non-perforated CPHB. The water moving out of the CPH holes generates additional turbulence on the seaside of the structure with higher reflection than the non-perforated CPHB. The same can be noticed in Figure 4.19. In order to identify the influence of perforations on the efficiency of the CPHB, the performance characteristics of the non-perforated and perforated CPHB are compared in Figure 4.20. Only the optimum perforated configuration (Pa = 50%, P = 19.2% and S/D = 0.25) is considered for the comparison study.
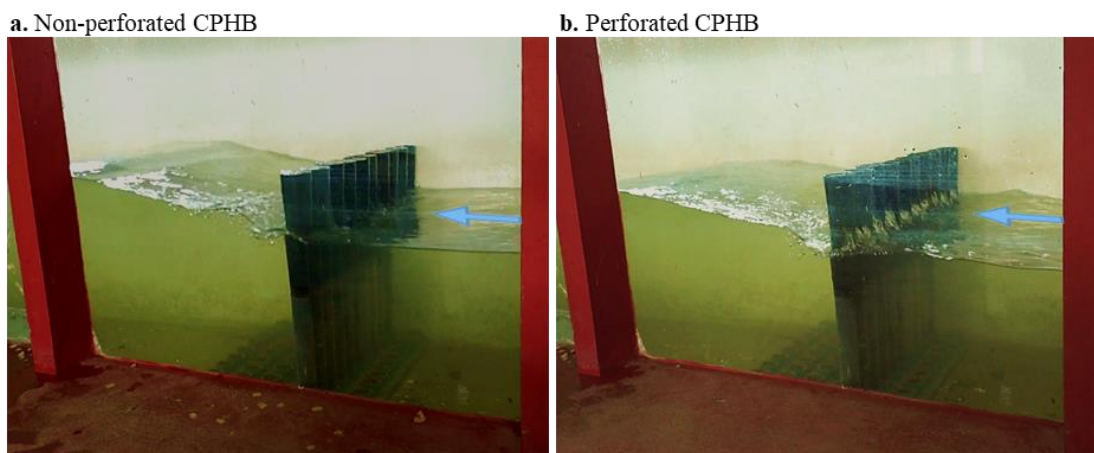
Figure 4.19 Wave interaction with the non-perforated and perforated CPHBs (Pa= 50%, P = 19.2 and S/D = 0.25) at 0.45 m depth of water

The enhancement in the attenuation capability of CPHB on introducing the perforations is clearly appealing in Figure 4.19 and Figure 4.20. The improvement in wave attenuation is less than 6% at lower wave steepness for all the considered depths of water. Whereas, a maximum reduction of 12.4% in K_t (0.662 to 0.58) is achieved at a depth of water of 0.45 m. An upsurge in both K_r and K_d is identified for the perforated structure irrespective of the depth of water. Introducing the perforations has almost doubled the K_r at 0.40 m depth of water.
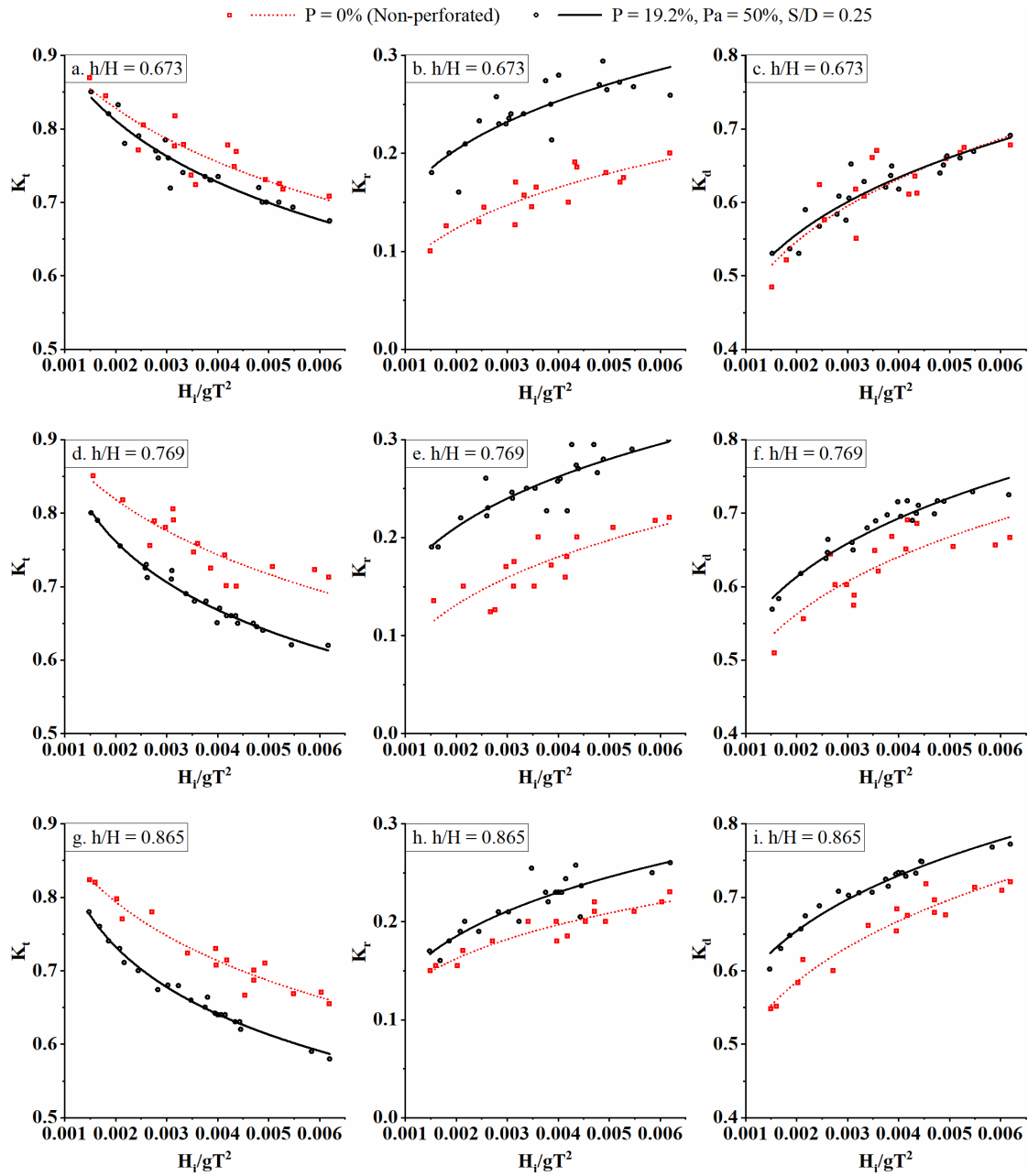
Figure 4.20. Comparison of performance between the non-perforated and perforated CPHBs

Also, a maximum increment of 13% in K_d is obtained at lower steepness when h = 0.45 m. The present study proved that providing the perforations on the surface of CPH is advantageous in achieving higher wave attenuation. It is also evident from the investigation that up to 12.4% reduction in K_t could be achieved by incorporating the

perforations on the surface of conical pile head. The obtained outcome is well matching with the literature (Kondo and Toma 1972; Rao et al. 2002; Rao and Rao 1999, 2001) where, 10% to 14% lesser K_t is reported through perforations.

4.2.3 Performance comparison of single row perforated CPHB with single and two rows of non-perforated CPHBs

In order to evaluate the performance characteristics of single row perforated CPHB, its performance is compared with those of single and two rows of non-perforated CPHBs in Figure 4.21. Under identical structural configuration (D/H_{max} = 0.4, Y/H_{max} = 1.5 and b/D = 0.1) and relative depth of water (h/H = 0.865), the performance of optimum configured perforated CPHB (Pa = 50%, P = 19.2% and S/D = 0.25) is compared with best performing non-perforated single and two rows (B/D = 0.4) of CPHB. For single row non-perforated CPHB, the K_t, K_r and K_d range between 0.66 to 0.82, 0.15 to 0.22 and 0.54 to 0.72, respectively. Introducing the second row of non-perforated CPHB with staggered arrangement resulted in lower K_t (0.58 to 0.77) with increased K_r (0.16 to 0.24) and K_d (0.64 to 0.79). However, depending on site conditions, there may be difficulties in driving/constructing two rows of closely spaced piles. To ward off such possibilities, perforations are introduced on the pile head surface, which resulted in reduced K_t (0.58 to 0.78) with higher K_r (0.17 to 0.265) and K_d (0.62 to 0.78).
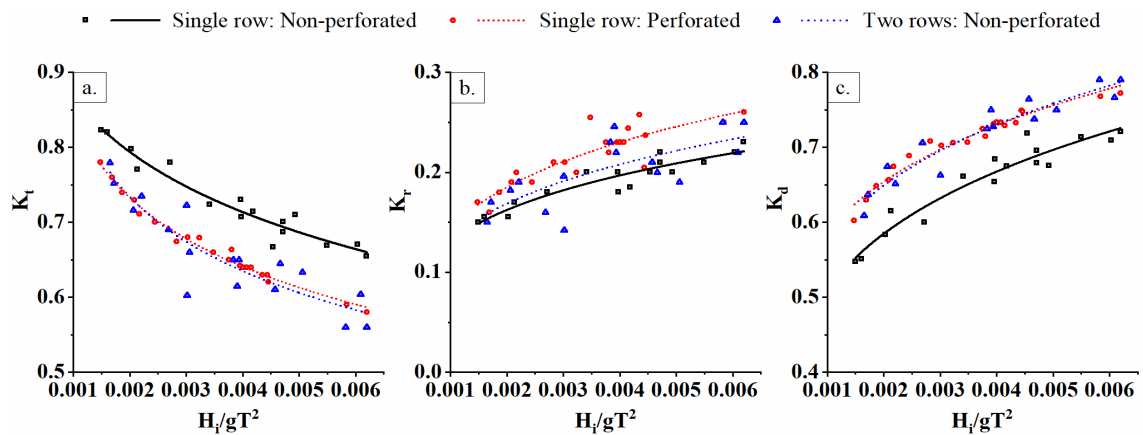
Figure 4.21 Performance comparison of single row perforated CPHB with single and two rows of non-perforated CPHBs

It is evident from the study that the performance of single row perforated CPHB and two rows of non-perforated CPHB are comparable. Therefore, it can be stated that introducing perforations with optimal configurations on a single row CPH surface is as efficient as introducing a second row of non-perforated piles.

4.2.4 Key findings

The following observations are recorded based on the physical model investigations carried out on the perforated CPHB.

1. The distribution of perforation (Pa) on CPH, percentage perforation (P) and the size of perforation (S/D) play a significant role in influencing the hydraulic performance of the perforated CPH.

2. Providing the perforations on 50% of the surface area of CPH (Pa = 50%) is found to be optimum; any other value of Pa resulted in reduced wave attenuation.

3. For all the considered combinations of Pa and S/D, increasing the percentage of perforations resulted in the reduction of K_t, and increase of K_r and K_d.

4. Perforations provided using an S/D of 0.25 are optimum.

5. The wave attenuation capability of the structure is more pronounced for the steep waves than the gentle waves by about 11.2 to 24.5%.

6. The wave attenuation capability of the proposed perforated single row CPHB structure is maximum when the Pa = 50%, P = 19.2% and S/D = 0.25.

7. A minimum K_t of 0.58 associated with a maximum K_r of 0.265 and K_d of 0.78 is realised for the above CPHB at a depth of water of 0.45 m.

8. The optimum configuration of perforated single row CPHB exhibits increased K_t by up to 12.4% when compared with non-perforated structure.

9. Introducing perforations with optimal configurations (i.e. Pa = 50%, P = 19.2% and S/D = 0.25) on a single row CPH surface is as efficient as introducing a second row of non-perforated piles.

4.3 NUMERICAL MODELLING OF CPHB

In the present study, only selected configurations of non-perforated and perforated CPHB are simulated using an open-source software REEF3D. The numerical results are validated by comparison with experimental data obtained. Before carrying out simulations of CPHB, the quality of the generated waves is examined under different grid sizes and CFL numbers to determine their optimal values for the present study. The range of grid sizes and CFL numbers employed are in accordance with Bihs et al. (2016a).

4.3.1 Validation of wave generation

The validation of the reconstructed wave is carried out in a two-dimensional (2D) NWT without placing the structure at a water depth of 0.40 m (h/H = 0.769). Since the reconstructed waves are unidirectional, the validation study is conducted in a 2D NWT. The width of the 2D tank is kept as one cell size with symmetric boundary conditions on both the side planes. The 2D tank is modelled with symmetric boundary conditions on both side planes. No turbulence modelling is used for simulations in the numerical wave tank without structures. To evaluate the accuracy of the free surface data, the experimental and numerical profiles for different grid sizes and CFL numbers are compared. Numerical simulations with finer grid sizes and smaller CFL numbers result in more accurate results, although with higher computational time.

To maintain the consistency between physical and numerical modelling, the time series data from the experiments are used to generate the same waves in NWT. The quality of wave generation is verified for steep ($H_i = 0.16$ m, T = 1.8 s) and gentle ($H_i = 0.06$ m, T = 2.0 s) wave heights for various grid sizes, as shown in Figure 4.22. For the grid size optimisation, the uniform grid sizes dx= 0.08 m, 0.04 m, 0.02 m and 0.01 m are considered while keeping the CFL number constant at 0.1. Table 4.1 presents the root-mean-square error (RMSE) values obtained by comparing the experimental data with the numerically reconstructed wave surface elevation.
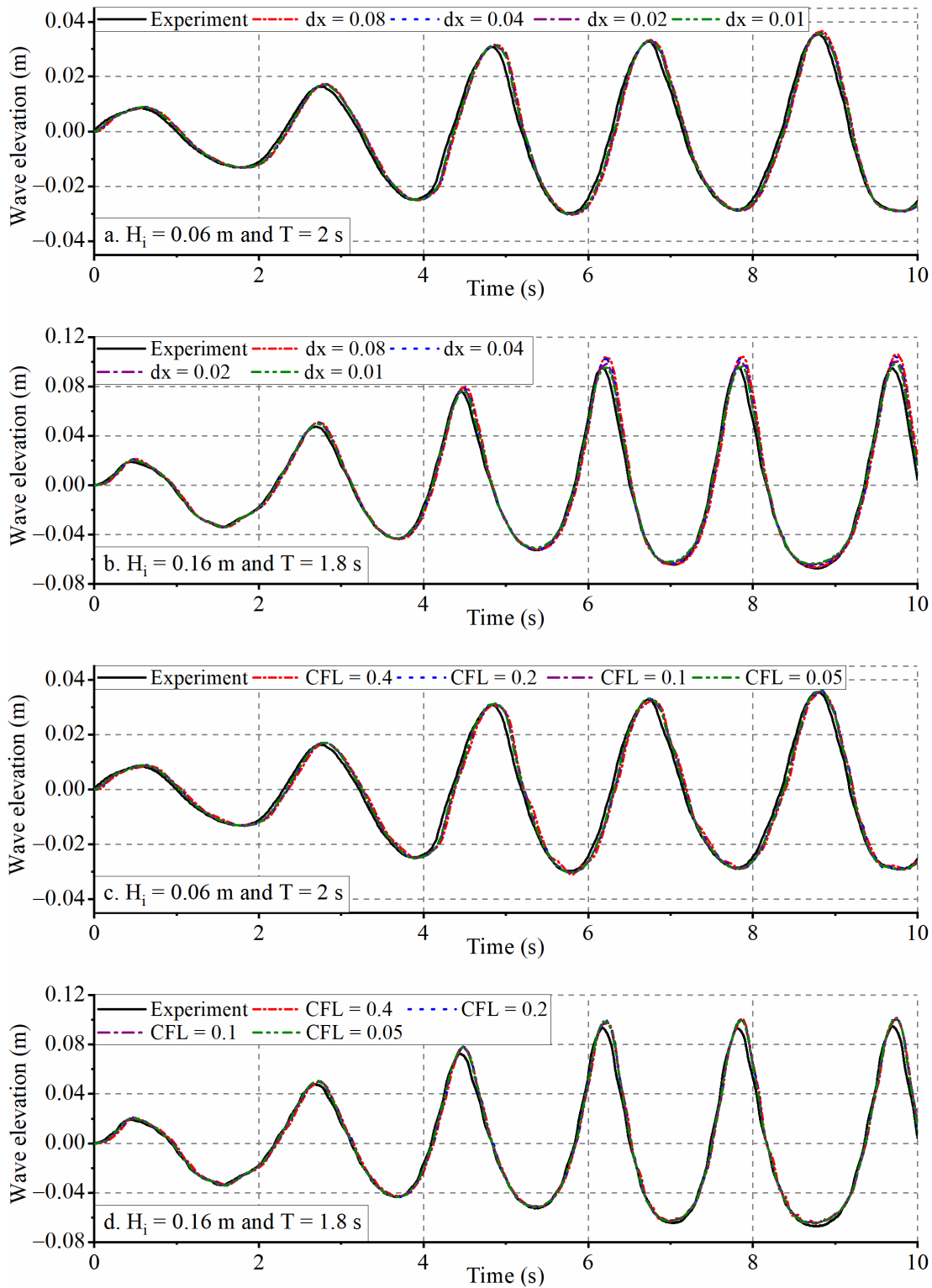
Figure 4.22 Influence of grid size (dx) and CFL number on the reconstruction of monochromatic waves

The grid size analysis clearly shows that lowering the grid size from 0.08 m to 0.04 m resulted in a reduction in the RMSE values. The free surface elevation is found to agree well with the measured data for a grid size of 0.02 m. Further reducing the grid size from 0.02 to 0.01 m shows a negligible improvement with higher computational time. It can be concluded from the grid refinement study that a grid size of 0.02 m is sufficient for accurate wave generation with a maximum RMSE of 0.0053 m. Therefore, dx = 0.02 m is used for further investigating the influence of CFL number on wave generation. The CFL numbers considered for the sensitivity study are 0.4, 0.2, 0.1 and 0.05, as shown in Figure 4.22 and the associated errors are listed in Table 4.1.

Table 4.1 Accuracy comparison between numerical and experimental wave profile

T (s)	H (m)	Grid size study (with CFL = 0.1)		CFL study (with dx = 0.02 m)	
		dx (m)	RMSE (m)	CFL No.	RMSE (m)
2.0	0.06	0.08	0.0033	0.40	0.0025
		0.04	0.0021	0.20	0.0025
		0.02	0.0020	0.10	0.0023
		0.01	0.0018	0.05	0.0023
1.8	0.16	0.08	0.0085	0.40	0.0068
		0.04	0.0053	0.20	0.0063
		0.02	0.0053	0.10	0.0055
		0.01	0.0036	0.05	0.0045

Similar to the grid refinement study, a CFL number of 0.1 appears to be optimal, where increasing the CFL number affects wave quality while decreasing the same resulted in negligible improvement and increased computational time. From the above sensitivity study on grid size and CFL number, it is clear that simulating the waves with a CFL number of 0.1 with a grid size lesser than or equal to 0.02 m results in an accurate reconstruction of free surface elevation. The computed RMSE values of the reconstructed waves are reasonable with reference to Aggarwal et al. (2018).

Further, it is essential to ensure that the quality of wave generation in 2D (11 m x 0.02 m x 0.8 m) and 3D (11 m x 0.355 m x 0.8 m) NWT is consistent. Hence, a simulation is run in a 3D NWT for $H_i = 0.16$ m and $T = 1.8$ s case by employing optimum grid size and CFL number (dx = 0.02 m and CFL = 0.1). It is found that the free surface elevations calculated in the 2D and the 3D NWT are in agreement.

While simulating the CPHB, a non-uniform grid distribution based on a Cartesian system is adopted in the present work to reduce computational effort. In the x-direction, a coarser grid size of 0.02 m is maintained at the generation and absorption zone. In the numerical simulations, a grid with a size of 0.004 m is employed to accurately characterise the CPHB structure. The grid sizes are varied gradually from 0.02 m to 0.004 by employing a sine-based stretching function (Figure 4.23). At the same time, a uniform grid size of 0.004 m is adopted in both y and z-directions. Using these non-uniform grids (Figure 4.23), a without-structure simulation is performed in 2D NWT to assess the reliability of wave generation. The free surface elevations of the 2D uniform grid and 2D non-uniform grid are seen to be in harmony. Therefore, it can be concluded that the accuracy of wave generation is unaffected by the non-uniform grid distribution adopted for the 3D NWT simulations.
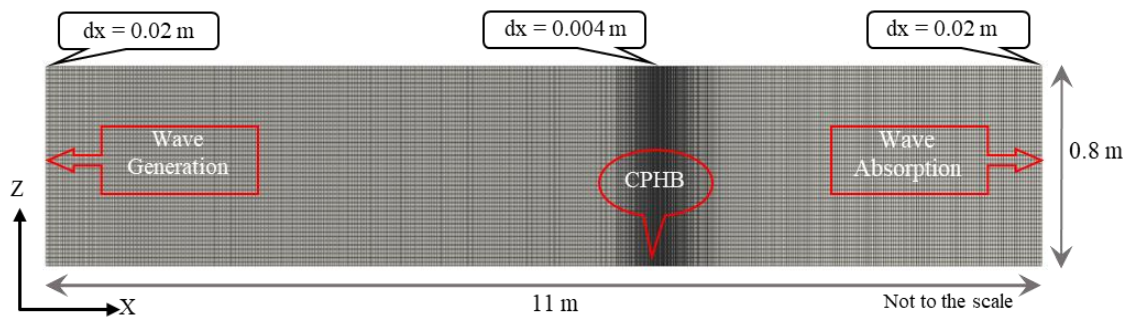
Figure 4.23 Typical representation of non-uniform grid in the numerical wave tank

4.3.2 Hydraulic performance of CPHB

Initially, the numerical investigation is conducted for non-perforated CPHB under monochromatic waves. The influence of pile head diameter on non-perforated CPHB

is investigated using two different diameter pile heads (D/H_{max} = 0.4 and 0.5) with constant Y/H_{max} of 1.5 and b/D of 0.1 at 0.40 m water depth (h/H = 0.769). The perforations with the optimum size and arrangement (Pa = 50%, P = 19.2%, and S/D = 0.25) obtained through physical modelling in the previous section (Section 4.2) are used for the perforated structure. The results of the non-perforated and perforated CPHBs are validated with the experimental data and analysed to arrive at the best-performing configuration of CPHBs. The study is carried out in various wave energy regions with intermediate water depth conditions. The different combinations of wave heights and periods considered for the simulation of monochromatic waves are listed in Table 4.2. The cases are selected such that the wave steepnesses (H_i/gT^2) are of the same range as that in the experiments.

Table 4.2 Simulated cases of monochromatic waves

Cases	T (Sec)	H_i (m)	L (m)	H_i/gT^2	Wave theory
M1	1.4	0.12	2.39	0.00624	Stokes 3rd order
M2	1.6	0.14	2.84	0.00557	Stokes 3rd order
M3	1.8	0.16	3.27	0.00503	Cnoidal
M4	1.8	0.10	3.27	0.00315	Stokes 3rd order
M5	2.0	0.16	3.70	0.00408	Cnoidal
M6	2.0	0.10	3.70	0.00255	Stokes 3rd order
M7	2.0	0.08	3.70	0.00204	Stokes 2nd order
M8	2.0	0.06	3.70	0.00153	Stokes 2nd order

4.3.2.1   Validation of numerical results with experimental data

The K_t, K_r and K_d of two non-perforated pile heads (D/H_{max} = 0.4 and 0.5) with Y/H_{max} = 1.5 and b/D = 0.1 at h = 0.40 m (h/H = 0.769) are compared to experimental data in Figure 4.24. Figure 4.25 presents the validation of numerical results with the experimental data for the case of perforated CPHB with D/H_{max} = 0.4, Y/H_{max} = 1.5, b/D = 0.1, Pa = 50%, P = 19.2%, S/D = 0.25 and h = 0.40 m. Best fit lines are drawn to gain a better understanding and interpretation of the results.
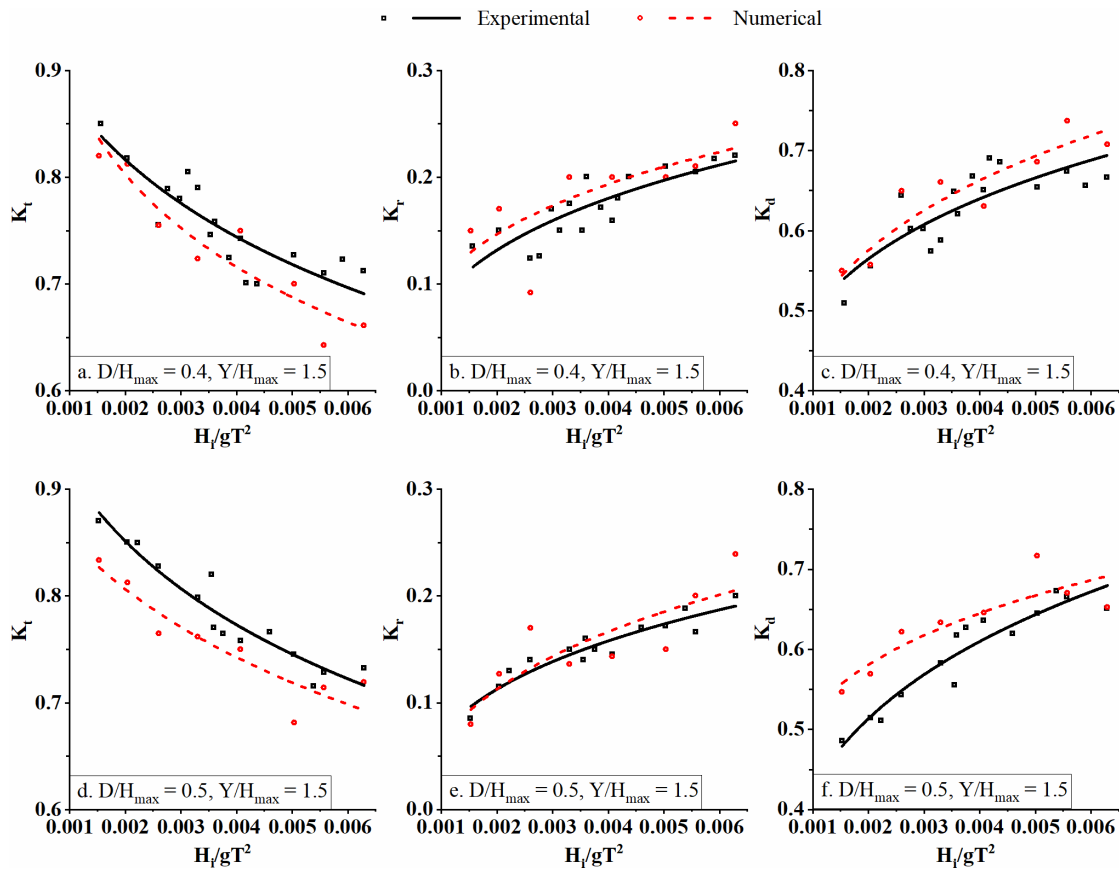
Figure 4.24 Comparison of numerical and physical modelling results for various D/H$_{max}$ of non-perforated CPHB with Y/H$_{max}$ = 1.5 and b/D = 0.1 at h = 0.40 m (h/H = 0.769)

The trend lines plotted for the numerical results of both non-perforated and perforated CPHB match with those of the experimental results to a reasonable extent. In the case of non-perforated CPHB, the numerical results are slightly under predicted for K$_t$ (less than 4%) and over predicted for K$_r$ and K$_d$ (less than 9%) for both the cases of D/H$_{max}$. For the perforated CPHB, the variation is slightly higher (up to 12%) compared to the non-perforated structure. The RMSE values calculated by comparing the experimental and numerical results are summarised in Table 4.3. The comparison of results shows that the numerically determined performance characteristics of both non-perforated and perforated CPHB are in relatively good agreement with the experimental data.
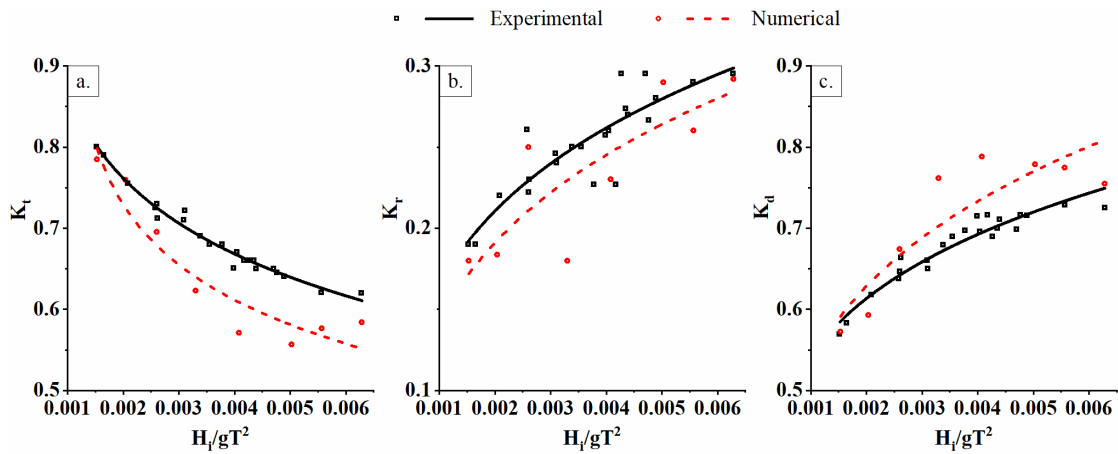
Figure 4.25 Comparison of numerical and physical modelling results for perforated CPHB

Table 4.3 Comparison of experimental and numerical results using RMSE

CPHB	D/H$_{max}$	RMSE		
		K$_t$	K$_r$	K$_d$
Non-perforated	0.4	0.0313	0.0142	0.0242
	0.5	0.0355	0.0090	0.0476
Perforated	0.4	0.0480	0.0170	0.0422

4.3.2.2   Effect of relative pile head diameter

Simulations of two different diameters (D/H$_{max}$ = 0.4 and 0.5) of non-perforated CPHB are performed to determine the influence of the pile head diameter and to arrive at the best performing configuration. Figure 4.26 presents the simulated images of the wave crest interaction with non-perforated CPHB for various D/H$_{max}$ at the same time step (t = 9.10 s). Due to the larger number and smaller spacing of pile heads, the horizontal velocity of waves (u$_x$) is obstructed to a significant amount in the case of D/H$_{max}$ = 0.4 compared to that for D/H$_{max}$= 0.5 (Figure 4.26). To overcome the obstruction, a relatively considerable amount of waves may enter into the hollow portion of the pile head for the D/H$_{max}$ = 0.4 case than for D/H$_{max}$ = 0.5. The water that enters the perforated pile head flushes out and results in additional energy loss, as demonstrated
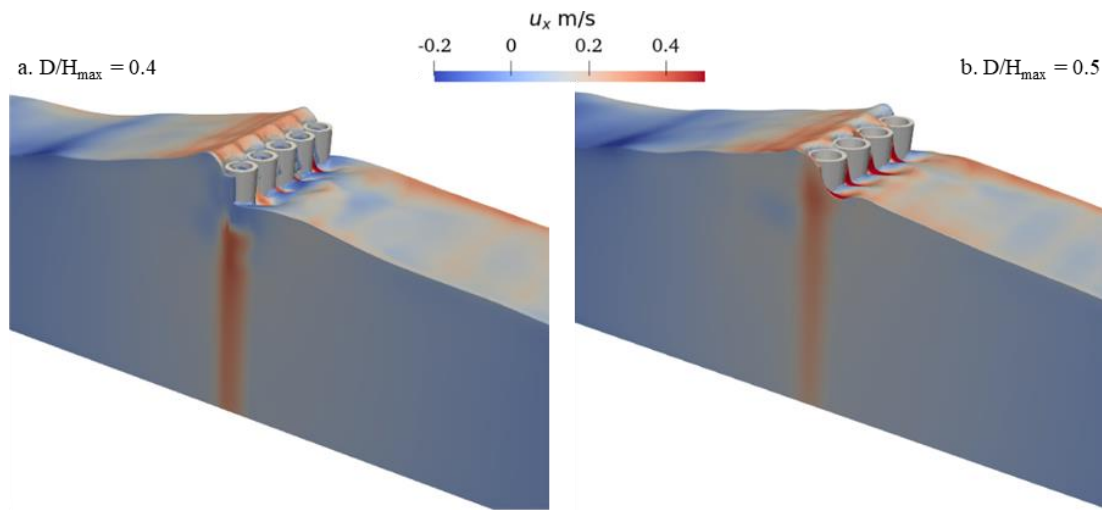
Figure 4.26 Simulated free surfaces with velocity magnitude (m/s) during the wave-structure interaction for different D/H$_{max}$ of non-perforated CPHB

in Figure 4.26a. When D/H$_{max}$ = 0.5, a relatively higher quantity of waves are transmitted between the pile heads with an intensified velocity, as seen in Figure 4.26b. The CPHB with D/H$_{max}$ = 0.4 configuration has a higher number of piles and about 9.8% higher blockage area compared to D/H$_{max}$ = 0.5. The higher blockage area increases the effectiveness in the obstruction of wave energy, leading to wave breaking over the structure along with higher wave reflection.

The plan view of the particle path lines during the propagation of the wave crest over the non-perforated CPHB is presented in Figure 4.27. When D/H$_{max}$ = 0.4, the horizontal propagation of the incident wave at the free surface is obstructed by the structure to a substantial extent. Whereas, for D/H$_{max}$ = 0.5, the wave easily propagates through the larger gaps without a significant reduction in velocity. In addition, the formation of vortices is clearly noticed on the lee side of the structure for D/H$_{max}$ = 0.4 (Figure 4.27a), which contributes to energy losses. When it comes to D/H$_{max}$ = 0.5, the energy dissipation through vortex formation is reduced, possibly due to lower blockage resulting from a long distance between the pile heads.
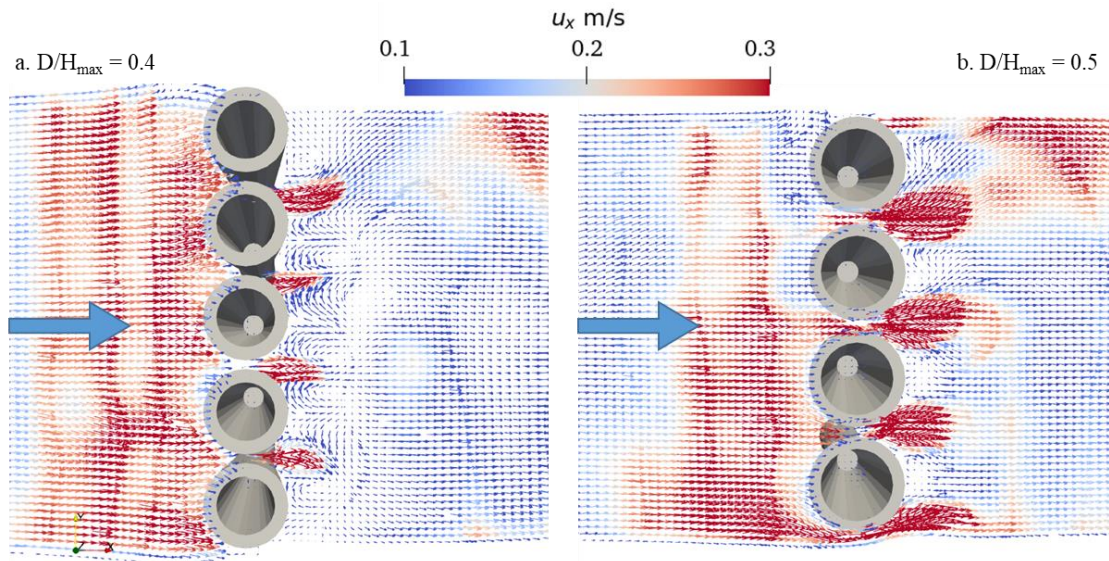
Figure 4.27 Plan view of particle path lines during the interaction of the wave crest with the non-perforated CPHB for different D/H$_{max}$ at t = 9.10 s
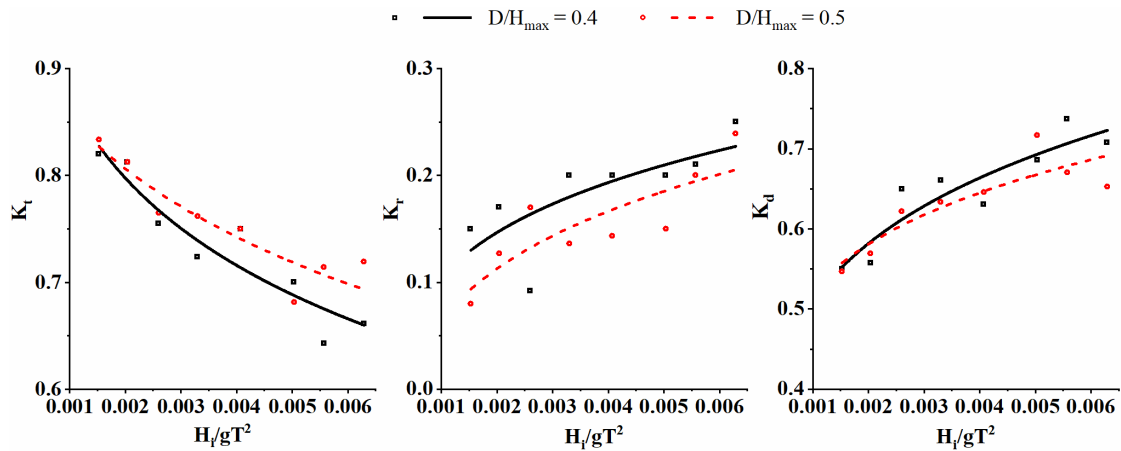
Figure 4.28 Performance comparison between different diameters of non-perforated CPHB with Y/H$_{max}$ = 1.5

The wave attenuation characteristics determined by numerical modelling are compared in Figure 4.28 to examine the influence of pile head diameter (D/H$_{max}$). For a higher wave steepness, D/H$_{max}$ = 0.4 exhibits about 8% lower K$_t$, 18.2% higher K$_r$ and 6% higher K$_d$ compared to D/H$_{max}$ = 0.5. At lower wave steepness, it is noticed that the K$_t$

and K_d are comparable. The lowest K_t of 0.64 is obtained for $D/H_{max} = 0.4$ at a higher wave steepness along with K_r of 0.22 and K_d of 0.73.

4.3.2.3   Effect of perforations

The key factors responsible for wave attenuation in pile breakwater are inertial resistance, contraction, vortex shedding and wave reflection. The idea behind providing a higher obstruction area near the free surface is to distort the orbital motion of the waves, which is maximum at the free surface. Figure 4.29 clearly demonstrates the changes in horizontal component of the orbital velocity (u_x) as the wave interacts with the non-perforated CPHB at different time instances (t). The increased area of the piles (CPHB) contributes to a comparatively higher obstruction than conventional pile breakwaters, due to which the horizontal velocity of the waves is obstructed (Figure 4.29b). Due to the obstruction, a part of the wave may flow through the gaps between the pile heads with an intensified velocity. Another part may flow over the pile head and enter the hollow portion of CPH (Figure 4.29c). This results in turbulence and energy dissipation along with partial reflection of waves, as presented in Figure 4.29c.

The gentle waves flow around the CPHB structure without entering the hollow part of the CPH. Therefore, to increase the wave-structure interaction, perforations are incorporated on the seaside surface of the CPH so that the waves, irrespective of their steepness, enter the hollow portion of the pile head. Under wave trough incidence, the water entered during crest incidence flows back through the perforations and confronts the following incident wave crest, creating a disturbance on the seaside of the structure. The best configuration of perforations (Pa = 50%, S/D = 0.25 and P =19.2%) obtained through physical modelling in the previous section (Section 4.2) is used in the present study. Figure 4.30 compares the changes in the horizontal velocity during the wave trough interaction with the non-perforated and perforated CPHB. It is noticed (Figure 4.30a and b) that water that entered the CPHB flows out of perforations, causing

110
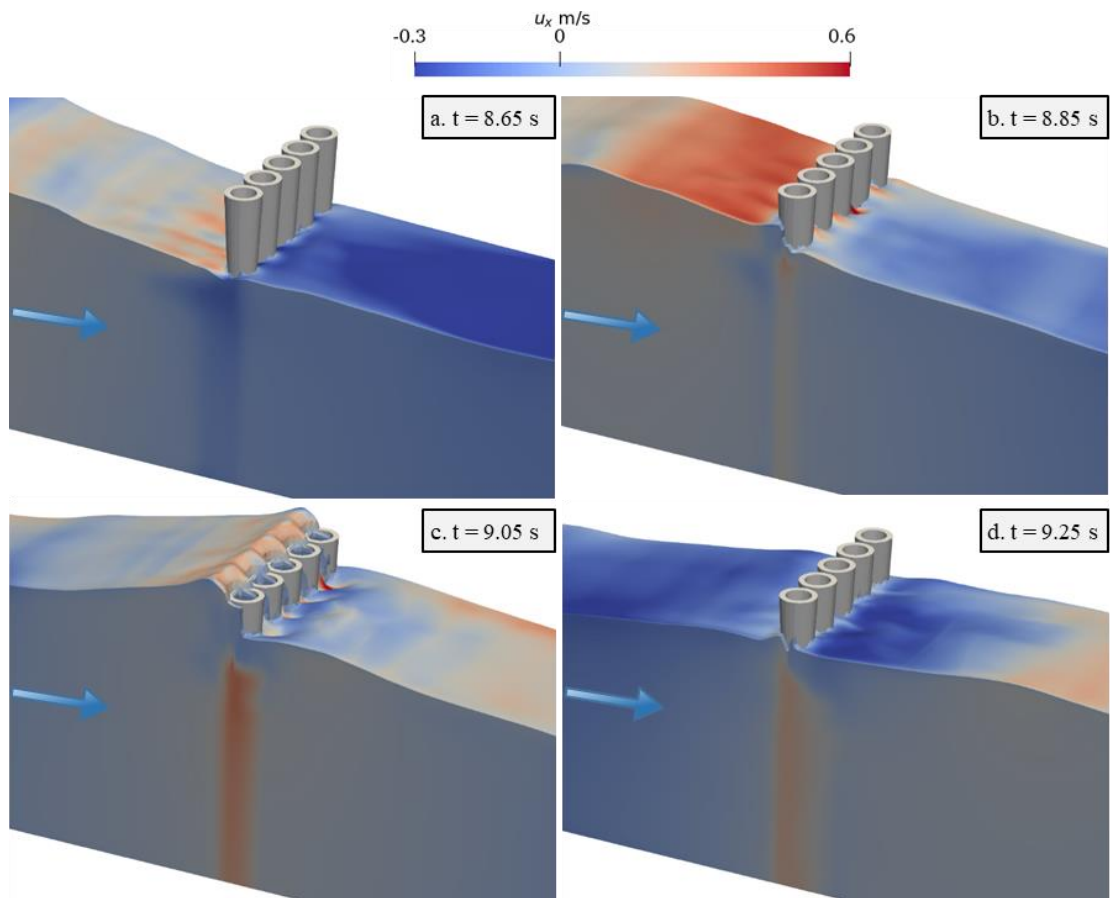
Figure 4.29 Wave interaction with the non-perforated CPHB (D/H$_{max}$ = 0.4) at different time instances (t)

comparatively higher reflection and increased turbulence on the seaside of the structure compared to the non-perforated structure.

The performance characteristics of non-perforated and perforated CPHB are compared in Figure 4.31 to determine the influence of the perforations. Introducing the perforations on the CPH reduces K_t by about 5% to 16.5%. The values of K_r and K_d increased by about 27.25% and 10.28% on average, respectively. A minimum K_t of 0.55 is calculated for the perforated CPHB at higher wave steepness, associated with a K_r and K_d of 0.28 and 0.81, respectively. The observed performances of the non-perforated and perforated CPHB are in agreement with the present experimental data.
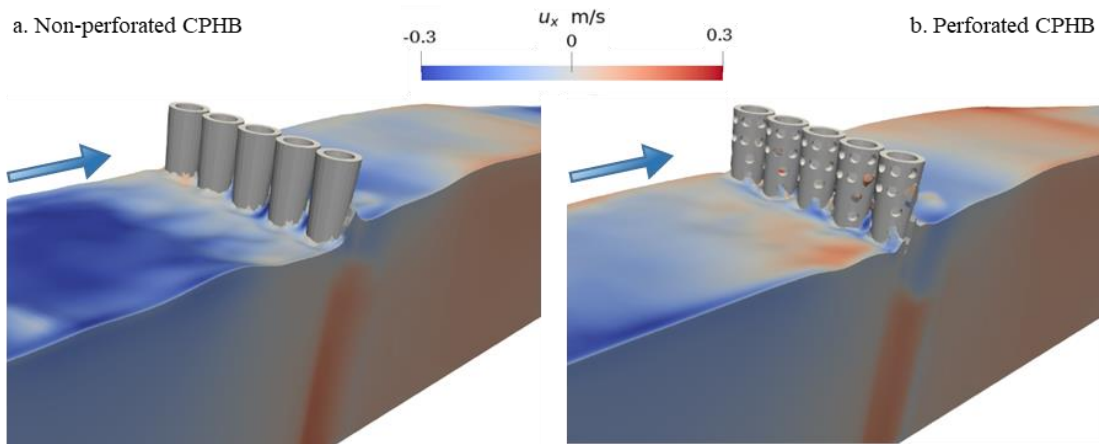
Figure 4.30 Simulated free surfaces of non-perforated and perforated CPHB cases with velocity magnitude (m/s)
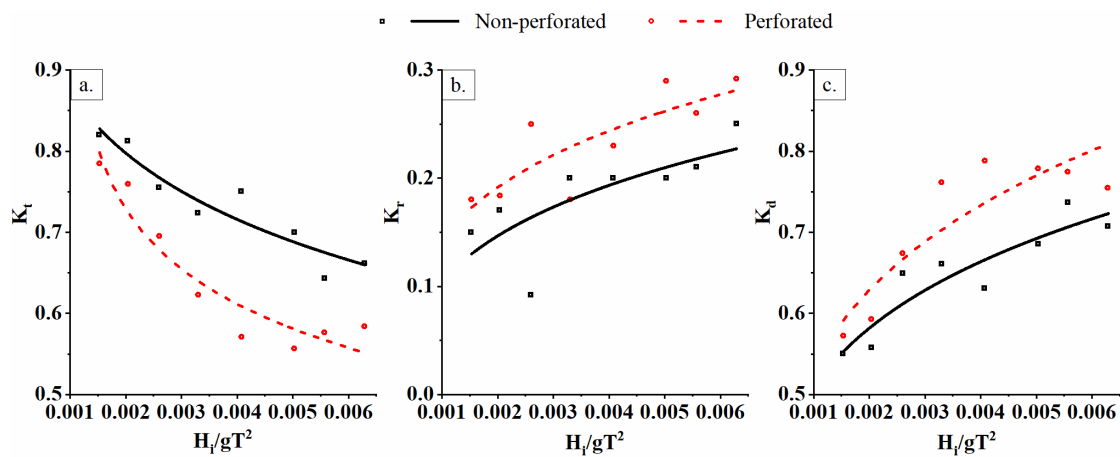
Figure 4.31 Performance comparison between non-perforated and perforated CPHB

The validation of the numerical results with the experimental data shows that the REEF3D is reproducing reliable results with acceptable RMSE values. Overall, the numerical model of the CPHB mimics the physical phenomenon of experimental studies.

4.3.3 Key findings

The numerical investigation of the performance characteristics of conical pile head breakwaters is carried out using the open-source CFD tool REEF3D. The following are the key findings drawn from the analysis of the results:

1. A sensitivity study on grid size and CFL number indicated that simulating the waves with a CFL number of 0.1 with a grid size lesser than or equal to 0.02 m results in an accurate reconstruction of free surface elevation.

2. In general, K_t is found to be indirectly proportional to the wave steepness, whereas K_r and K_d exhibit the opposite pattern.

3. For non-perforated CPHB, the numerical results are slightly under predicted for K_t (less than 4%) and over predicted for K_r and K_d (less than 9%) for both the cases of D/H_{max}. For the perforated CPHB, the variation is slightly higher (up to 12%) compared to the non-perforated structure.

4. The comparison between the experimental and numerical results indicates that the numerically determined performance characteristics of both non-perforated and perforated CPHB are in relatively good agreement with the experimental data.

5. For a higher wave steepness, $D/H_{max} = 0.4$ exhibits about 8% lower K_t, 18.2% higher K_r and 6% higher K_d compared to $D/H_{max} = 0.5$.

6. At lower wave steepness, it is noticed that the K_t and K_d are comparable.

7. The lowest K_t of 0.66 is obtained for non-perforated CPHB with $D/H_{max} = 0.4$ at a higher wave steepness along with K_r of 0.23 and K_d of 0.72.

8. Introducing perforations with the optimum configuration (Pa = 50%, S/D = 0.25 and P = 19.2%) on the CPHs enhanced the transmission capability of the CPHB by about 5% to 16.5%. The values of K_r and K_d increased by about 27.25% and 10.28% on average, respectively.

9. Validation of the numerical results with the experimental data shows that REEF3D produces comparable results with acceptable RMSE values.

4.4 EMPIRICAL EQUATIONS

4.4.1 Development of equations

Predicting the performance characteristics of CPHB quickly using empirical equations would be handy from the engineering point of view. Therefore, a set of empirical equations is derived for the K_t and K_r of CPHB (equations 4.1 and 4.2) using the data fitting technique. The experimental data of the present study on non-perforated and perforated CPHB are used to develop the empirical equations. 70% of the data are used as training set and the remaining 30% is used to evaluate the model performance (Nguyen et al. 2021). In this process, several equations are obtained and the best equations are chosen based on the coefficient of determination (R^2) and relative root mean square error (RrmsE) values. The RrmsE is calculated by employing a similar method followed by Rattanapitikon (2007) and Nam et al. (2017). These empirical equations are applicable for both non-perforated and perforated CPHBs. The equations are expressed in terms of the structural (D/H_{max}, Y/H_{max}, $Y/2h$, b/D and B/D) and perforation characteristics (Pa, P, and S/D) of CPHB along with wave parameters (H_i/gT^2). The developed equations for K_t and K_r are given by,

$$K_t = e^{\left[S_{Kt}\right]} - K_{tp} \tag{4.1}$$

$$\text{Where, } S_{Kt} = -\frac{32\, m_6}{m_1} - \frac{m_4}{157\, m_3} + \frac{1076\, m_6^2}{m_1^2\, m_2} + \frac{m_1^2\, m_4\, m_5}{1076\, m_2\, m_6}$$

$$K_r = S_{Kr} + K_{rp} \tag{4.2}$$

$$\text{Where, } S_{Kr} = \frac{m_2\, m_6}{13\, m_1 m_6 + m_1 m_3 m_5 - m_4 m_5 m_6 - 3\, \bar{m}_3^3 m_5}$$

Where, $m_1 = D/H_{max}$, $m_2 = Y/H_{max}$, $m_3 = b/D$, $m_4 = N + B/D$, $m_5 = Y/2h$, $m_6 = H_i/gT^2$, $m_7 = Pa$ in %, $m_8 = P$ in % and $m_9 = S/D$. N is the number of CPHB rows

placed at a clear distance of B, which is assumed to be zero for a single row of CPHB (i.e. N = 1). K_{tp} and K_{rp} are the perforation factors of wave transmission and reflection coefficients, respectively, which are given by,

$$
K_{tp} \begin{cases} = 0 \ \dots\dots\dots\dots\dots\dots\dots\dots\dots\dots\dots\dots\dots\dots\dots \text{ For non-perforated CPHB} \\[2em] = m_5\,m_9^2 \ + \dfrac{m_6\,m_7\,m_8}{28} - \dfrac{m_5^3\,m_6\,m_7^2\,m_8}{21} - 8\,m_6 \ \dots \text{ For perforated CPHB} \end{cases}
$$

$$(4.3)$$

$$
K_{rp} \begin{cases} = 0 \ \dots\dots\dots\dots\dots\dots\dots\dots\dots\dots\dots\dots\dots\dots\dots \text{ For non-perforated CPHB} \\[2em] = 4\,m_6\,m_9 + m_5^4\,m_8 - \dfrac{m_5\,m_7^2}{26412} - e^{\left(\frac{-m_7}{7}\right)} \ \dots\dots\dots \text{ For perforated CPHB} \end{cases}
$$

$$(4.4)$$

4.4.2 Validation of equations

The experimental data of the present study on non-perforated and perforated CPHBs are considered to validate the potential of the developed empirical equations. The validation of empirical equation results with the experimental data is presented in Figure 4.33 and Figure 4.32 for non-perforated and perforated CPHBs, respectively. The R^2 and RrmsE values computed for the K_t and K_r of proposed empirical equations are listed in Table 4.4. A reasonably good agreement is obtained between the predicted values and experimental data for both non-perforated and perforated CPHBs. Hence, it can be stated that the proposed empirical equations are reliable in predicting the K_t and K_r of both non-perforated and perforated CPHBs within the limits of test conditions.
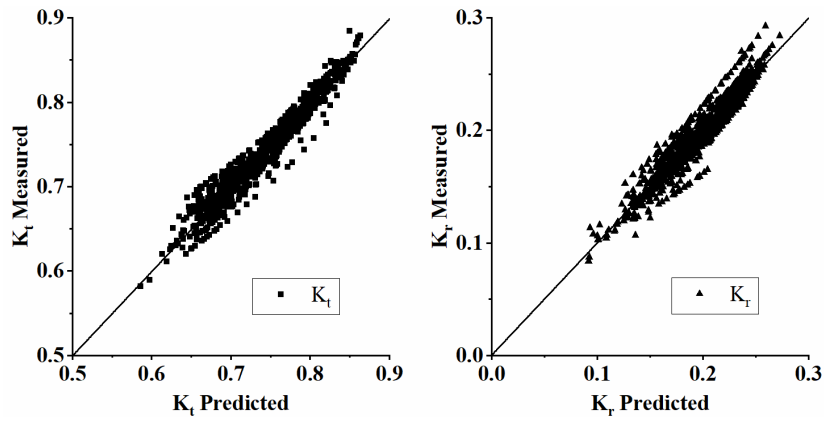
Figure 4.32 Validation of empirical predictions with the experimental data of perforated CPHB
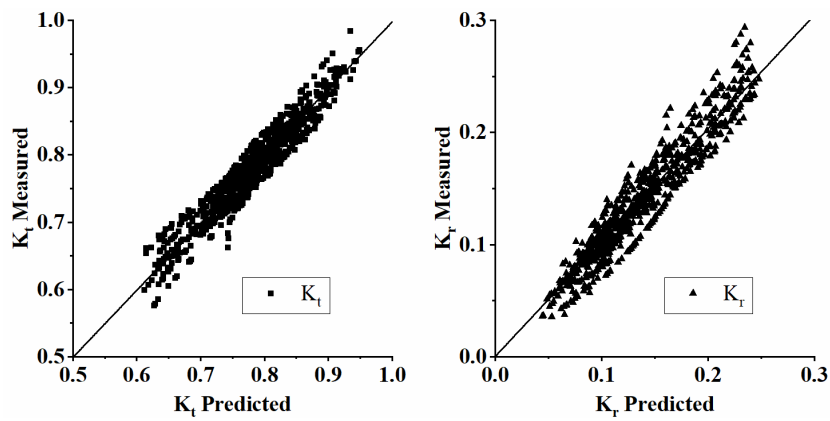
Figure 4.33 Validation of empirical predictions with the experimental data of non-perforated CPHB

Table 4.4 R^2 and RrmsE values for proposed empirical equations

Structure	K_t		K_r	
	R^2	RrmsE (%)	R^2	RrmsE %
Non-perforated CPHB	0.92	2.56	0.91	10.55
Perforated CPHB	0.94	1.73	0.90	5.36

4.4.3 Key findings

Based on the analysis of results, the following observations are documented on empirical equations developed:

1. The Transmission coefficient (K_t) of non-perforated and perforated CPHBs may be predicted by,

$$K_t = e^{\left[S_{K_t}\right]} - K_{tp}$$

2. The reflection coefficient (K_r) of both non-perforated and perforated CPHBs may be predicted by,

$$K_r = S_{Kr} + K_{rp}$$

3. R^2 of 0.92 and RrmsE of 2.56% are obtained for the equation to predict K_t of non-perforated CPHB. For the same structure, R^2 of 0.91 and RrmsE of 10.55% are obtained for the equation to predict K_r.

4. For the perforated CPHB, R^2 of 0.94 and RrmsE of 1.73% are achieved for the equation of K_t. Similarly, an R^2 of 0.90 and RrmsE of 5.36% are achieved for the equation of K_r.

5. A reasonably good agreement may be seen between the predicted values and experimental data for both non-perforated and perforated CPHBs.

6. The proposed empirical equations are reliable in predicting the K_t and K_r of both non-perforated and perforated CPHB within the limits of test conditions.

4.5 COMPARISON WITH OTHER STUDIES

4.5.1 Perforated hollow pile breakwater

A comparative study between the proposed structure and perforated hollow pile breakwater is carried out in order to examine the effectiveness of the CPHB. Perforated hollow pile breakwater consists of an array of perforated hollow cylindrical piles where the piles have uniform diameters throughout the length. The wave attenuation characteristics of perforated hollow pile breakwater are estimated based on the theoretical approach as there are no data available in the literature corresponding to the structural configuration and test limits of the present study. Therefore, the hybrid equations developed by Suvarna et al. (2021) for perforated hollow pile breakwater are adopted to extract the data. The summary of the development of hybrid equations is discussed in detail in section 2.3 for a better understanding.

The comparative study quantifies the efficiency of the proposed CPHB structure over perforated hollow pile breakwater by keeping the same number of piles in both cases. For the comparative analysis, best performing perforated CPHB with a structural configuration of $D/H_{max} = 0.4$, $Y/H_{max} = 1.5$ and $b/D = 0.1$ ($b_0/D = 0.76$), perforation of $Pa = 50\%$, $P = 19.2\%$ and $S/D = 0.25$, and $h = 0.45$ m is considered. The wave attenuation parameters of the perforated hollow pile breakwater are estimated using similar perforation characteristics of CPHB, i.e. $Pa = 50\%$, $P = 19.2\%$ and $S/D = 0.25$. The comparison of K_t, K_r and K_d between perforated CPHB and perforated hollow pile breakwater is illustrated in Figure 4.34.

The range of K_t values obtained for perforated hollow pile breakwater is between 0.96 and 0.89, whereas, for the perforated CPHB structure, the K_t ranges between 0.78 and 0.58. About 18.7% lesser K_t is noticed at lower wave steepness for CPHB than the perforated hollow pile structure. Similarly, at higher wave steepness, about 35% lesser K_t is obtained. The K_r for perforated hollow pile breakwater ranges between 0.04 and 0.1 whereas, for the perforated CPHB, the K_r observed is between 0.17 and 0.265. At the same time, the K_d obtained for the perforated CPHB (0.62 to 0.79) is about double the perforated hollow pile structure (0.29 to 0.43). The above analysis clearly proves
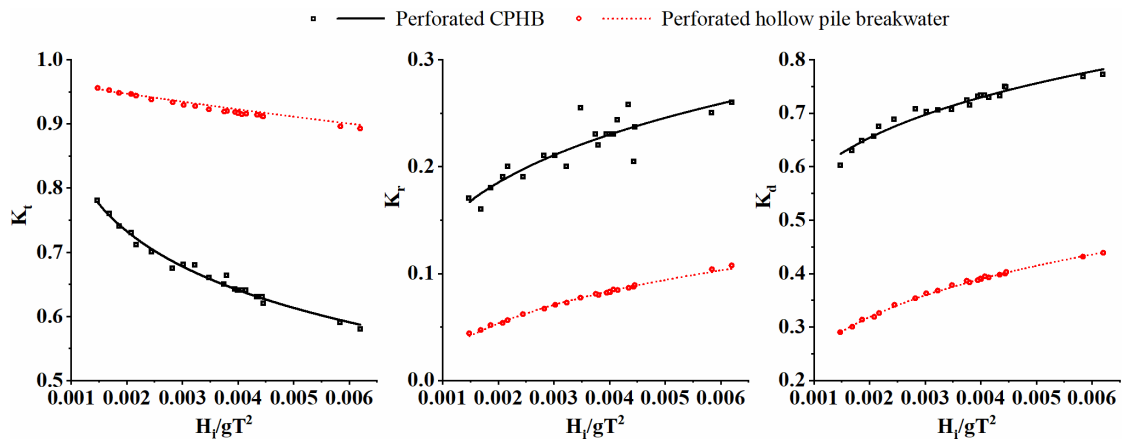
Figure 4.34 Comparison between the perforated CPHB and perforated hollow pile breakwater with the same number of pile units

that the perforated CPHB is superior in performance compared to the perforated hollow pile breakwater.

4.5.2 Other pile structures

To prove the relevance of the present study, the performance characteristics of the perforated CPHB are compared with those of other similar research works (Figure 4.35) conducted on pile types of breakwaters. The results of optimum configured perforated CPHB (D/H_{max} = 0.4, Y/H_{max} = 1.5, b/D = 0.1, Pa = 50%, P = 19.2%, S/D = 0.25 and h = 0.45 m) is compared with the perforated hollow pile breakwater (Rao and Rao 1999), suspended perforated pipe breakwater (Rao and Rao 2001), rectangular pile breakwater (Huang 2007) and zigzag porous screen breakwater (Mani 2009).

The behaviour of K_t, K_r and K_d of perforated CPHB is matching well with the other compared structures. From Figure 4.35, it is perceptible that a lower K_t and higher K_d are achieved than the compared pile structures. The K_r of the perforated CPHB is higher than the suspended perforated pipe breakwater, rectangular pile breakwater and zigzag porous screen breakwater, and lesser than the perforated hollow pile breakwater.

119

Table 4.5 Comparison of perforated CPHB performance with other pile structures

Reference	Type of breakwater	Structural details			Number of pile units per m	Structure performance		
		d (m)	b_0/d	P (%)		K_t	K_r	K_d
Rao and Rao (1999)	Perforated hollow pile breakwater	0.034	0.15	25	25.96	0.66 to 0.73	0.22 to 0.30	0.64 to 0.69
Rao and Rao (2001)	Perforated suspended pipe breakwater	0.034	0.15	25	25.96	0.67 to 0.79	0.16 to 0.22	0.59 to 0.71
Huang (2007)	Rectangular pile breakwater	0.006	1.77	21	56.41	0.73 to 0.88	0.09 to 0.28	0.49 to 0.64
Mani (2009)	Zigzag porous screen breakwater	0.040	0.22	40	20.49	0.67 to 0.83	0.16 to 0.18	0.57 to 0.73
Present study	Perforated CPHB	0.040	0.76	19.2	14.20	0.58 to 0.78	0.17 to 0.26	0.62 to 0.78

In order to understand the possible benefits of perforated CPHB over other similar pile structures, their performances are compared and listed in Table 4.5. It is found that the wave attenuation characteristics of the CPHB structure are in line with the other structures with a minimal number of pile units. The number of CPHB units per meter length is about 45.3% less than both hollow pile breakwaters and suspended pipe breakwaters, 74.8% less than rectangular pile breakwaters and 30.7% less than zigzag porous screen breakwaters. Considering the test conditions/parameters of the present research work, it appears that the perforated CPHB tested herein is successful and a
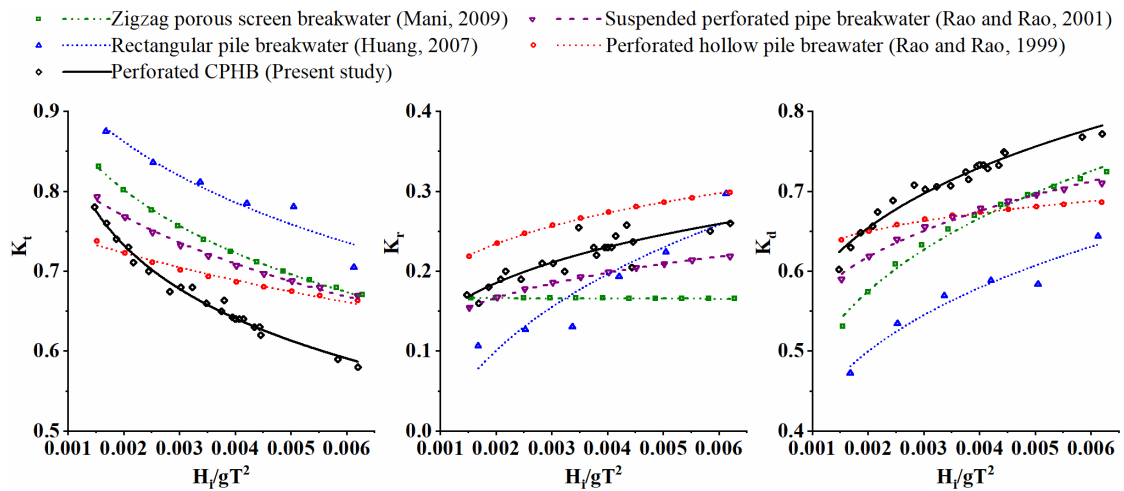
Figure 4.35 Comparison between perforated CPHB and other pile structures

better performing pile breakwater structure compared to most of the other similar structures compared.

Considering the number of pile units required per meter width to obtain comparable performance, it appears that the present perforated CPHB structure has the potential to be economical in construction. However, the exact size, construction at the site and site conditions need to be considered in proving the exact economy achieved. This aspect is beyond the scope of the present research and is not explored.

4.5.3   Key findings

The following are the major findings derived after evaluating the perforated CPHB performance with the results of other studies.

1. Introducing the best performing configuration of perforated hollow conical pile head over the conventional pile breakwater improves the wave attenuation characteristics of the structure.

2. The wave attenuation characteristics of the perforated CPHB structure are in line with the other structures with a minimal number of pile units.

3. The wave attenuation capacity of the CPHB structure is comparable with other pile structures with minimal reflection and higher energy dissipation.

4. The range of the K_t values obtained for perforated hollow pile breakwater is between 0.96 and 0.89 whereas, for the perforated CPHB, the K_t ranges between 0.78 and 0.58.

5. The K_r for perforated hollow pile breakwater ranges between 0.04 and 0.1 whereas, for the perforated CPHB, the K_r observed is between 0.17 and 0.26. At the same time, the K_d obtained for the perforated CPHB (0.62 to 0.78) is about double the perforated hollow pile structure (0.29 to 0.43).

6. The comparative study between the perforated CPHB and perforated hollow pile breakwater (PHPB) showed that CPHB is about 18.7% to 35% more effective in wave attenuation than PHPB.

7. The proposed perforated CPHB with optimum configuration (D/H_{max} = 0.4, Y/H_{max} = 1.5, b/D = 0.1, Pa = 50%, P = 19.2% and S/D = 0.25) is superior in performance compared to the perforated hollow pile breakwater.

8. The number of CPHB units per meter length is about 45.3% less than both hollow pile breakwaters and suspended pipe breakwaters, 74.8% less than rectangular pile breakwaters and 30.7% less than zigzag porous screen breakwaters.

CHAPTER 5

SUMMARY AND CONCLUSIONS

5.1 BACKGROUND

Pile breakwaters can serve as an alternative to conventional breakwaters when partial wave attenuation is acceptable. Increasing the size of the pile breakwater in the vicinity of the free surface increases the hydraulic efficiency, as most of the wave energy is concentrated around the free surface. Therefore, a conical pile head breakwater (CPHB) is proposed in the present study by gradually widening the diameter of piles towards the free surface. The hydraulic performance of the CPHB is investigated while monochromatic waves with varying wave heights and period at different depths of water attack the structure. The influence of relative pile head diameter (D/H_{max}), relative pile head height (Y/H_{max}) and relative clear spacing between the CPHs (b/D) on the performance characteristics (K_t, K_r and K_d) of non-perforated CPHB are investigated comprehensively and the best performing structural configuration is evolved. To improve the performance of the CPHB structure, a second row of CPHB is introduced in a staggered manner. The influence of clear spacing between the two rows of pile heads (B/D) on the performance of CPHB is investigated through physical modelling studies. However, depending on site conditions, there may be difficulties in driving/construction of closely spaced two rows of piles.

To overcome this problem, an attempt is made to enhance the performance of single row CPHB structure by incorporating perforations on the pile head. The influence of perforations on the K_t, K_r and K_d of perforated CPHB is explored through physical model studies. The effect of distribution of perforations around the pile head (Pa), percentage of perforations (P) and size of perforations (S/D) on the wave attenuation characteristics are evaluated to arrive at an optimum configuration.

Selected CPHB configurations are simulated using an open-source computational fluid dynamics model REEF3D and the numerical results are validated with the experimental data. In addition, a set of empirical equations is developed based on the experimental values for quick prediction of K_t and K_r. The estimated values of K_t and K_r are in line with the experimental data. Finally, to prove the relevance of the present study, the performance characteristics of the perforated CPHB are compared with those of other similar research works. The important conclusions derived based on the extensive investigations conducted on non-perforated and perforated CPHBs under selected test conditions are presented in the subsequent section.

5.2 CONCLUSIONS

5.2.1 Non-perforated CPHB

The following conclusions are derived based on the extensive experiments carried out on non-perforated CPHB:

1. In general, the transmission coefficient (K_t) decreases with an increase in wave steepness (H_i/gT^2) whereas, K_r and K_d follow the opposite trend.

2. K_t is directly proportional to D/H_{max} and b/D, and inversely proportional to Y/H_{max}. At the same time, K_r and K_d demonstrate the opposite behaviour.

3. The wave attenuation, wave reflection and energy dissipation of the CPHB are more pronounced for steep incident waves than for gentle waves.

4. The structural configuration of $D/H_{max} = 0.4$, $Y/H_{max} = 1.5$ and $b/D = 0.1$ is the best performing model in case of a single row of CPHB with the least K_t of 0.66 along with $K_r = 0.22$ and $K_d = 0.72$.

5. In the case of two staggered rows of CPHB, the B/D of 0.4 is the optimum spacing between the rows, which provided a minimal K_t of 0.58 with K_r of 0.24 and K_d of 0.79.

6. The addition of the second row of CPHB with $D/H_{max} = 0.4$, $Y/H_{max} = 1.5$, $b/D = 0.1$ and $B/D = 0.4$ configuration in staggered arrangement reduces the K_t by a maximum of 12.34% compared to a single row. However, from the practical point of view, providing whether single or double row structure to achieve an

extra 12.34% reduction in K_t is a matter of judgement considering site conditions. Therefore, efforts are made to introduce perforations on the best model of single row CPHB and achieve improved performance.

5.2.2 Perforated CPHB

The following conclusions are recorded based on the physical model investigation carried out on the perforated CPHB:

1. The distribution of perforations (Pa) on CPH, percentage of perforations (P) and the size of perforations (S/D) play a significant role in influencing the hydraulic performance of the perforated CPHB.

2. The wave attenuation capability of the structure is more pronounced for steep waves than the gentle waves by about 11.2 to 24.5%.

3. The wave attenuation capability of the proposed perforated CPHB structure is maximum when $D/H_{max} = 0.4$, $Y/H_{max} = 1.5$ and $b/D = 0.1$ with Pa = 50%, P = 19.2% and S/D = 0.25.

4. A minimum K_t of 0.58 associated with a maximum K_r of 0.265 and K_d of 0.78 is realised for the optimum configuration of CPHB at a water depth of 0.45 m.

5. The perforated CPHB seems to be more efficient in wave attenuation than the non-perforated CPHB by up to 12.4%.

6. Introducing perforations with optimal configurations on a single row of CPHB is as efficient as introducing a second row of non-perforated CPHB with the staggered arrangement.

5.2.3 Numerical modelling of CPHB

The following conclusions are derived based on the numerical simulations carried out using an open-source CFD tool REEF3D.

1. Validation of the numerical results with the experimental data shows that REEF3D produces reliable results with acceptable RMSE values.

2. For non-perforated CPHB, the numerical results are under predicted for K_t (less than 4%) and over predicted for K_r and K_d (less than 9%). For the perforated

CPHB, the variation is slightly higher (up to 12%) compared to the non-perforated structure.

3. Introducing perforations with the optimum configuration (Pa = 50%, S/D = 0.25 and P = 19.2%) on the CPHs enhanced the transmission capability of the CPHB by about 5% to 16.5%. The values of K_r and K_d increased on an average of about 27.25% and 10.28%, respectively.

4. Overall, the numerical model of the CPHB mimics the physical phenomenon of experimental studies, and the perforated CPHB with the proposed configuration is capable of reducing wave transmission by up to 42%. Hence, taking the site characteristics into consideration, the CPHB may be considered as one of the options among various solutions designed for wave attenuation/damping purposes.

5.2.4 Empirical equations

The following conclusions are obtained based on the validation of empirical predictions with the experimental data:

1. The empirical equation for predicting the transmission coefficient (K_t) and reflection coefficient (K_r) of non-perforated and perforated CPHBs are, respectively,

$$K_t = e^{\left[S_{Kt}\right]} - K_{tp}$$

$$K_r = S_{Kr} + K_{rp}$$

2. A reasonably good agreement is obtained between the predicted values and experimental data for both types of structure.

3. The empirical equations estimate the K_t and K_r values accurately with a high coefficient of determination ($R^2 \geq 0.90$). Therefore, it can be stated that the proposed empirical equations are reliable in predicting the K_t and K_r of both non-perforated and perforated CPHBs within the limits of test conditions.

126

5.2.5 Performance comparison with other studies

The following are the primary conclusions reached after comparing the performance of perforated CPHB with other pile structures:

1. Introducing the best performing configuration of conical hollow pile head over the conventional pile breakwater improves the wave transmission characteristics of the structure with higher wave dissipation.

2. The wave attenuation capacity of the CPHB structure is comparable with other pile types of breakwaters with minimal reflection and higher energy dissipation.

3. The proposed perforated CPHB with optimum configuration ($D/H_{max} = 0.4$, $Y/H_{max} = 1.5$, $b/D = 0.1$, $Pa = 50\%$, $P = 19.2\%$ and $S/D = 0.25$) is about 18.7% to 35% more effective in wave attenuation than the perforated hollow pile breakwater.

5.2.6 Summary

The conclusions of the present investigation are summarised below:

1. The structural parameters (D/H_{max}, Y/H_{max} and b/D) and perforation characteristics (Pa, P and S/D) of CPHB play a significant role in influencing the hydraulic performance of the structure.

2. For single row non-perforated CPHB, the structural configuration of $D/H_{max} = 0.4$, $Y/H_{max} = 1.5$ and $b/D = 0.1$ is the best performing model with the least K_t of 0.66 along with K_r of 0.22 and K_d of 0.72.

3. For staggered two rows of CPHB, $D/H_{max} = 0.4$, $Y/H_{max} = 1.5$, $b/D = 0.1$ and $B/D = 0.4$ is the optimum configuration which provided a minimal K_t of 0.58 with $K_r = 0.24$ and $K_d = 0.79$ and it reduces the K_t by a maximum of 12.34% compared to a single row.

4. The perforated CPHB attenuates the waves by up to an increased efficiency of 12.4% compared to that of a non-perforated structure.

5. Introducing perforations with optimal configurations ($Pa = 50\%$, $P = 19.2\%$ and $S/D = 0.25$) on a single row CPH surface is as efficient as introducing second row of non-perforated piles with staggered arrangement.

6. The validation of the numerical results with the experimental data proved that REEF3D is reliable in simulating the CPHB structure.

7. Empirical equations to predict the hydraulic performance of non-perforated and perforated CPHBs are,

$$K_t = e^{\left[S_{Kt}\right]} - K_{tp} \quad \text{and}$$

$$K_r = S_{Kr} + K_{rp}$$

8. The optimum configuration of single row CPHB is $D/H_{max} = 0.4$, $Y/H_{max} = 1.5$ and $b/D = 0.1$ with $Pa = 50\%$, $P = 19.2\%$ and $S/D = 0.25$.

5.3 RESEARCH CONTRIBUTION

The research contributions of the present study are:

1. Developed a novel concept of conical pile head breakwater and evaluated its hydraulic performance by considering different configurations of CPHB under varying wave climates through physical modelling studies.

2. The influence of perforations has been investigated in enhancing the CPHB performance.

3. Derived a set of empirical equations for computing the hydraulic performance of the CPHB.

4. Simulated and validated the selected cases of CPHB by employing an open-source tool REEF3D.

5.4 LIMITATIONS OF THE STUDY

The primary limitation in the present experimental study on CPHB is that the structure is investigated under unidirectional monochromatic waves in a two-dimensional flume with a rigid seabed. Whereas, the porotype will be subjected to multidirectional random waves with varying seabed. Even though the monochromatic waves are proven to give conservative results (Neelamani and Rajendran 2002a; Neelamani and Vedagiri 2001), it is suggested to verify the performance under random waves with mobile bed conditions before implementing them in the field. Further, the empirical equations

developed predict the performance of CPHB under limited laboratory conditions, which may be further tuned for practical applications.

5.5 FUTURE SCOPE

Further research may be carried out on optimum perforated conical pile head structure with varying patterns of perforations such as horizontal or vertical slits. Also, site-specific optimization of CPHB profile to suit the particular wave climate at a given location for the practical implementation may be necessary. Investigations with different shapes of pile heads, such as rectangular, can be considered as another possible subject for future research.

FREE SURFACE RECONSTRUCTION USING DIRICHLET INLET BOUNDARY CONDITION

The spectrum decomposition technique for the harmonic components is used in the present approach to reconstruct the free surface elevation in numerical wave tank (Aggarwal et al. 2018). The Fourier analysis separates the variability of a time series into components at each harmonic frequency and approximates a function as a sum of the sine and cosine terms. The wave signal in experimental wave flumes recorded at a target location is composed of incident and reflected signals:

$$x(t) = x_{in}(t) + x_r(t) \tag{AI-1}$$

where $x_{in}(t)$ and $x_r(t))$ are the incident and reflected wave signals.

Further, the wave signal can be decomposed to multiple harmonic components using FFT which can be represented as (Hoffmann, 2009):

$$x(t) = \frac{a_0}{2} + \sum_{i=1}^{\infty}\left(a_i \cos\frac{2\pi it}{T} + b_i \cos\frac{2\pi it}{T} \right) \tag{AI-2}$$

where a_0, a_i and b_i are Fourier coefficients and T is the wave period.

The frequency of the 0th and i^{th} ($i \geq 1$) harmonic are given as:

$$\omega_0 = \frac{2\pi}{T} \tag{AI-3}$$

$$\omega_i = \frac{2\pi i}{T} \tag{AI-4}$$

The amplitudes A_i and phases Φ_i can be computed from the Fourier coefficients using:

$$A_i = \sqrt{a_i^2 + b_i^2} \tag{AI-5}$$

$$\Phi_i = \arctan \frac{b_i}{a_i} \tag{AI-6}$$

The free surface signal of the wave can be further written in terms of the Fourier amplitudes and phases as:

$$x(t) = \frac{A_0}{2} + \sum_{i=1}^{\infty} \left(A_i \cos \left(i\omega_0 t + \Phi_i \right) \right) \tag{AI-7}$$

The computed Fourier components are re-tested by computing the autocorrelation function and the cross-spectral density. The autocorrelation function for a random process $x(t)$ is defined as the average value of the product $x(t)\, x\,(t + \tau)$. With the assumption of a stationary process, the value of $E[x(t)\, x\,(t + \tau)]$ is dependent only on the time separation τ. The autocorrelation function $R_x(\tau)$ can be related to the spectral density (Newland 1993):

$$R_x(\tau) = \int_{-\infty}^{\infty} S_x(\omega)\, e^{j\omega t}\, d\omega \tag{AI-8}$$

where j is the square root of negative unity.

In the next step, the crosscorrelation functions of the input $R_{xy}(\tau)$ and output signals; i.e., $y(t)$, $R_{yx}(\tau)$ are linked in terms of the cross-spectral densities using the inverse FFT:

$$S_{xy}(\omega) = S_{yx}^{*}(\omega)$$

Where, S_{xy} is the cross-spectral density and $S_{yx}^{*}(\omega)$ is the complex conjugate of the cross-spectral density.

After the cross-spectral densities of both the input and output signals are computed, the computed wave amplitudes (A_i), angular frequencies (ω_i) and the phase angles (Φ) are used as the inputs for the numerical model. The irregular wave signal is generated by the superposition of the linear regular wave components in the next step with the Dirichlet inlet boundary condition as:

$$\eta = \sum_{i=1}^{N} A_i \cos(k_i x - \omega_i t + \Phi_i) \qquad \text{(AI-9)}$$

$$\omega_i^2 = gk_i \tanh k_i h \qquad \text{(AI-10)}$$

Similarly, the horizontal velocity u and the vertical velocity w are also reconstructed by superposition of the individual velocity components:

$$u = \sum_{i=1}^{N} \omega_i A_i \frac{\cosh\{|k_i|(z+h)\}}{\sinh(|k_i|h)} \cos(k_i x - \omega_i t + \Phi_i) \qquad \text{(AI-11)}$$

$$w = \sum_{i=1}^{N} \omega_i A_i \frac{\sinh\{|k_i|(z+h)\}}{\sinh(|k_i|h)} \sin(k_i x - \omega_i t + \Phi_i) \qquad \text{(AI-12)}$$

Where, k_i is the wave number, N is total number of components, h is water depth, and z is height of the point of interest from the free surface. In this manner, the target experimental or theoretical wave signal is generated at the inlet boundary.

TRENDLINE SELECTION

In the present study, physical modelling studies are performed and the hydraulic performance characteristics (K_t, K_r and K_d) are plotted with wave steepness (H_i/gT^2). The trend lines are drawn for the discrete data in order to clearly comprehend CPHB performance and evaluate the results. The R^2 values obtained for logarithmic, linear, exponential and polynomial trend lines for a typical case of perforated CPHB (D/H_{max} = 0.4, Y/H_{max} = 1.5, b/D = 0.1, Pa = 50%, P = 19.2%, S/D = 0.25 and h = 0.45 m) are illustrated for logarithmic, linear, exponential and polynomial trend lines in Figure AII-1, Figure AII-2, Figure AII-3 and Figure AII-4, respectively. As evident from the figures, the logarithmic trend line is found to be better fitting with the highest R^2 values than the other types considered. In order to evaluate the results and understand the CPHB performance, logarithmic trend lines are employed for all the plots.

Figure AII-1 Logarithmic trend line plotted for a typical case of CPHB (D/H_{max} = 0.4, Y/H_{max} = 1.5, b/D = 0.1, Pa = 50%, P = 19.2%, S/D = 0.25 and h = 0.45 m)

Figure AII-2 Linear trend line plotted for a typical case of CPHB (D/H$_{max}$ = 0.4, Y/H$_{max}$ = 1.5, b/D = 0.1, Pa = 50%, P = 19.2%, S/D = 0.25 and h = 0.45 m)

Figure AII-3 Exponential trend line plotted for a typical case of CPHB (D/H$_{max}$ = 0.4, Y/H$_{max}$ = 1.5, b/D = 0.1, Pa = 50%, P = 19.2%, S/D = 0.25 and h = 0.45 m)

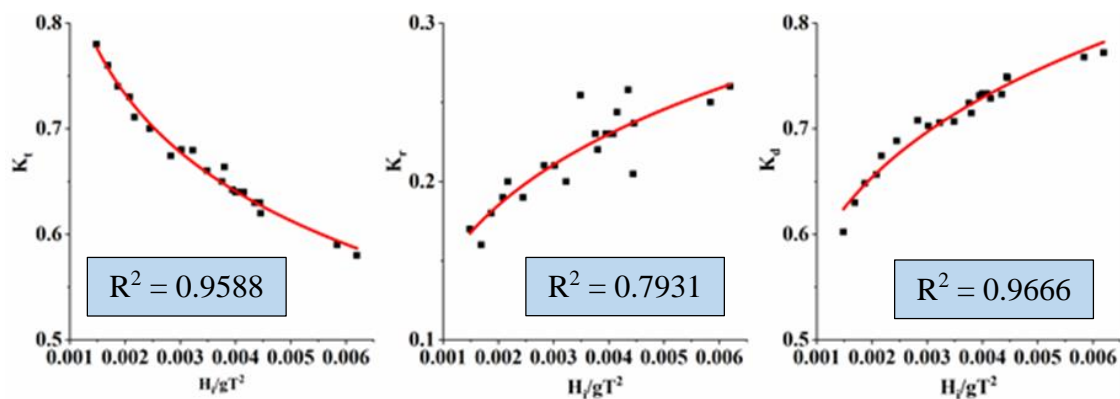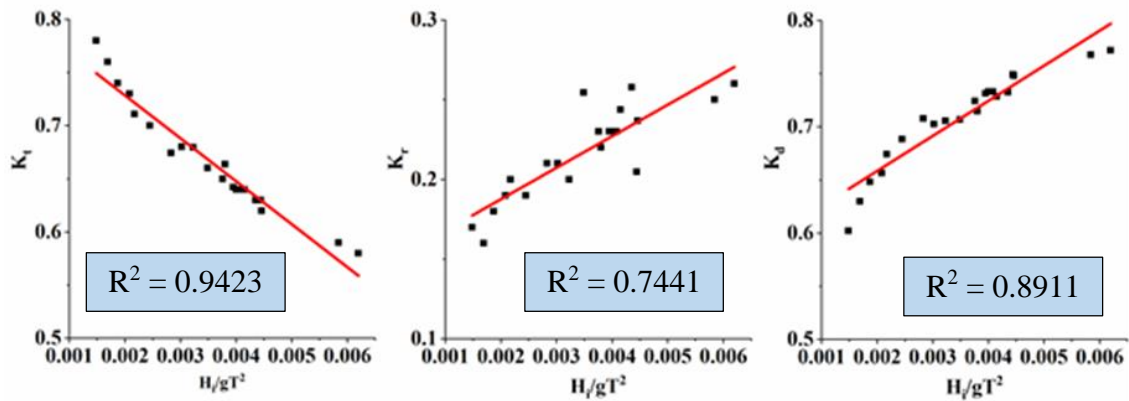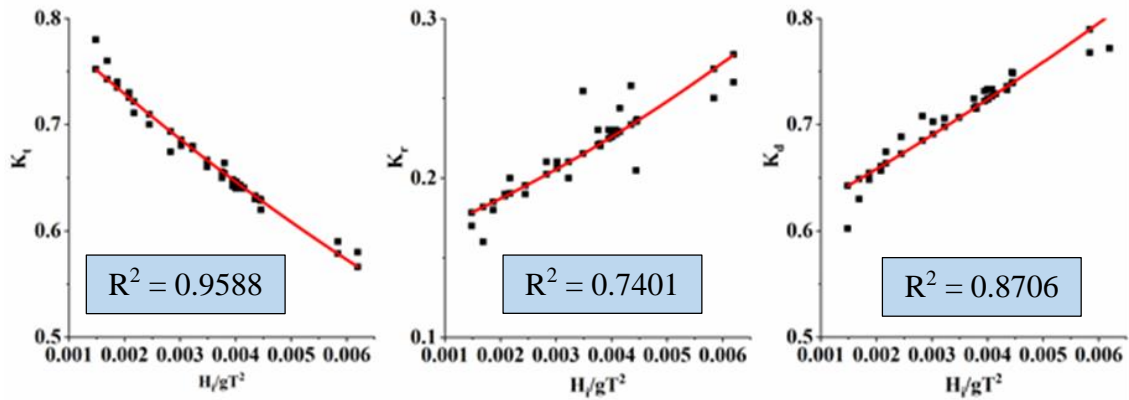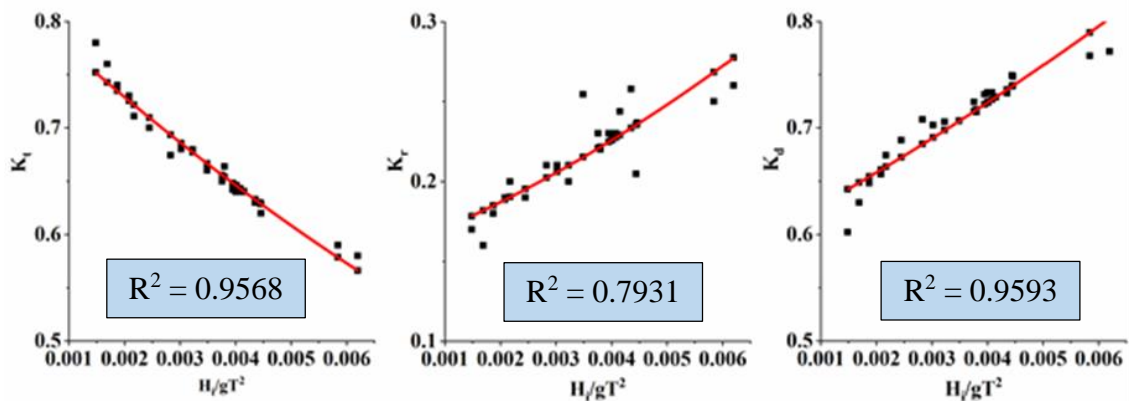**Figure AII-4 Exponential trend line plotted for a typical case of CPHB (D/H$_{max}$ = 0.4, Y/H$_{max}$ = 1.5, b/D = 0.1, Pa = 50%, P = 19.2%, S/D = 0.25 and h = 0.45 m)**

APPENDIX-III

UNCERTAINTY ANALYSIS

Physical modelling test facilities varies in terms of facilities, apparatus, experimental methodologies and size. As a result, a testing facility must give probable lower and higher margins that may be used with an acceptable degree of confidence. Uncertainty analysis refers to such a research for an experimental test method at a specific facility. Uncertainty describes the degree of goodness of a measurement or experimentally determined result. It is an estimate of experimental error. It is possible to conduct experiments in a scientific manner and predict the accuracy of the results with the help of uncertainty analysis. The confidence interval gives an estimated range of values, which is likely to include an unknown population parameter. The 95% confidence interval limits must always be estimated and this concept of confidence level is fundamental to uncertainty analysis (Misra 2001).

A best-fit curve can include both 95% confidence band and the 95% prediction band. Confidence band tells about 95% sure that the true best fit curve lies within the confidence band. The prediction band tells about the scatter of the data. If data points are considered, 95% points are expected to fall within the prediction band. Since the prediction band has to account for uncertainty in the curve itself as well as scatters around the curve, it is much wider than the confidence band. The 95% confidence bands have a 95% chance of containing the true best fit curve and the 95% prediction bands include 95% of the data points. Also the 95% confidence and prediction bands have been accepted to be reliable enough for usage under the adoption of uncertainty analysis (Misra 2001).

To evaluate uncertainty in the present test results, 95% confidence and prediction bands are plotted for the typical cases of CPHB. Figure AIII-1 presents the 95% confidence and prediction bands for the plots showing the variation of K_t, K_r and K_d for best performing non-perforated CPHB configuration ($D/H_{max} = 0.4$, $Y/H_{max} = 1.5$ and b/D =

0.1) at 0.45 m depth of water. Overall, based on uncertainty analysis, it can be stated that the test results reported on non-perforated and perforated CPHB in the present study are reliable.
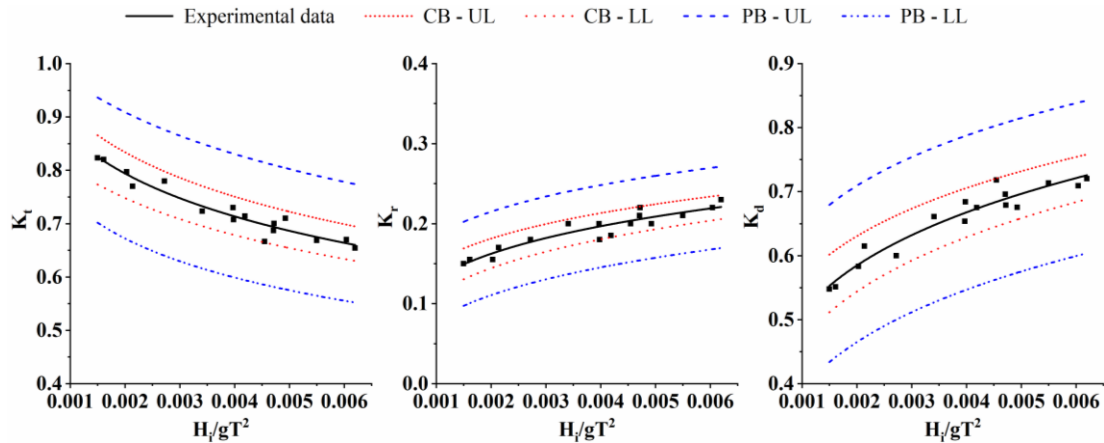
Figure AIII-1 Variation of K_t, K_r and K_d for best performing non-perforated CPHB (D/H_{max} = 0.4, Y/H_{max} = 1.5 and b/D = 0.1) at 0.45 m depth of water with 95% confidence and prediction bands
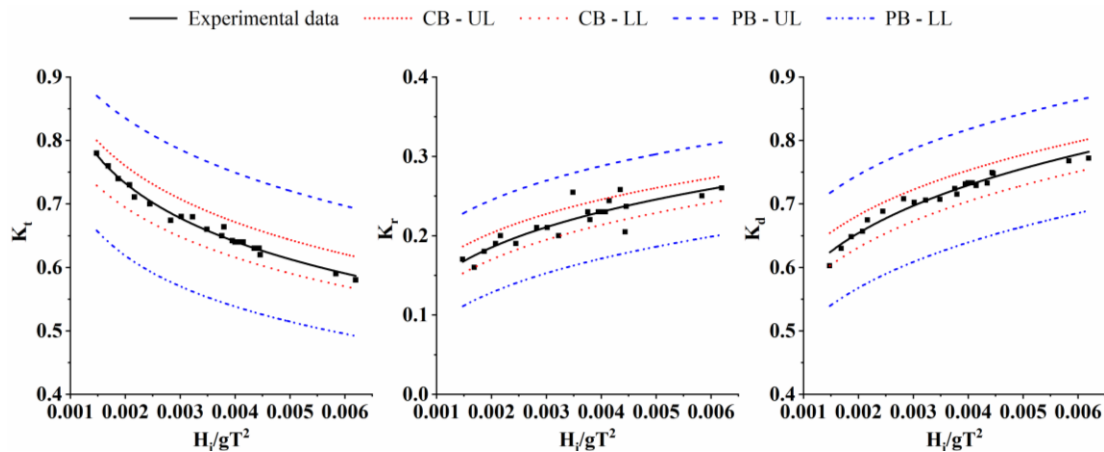
Figure AIII-2 Variation of K_t, K_r and K_d for best performing perforated CPHB (D/H_{max} = 0.4, Y/H_{max} = 1.5, b/D = 0.1, Pa = 50%, P = 19.2% and S/D = 0.25) at 0.45 m depth of water with 95% confidence and prediction bands

REFERENCES

Afshar, M.A. (2010). "Numerical wave generation in OpenFOAM." *Master's thesis*, Department of Shipping and Marine Technology, Chalmers University of Technology Gothenburg, Sweden.

Aggarwal, A., Pákozdi, C., Bihs, H., Myrhaug, D. and Alagan Chella, M. (2018). "Free surface reconstruction for phase accurate irregular wave generation.*" Journal of Marine Science and Engineering*, 6(105), 1-23.

Aggarwal, A., Bihs, H., Shirinov, S. and Myrhaug, D. (2019). "Estimation of breaking wave properties and their interaction with a jacket structure." *Journal of Fluids and Structures,* 91, 102722.

Ahmad, N., Bihs, H., Myrhaug, D., Kamath, A. and Arntsen, Ø.A. (2019). "Numerical modeling of breaking wave induced seawall scour." *Coastal Engineering,* 150, 108-120.

Anuar, N. M. and Sidek, F. J. (2012). "Wave characteristics around perforated piles in a two rows arrangement." *Malaysian Journal of Civil Engineering*, 24, 48-66.

Bihs, H., Chella, M.A., Kamath, A. and Arntsen, Ø.A. (2017). "Numerical investigation of focused waves and their interaction with a vertical cylinder using REEF3D." *Journal of Offshore Mechanics and Arctic Engineering*, 139, 41101-41108.

Bihs, H., Kamath, A., Chella, M.A., Aggarwal, A. and Arntsen, Ø.A. (2016a). "A new level set numerical wave tank with improved density interpolation for complex wave hydrodynamics." *Computers and Fluids*, 140, 191-208.

Bihs, H., Kamath, A., Chella, M.A., Aggarwal, A. and Arntsen, Ø.A. (2016b). "Breaking wave interaction with tandem cylinders under different impact scenarios." *Journal of Waterway, Port, Coastal, and Ocean Engineering*, 142(5), 1-14.

Bovin, R. (1964). "Comments on vertical breakwaters with low coefficients of reflection." *Dock and Harbour Authority*, London, 45, 56-61.

Brackbill, J.U., Kothe, D.B. and Zemach, C. (1992) "A continuum method for modeling surface tension." *Journal of computational physics*, 100(2), 335-354.

Chorin, A. J. (1968). "Numerical solution of the Navier-Stokes." *Mathematics of Computation,* 22(104), 745-762.

Costello, R. D. (1952). "Damping of water waves by vertical circular cylinders." *American Geophysical Union*, 33(4), 513–519.

Davidson, P. A. (2015). "Turbulence: An introduction for scientists and engineers." *Oxford university press*.

Deo M. C. (2013). "Waves and Structures." Powai, Mumbai: Indian Institute of Technology. Bombay. http://www.civil.iitb.ac.in/~mcdeo/waves.html

Duclos, G., Clément, A.H., Gentaz, L. and Colmard, C. (2001). "Experimental and numerical study of a half-submerged pile-supported breakwater." *Proc., 11th International Offshore and Polar Engineering Conference*, OnePetro.

Elsharnouby, B., Soliman, A., Elnaggar, M. and Elshahat, M. (2012). "Study of environment friendly porous suspended breakwater for the Egyptian Northwestern Coast." *Ocean Engineering*, 48, 47-58.

Günaydin, K. and Kabdaşli, M. S. (2004). "Performance of solid and perforated U-type breakwaters under regular and irregular waves." *Ocean Engineering*, 31, 1377-1405.

Günaydın, K. and Kabdaşlı, M.S. (2007). "Investigation of Π-type breakwaters performance under regular and irregular waves." *Ocean Engineering*, 34(7), 1028-1043.

Hagiwara, K. (1984). "Analysis of upright structure for wave dissipation using integral equation." *Proc. 19ᵗʰ Coastal Engineering Conference,* Houstan, Texas, Published by ASCE, New York, 2810-2826.

Hayashi, T. and Masataro, H. (1968). "Closely spaced pile breakwater as a protection structure against beach erosion." *Coastal Engineering,* 11, 606-621.

Hayashi, T., Hattori, M., Kano, T. and Shirai, M. (1966). "Hydraulic research on the closely spaced pile breakwater." *Coastal Engineering in Japan*, 9(1), 107-117.

Herbich, J.B. (1990). "Pile and offshore breakwaters." *Handbook of coastal and ocean engineering*, Gulf Publishing Company, 895-904.

Herbich, J.B. and Douglas, B. (1988). "Wave transmission through a double row of pile breakwater." *Proc. 21ˢᵗ Coastal Engineering Conference*, Torremolinos, Spain, Published by ASCE, New York, N. Y., 2229-2241.

Higuera, P., Lara, J. L. and Losada, I. J. (2013a). "Realistic wave generation and active wave absorption for Navier - Stokes models application to OpenFOAM®." *Coastal Engineering*, 71, 102-118.

Higuera, P., Lara, J. L. and Losada, I. J. (2013b). "Simulating coastal engineering processes with OpenFOAM®." *Coastal Engineering,* 71, 119-134.

Hildebrandt, A. and Sriram, V. (2014). "Pressure distribution and vortex shedding around a cylinder due to a steep wave at the onset of breaking from physical and numerical modeling." *Proceedings of the International Offshore and Polar Engineering Conference*, 405-410.

Hoffmann, J. (2009). *MATLAB and Simulink*, Addison Wesley Longman, Boston, MA, USA.

Hsu, H.H. and Wu, Y.C. (1999). "Scattering of water wave by a submerged horizontal plate and a submerged permeable breakwater." *Ocean Engineering*, 26(4), 325-341.

Hu, H., Wang, K.H. and Williams, A.N. (2002). "Wave motion over a breakwater system of a horizontal plate and a vertical porous wall." *Ocean Engineering*, 29(4), 373-386.

Huang, Z. (2007). "Wave interaction with one or two rows of closely spaced rectangular cylinders." *Ocean Engineering*, 34(11–12), 1584-1591.

Hughes, S. A. (1993). "Physical models and laboratory techniques in coastal engineering." *Advanced Series in Ocean Engineering*, 7, World Scientific, Singapore.

Hutchinson, P.S. and Raudkivi, A.J. (1984). "Case history of a spaced pile breakwater at Halfmoon bay marina, Auckland, New-Zealand." *Proc. 19ᵗʰ Coastal Engineering Conference*, Houstan, Texas, Published by ASCE, New York, N.Y., 2530-2535.

Isaacson, M. (1991). "Measurement of regular wave reflection." *Journal of Waterway, Port, Coastal, and Ocean Engineering*, 117(6), 553-569.

Isaacson, M., Premasiro, S. and Yang, G. (1998). "Wave interaction with vertical slotted barrier." *Journal of Waterway, Port, Coastal, and Ocean Engineering*, 124(June), 118-126.

Jeya, T.J., Sriram, V. and Sundar, V. (2021). "Hydrodynamic characteristics of vertical and quadrant face pile supported breakwater under oblique waves." Proceedings of the Institution of Mechanical Engineers, *Journal of Engineering for the Maritime Environment*, 236(1), 62-73.

Ji, C.H. and Suh, K.D. (2010). "Wave interactions with multiple-row curtainwall-pile breakwaters." *Coastal Engineering*, 57(5), 500-512.

Jiang, G. S. and Shu, C. W. (1996). "Efficient implementation of weighted ENO schemes." *Journal of Computational Physics*, 126(1), 202-228.

Kakuno, S. and Liu, P.L.F. (1993). "Scattering of water waves by vertical cylinders." *Journal of Waterway, Port, Coastal and Ocean Engineering*, 119(3), 302-322.

Kamath, A., Chella, M. A., Bihs, H. and Arntsen, Ø. A. (2015). "Evaluating wave forces on groups of three and nine cylinders using a 3D numerical wave tank." *Engineering Applications of Computational Fluid Mechanics*, 9(1), 343-354.

Kamath, A., Bihs, H., Alagan Chella, M. and Arntsen, Ø. A. (2016). "Upstream-cylinder and downstream-cylinder influence on the hydrodynamics of a four-cylinder group." *Journal of Waterway, Port, Coastal, and Ocean Engineering*, 142(4), 4016002-4016012.

Kamath, A., Travis Roy, Betsy R. Seiffert and Bihs, H. (2022). "Experimental and numerical study of waves breaking over a submerged three-dimensional bar." *Journal of Waterway, Port, Coastal, and Ocean Engineering*, 148(2), 04021052.

Kono, T. and Tsukayama, S. (1981). "Wave deformation on a barrier reef." *Proc. Japan Society of Civil Engineers*, Japan, 27-38.

Kondo, H. and Toma, S. (1972). "Reflection and transmission for a porous structure." *Proc. l3th Coastal Engineering Conference*, Vancouver, B.C., Canada. Published by ASCE, New York, N.Y., 1847-1866.

Koraim, A.S. (2014). "Hydraulic characteristics of pile supported L-shaped bars used as a screen breakwater." *Ocean Engineering,* 83, 36-51.

Koraim, A.S., Iskander, M. M. and Elsayed, W.R. (2014). "Hydrodynamic performance of double rows of piles suspending horizontal C shaped bars." *Coastal Engineering,* 84, 81-96.

Koraim, A.S. and Salem, T.N. (2012). "The hydrodynamic characteristics of a single suspended row of half pipes under regular waves." *Ocean Engineering*, 50, 1-9.

KREC Study Team (1994). "Study on coastal erosion (Dakshina Kannada district), input to environmental master plan study." *Karnataka Regional Engineering College*, Surathkal, Karnataka, India, 80-125.

Kriebel, D. L. (1992). "Vertical wave barriers: Wave transmission and wave forces." *Proc. 23rd Int. Conf. on Coastal Engineering,* 1313-1326.

Laju, K., Sundar, V. and Sundaravadivelu, R. (2005). "Studies on pile supported skirt breakwater." *Proc. 1st International Conference on Coastal Zone Management and Engineering,* Middle East, Dubai, United Arab Emirates.

Laju, K., Sundar, V. and Sundaravadivelu, R. (2011). "Hydrodynamic characteristics of pile supported skirt breakwater models." *Applied Ocean Research*, 33(1), 12-22.

Lean, G.H. (1967). "A simplified theory of permeable wave absorbers." *Journal of Hydraulic Research*, 5(1), 15-30.

Liu, H., Ghidaoui, M. S., Huang, Z., Yuan, Z. and Wang, J. (2011). "Numerical investigation of the interactions between solitary waves and pile breakwaters using BGK-based methods." *Computers and Mathematics with Applications*, 61(12), 3668-3677.

Liu, Y. and Li, Y.C. (2011). "Wave interaction with a wave absorbing double curtain-wall breakwater." *Ocean Engineering*, 38(10), 1237-1245.

Mani, J. S. (2009). "Experimental and numerical investigations on zigzag porous screen breakwater." *Natural Hazards*, 49(2), 401–409.

Mani, J.S. and Jayakumar, S. (1995). "Wave transmission by suspended pipe breakwater." *Journal of Waterway, Port, Coastal, and Ocean Engineering*, 121(6), 335-338.

Martin, T., Kamath, A. and Bihs, H. (2020). "A Lagrangian approach for the coupled simulation of fixed net structures in a Eulerian fluid model." *Journal of Fluids and Structures*, 94, 102962.

Mei, C. C. (1989). *The applied dynamics of ocean surface waves*. World Scientific, Singapore.

Miquel, A., Kamath, A., Alagan Chella, M., Archetti, R. and Bihs, H. (2018). "Analysis of different methods for wave generation and absorption in a CFD-based numerical wave tank." *Journal of Marine Science and Engineering*, 6(2), 1-20.

Misra, S.C. (2001). ''Uncertainty analysis in hydrodynamic tests.'' *Proc. 1st International Conference on Ocean Engineering*, 207–214.

Mo, W., Irschik, K., Oumeraci, H. and Liu, P. L. (2007). "A 3D numerical model for computing non-breaking wave forces on slender piles." *Journal of Engineering Mathematics*, 58(1), 19-30.

Mojtahedi, A., Beiragh, M. S., Farajpour, I. and Mohammadian, M. (2020). "Investigation on hydrodynamic performance of an environmentally friendly pile breakwater." *Ocean Engineering*, 217, 107942.

Nam, P.T., Larson, M., Hanson, H. and Oumeraci, H. (2017). "Model of nearshore random wave transformation: Validation against laboratory and field data." *Ocean Engineering*, 135, 183-193.

Neelamani, S. and Reddy, M.S. (1992). "Wave transmission and reflection characteristics of a rigid surface and submerged horizontal plate." *Ocean Engineering*, 19(4), 327-341.

Neelamani, S. and Vedagiri, M. (2001). "Wave interaction with partially immersed twin vertical barriers." *Ocean Engineering*, 29(2), 215-238.

Neelamani, S. and Rajendran, R. (2002a). "Wave interaction with T-type breakwaters." *Ocean Engineering*, 29(2), 151-175.

Neelamani, S. and Rajendran, R. (2002b). "Wave interaction with ⊥-type breakwaters." *Ocean Engineering*, 29(5), 561-589.

Newland, D.E. (1993). "Random vibrations, spectral and wavelet analysis." *Longman Scientific and Technical*: Harlow, UK.

Nguyen, Q. H., Ly, H. B., Ho, L. S., Al-Ansari, N., Le, H. V., Tran, V. Q., Prakash, I. and Pham, B.T. (2021). "Influence of data splitting on performance of machine learning models in prediction of shear strength of soil." *Mathematical Problems in Engineering*, 1-15.

Osher, S. and Sethian, J. A. (1988). "Fronts propagating with curvature-dependent speed: Algorithms based on Hamilton-Jacobi formulations." *Journal of Computational Physics*, 79, 12-49.

Park, W. S., Kim, B. H., Suh, K. D. and Lee, K. S. (2000). "Scattering of irregular waves by vertical cylinders." *Coastal Engineering*, 42(2), 253-271.

Peng, D., Merriman, B., Osher, S., Zhao, H. and Kang, M. (1999). "A PDE-based fast local level set method." *Journal of Computational Physics*, 155, 410-438.

Ramnarayan, S. K., Sannasiraj, S. A. and Sundar, V. (2020). "Hydrodynamic characteristics of curved and vertical front face pile-supported breakwaters in regular waves." *Ocean Engineering*, 216, 108105.

Ramnarayan, S.K., Sannasiraj, S.A. and Sundar, V. (2021). "Hydrodynamic characteristics of curved front face pile-supported breakwaters in random waves." *Applied Ocean Research*, 117, 102922.

Ramnarayan, S. K., Sundar, V. and Sannasiraj, S. A. (2022). "Hydrodynamic performance of concave front pile-supported breakwaters integrated with a louver wave screen." *Ocean Engineering*, 254, 111394.

Rao, S. and Rao, N.B.S. (2001). "Laboratory investigation on wave transmission through suspended perforated pipes." *ISH Journal of Hydraulic Engineering*, 7(1), 23-32.

Rao, S., Shirlal, K.G. and Rao, N.B.S. (2002). "Wave transmission and reflection for two rows of perforated hollow piles." *Indian Journal of Marine Sciences*, 31(4), 283-289.

Rao, S. and Rao, N.B.S. (1999). "Laboratory investigation on wave reflection characteristics of suspended perforated pipe breakwater." *ISH Journal of Hydraulic Engineering,* 5(1), 22-32.

Rao, S., Rao, N.B.S. and Sathyanarayana, V.S. (1999). "Laboratory investigation on wave transmission through two rows of perforated hollow piles." *Ocean Engineering*, 26(7), 675-699.

Rattanapitikon, W., (2007). "Calibration and modification of energy dissipation models for irregular wave breaking." *Ocean Engineering*, 34(11-12), 1592-1601.

Reedijk, B. and Muttray, M. (2009). "Pile row breakwaters at Langkawi, Malaysia, 10 years of beach development." *Coastal Structures 2007*, World Scientific Publishing Company, Singapore, 562-573.

Sarpkaya, T. (1976). "Vortex shedding and resistance in harmonic flow about smooth and rough circular cylinders at high Reynolds numbers." *Naval Postgraduate School, Monterey, CA, United States*.

Sasikumar, A., Kamath, A. and Bihs, H. (2020). "Modeling porous coastal structures using a level set method based VRANS-solver on staggered grids." *Coastal Engineering Journal*, 62(2), 198-216.

Schäffer, Hemming A. and Klopman, Gert. (2000) "Review of multidirectional active wave absorption methods." *Journal of Waterway, port, coastal, and ocean engineering*, 126(2), 88-97.

Shu, C. W. and Osher, S. (1988). "Efficient Implementation of Essentially Non-oscillatory Shock-Capturing Schemes." *Journal of Computational Physics*, 77, 439-471.

Srineash, V. K., Kamath, A., Murali, K. and Bihs, H. (2020). "Numerical simulation of wave interaction with submerged porous structures and application for coastal resilience." *Journal of Coastal Research*, 36(4), 752-770.

Straub, L. G., Bowers, C. E. and Herbich, J. B. (1957). "Laboratory tests of permeable wave absorbers." *Coastal Engineering Proceedings*, 6, 44-44.

Suh, K.D. D., Shin, S. and Cox, D. T. (2006). "Hydrodynamic characteristics of pile-supported vertical wall breakwaters." *Journal of Waterway, Port, Coastal, and Ocean Engineering,* 132(2), 83.

Suh, K., Jung, H. Y. and Chong, K. P. (2007). "Wave reflection and transmission by curtainwall – pile breakwaters using circular piles." *Ocean Engineering*, 34, 2100-2106.

Suh, K., Ji, C. and Kim, B. H. (2011). "Closed-form solutions for wave reflection and transmission by vertical slotted barrier." *Coastal Engineering*, 58(12), 1089-1096.

Sundar, V. and Subbarao, B. V. V. (2003). "Hydrodynamic performance characteristics of quadrant front-face pile-supported breakwater." *Journal of Waterway, Port, Coastal, and Ocean Engineering*, 129(1), 22-33.

Suvarna, P. S., Sathyanarayana, A. H., Umesh, P. and Shirlal, K. G. (2020). "Laboratory investigation on hydraulic performance of enlarged pile head breakwater." *Ocean Engineering*, 217, 107989.

Suvarna, P. S., Sathyanarayana, A. H., Umesh, P. and Shirlal, K. G. (2021). "Hydraulic performance of perforated enlarged pile head breakwaters through laboratory investigation." *Ocean Engineering*, 241, 110089.

Teh, H. M., Venugopal, V. and Bruce, T. (2012). "Hydrodynamic characteristics of a free-surface semicircular breakwater exposed to irregular waves." *Journal of Waterway, Port, Coastal, and Ocean Engineering*, 138(2), 149-163.

Teh, H.M., Venugopal, V. and Bruce, T. (2013). "Performance enhancement of a perforated free surface semicircular breakwater." *Proc. 23rd International Offshore and Polar Engineering Conference*. OnePetro.

Teh, H.M. (2013). "Hydraulic performance of free surface breakwaters: A review." *Sains Malaysiana*, 42(9), 1301-1310.

Truitt, C. L. and Herbich, J. B. (1987). "Transmission of random waves through pile breakwaters." *Proc. 20th Coastal Engineering Conference*, Taipei, Taiwan, Published by ASCE, NewYork, N. Y., 2303-2313.

Van der Vorst, H. A. (1992). "Bigstab: A fast and smoothly converging variant of Bi-CG for the solution of nonsymmetric linear systems." *SIAM Journal on Scientific and Statistical Computing*, 13(2), 631-644.

Wang, W., Kamath, A., Martin, T., Pákozdi, C. and Bihs, H. (2020). "A comparison of different wave modelling techniques in an open-source hydrodynamic framework." *Journal of Marine Science and Engineering*, 8(7), 526-553.

Wang, G., Ren, B. and Wang, Y. (2016). "Experimental study on hydrodynamic performance of arc plate breakwater." *Ocean Engineering*, 111, 593-601.

Weele, Van J. and Herbich, J.B. (1972). "Wave reflection and transmission for pile arrays." *Proc. 13th Coastal Engineering Conference*, Vancouver, B.C., Canada. Published by ASCE, New York, N.Y., 1935-1953.

Weigel, R.L. (1961). "Closely spaced piles as breakwater." *Dock and Harbour Authority*, 42(491), 150.

Wilcox, D. C. (1998). "Turbulence Modelling for CFD." *DCW Ind. Inc*, La Canada, California. 2, 103-217

Xuan, T. Le, Tran Ba, H., Manh, H. Le, Van, D. Do, Minh Nguyen, N., Wright, D. P., Bui, V. H., Mai, S. T. and Tran Anh, D. (2020). "Hydraulic performance and wave transmission through pile-rock breakwaters." *Ocean Engineering*, 218, 108229.

Yin, M., Zhao, X., Luo, M. and Sun, H. (2021). "Flow pattern and hydrodynamic parameters of pile breakwater under solitary wave using OpenFOAM." *Ocean Engineering*, 235, 109381.

Zhang, R. and Stive, M.J. (2019). "Numerical modelling of hydrodynamics of permeable pile groins using SWASH." *Coastal Engineering*, 153, 103558.

Zhao, X. and Ning, D. (2018). "Experimental investigation of breakwater-type WEC composed of both stationary and floating pontoons." *Energy*, 155, 226-233.

Zhu, D.T. (2011). "Hydrodynamic characteristics of a single row pile breakwater." *Coastal Engineering*, 58(5), 446-451.

Zhu, D.T. (2013). "Full wave solution for hydrodynamic behaviours of pile breakwater." *China Ocean Engineering,* 27(3), 323-334.

Zhu, D.T. and Yao Feng Xie (2015). "Hydrodynamic characteristics of offshore and pile breakwaters." *Ocean Engineering,* 104, 257-265.

JOURNAL PAPERS

1. Sathyanarayana, Arunakumar Hunasanahally, Praveen S. Suvarna, Pruthviraj Umesh, and Kiran G. Shirlal (2021). "Performance characteristics of a conical pile head breakwater: An experimental study." *Ocean Engineering*, 235, 109395. https://doi.org/10.1016/j.oceaneng.2021.109395

2. Sathyanarayana, Arunakumar Hunasanahally, Praveen S. Suvarna, Pruthviraj Umesh, Kiran G. Shirlal, Hans Bihs, and Arun Kamath (2022). "Numerical Modelling of an Innovative Conical Pile Head Breakwater." *Water*, 14(24), 4087. https://doi.org/10.3390/w14244087

3. Sathyanarayana, Arunakumar Hunasanahally, Praveen S. Suvarna, Pruthviraj Umesh, and Kiran G. Shirlal (2023)."Investigation on innovative pile head breakwater for coastal protection." *Proceedings of the Institution of Mechanical Engineers, Part M: Journal of Engineering for the Maritime Environment*, 14750902231155677.
   https://doi.org/10.1177/1475090223115567

CONFERENCE PAPER

1. Sathyanarayana, Arunakumar Hunasanahally, Nikhil V V, Praveen S. Suvarna, Pruthviraj Umesh, and Kiran G. Shirlal (2022)." Hydraulic characteristics of two rows of perforated pile head breakwater." Proc. 27th International Conference on Hydraulics, Water Resources, Environmental and Coastal Engineering (HYDRO 2022), Punjab Engineering College, Chandigarh, India.

NAME	**:**	**ARUNAKUMAR H S**
Date of Birth	**:**	17-04-1991
Mobile	**:**	+919731517959
Email	**:**	arunsaligram17@yahoo.com
Permanent Address	**:**	Door No. 104, Hanumantha Nagara,
		Bherya Road, Saligrama,
		K.R. Nagara, Mysuru,
		Karnataka - 571604
Qualifications	**:**	B.E. (Civil Engineering)
		M.Tech (Marine Structure)
Publications	**:**	International journals - 5
		International conferences - 4